CCI Land Surface Temperature

Product Validation and Intercomparison Report (PVIR)

WP4B.2 – DEL4.1

Ref.: LST-CCI-D4.1-PVIR

Date: 3-Jun-2020

Organisation: Consortium CCI LST

Signatures

	Name	Organisation	Signature
Written by	Maria Martin	KIT	
Reviewed by	Darren Ghent	ULeic	
Approved by			
Authorized by			

Change log

Version	Date	Changes
1.0	3-Jun-2020	First version

Table of Content

List of Figures

List of Tables

0. Executive Summary

Within the land surface temperature (LST) Climate Change Initiative project (LST_cci), which is part of the European Space Agency (ESA) Climate Change Initiative (CCI), a set of LST products from major satellites is developed. These LST data sets can be used for various applications within climate science.

For users to understand these data sets well and take them up, information on their quality is crucial. This is achieved within the project by validation of the developed data sets by an independent validation team, which ensures impartial results of the validation analysis.

This documents reports the results and interpretations of the validations carried out within LST_cci, which are split in two parts. First is the more straightforward approach of validating the satellite data sets against in situ point measurements, and second is the intercomparison of the data sets with third party data sets which are used as reference. This gives additional insights in the quality of the developed data. The results are presented in terms of bias for the in situ validation, difference for the intercomparisons, and accuracy and robust standard deviation for both with reference to the LST_cci requirements.

For the in situ validation, five infrared CCI LST products, for sensors Aqua-MODIS, Terra-MODIS, ATSR-2, AATSR, and SLSTR-A, and three microwave LST_cci products, from sensors SSMI-13, SSMI-17 and SSMI-18, are validated against in situ data from 13 globally distributed stations. The LST_cci products from these sensors are henceforth identified by 6 character codes: MODISA (for Aqua-MODIS), MODIST (for Terra-MODIS), ATSR_2 (for ATSR-2), ATSR_3 (for AATSR), SLSTRA (for SLSTR-A), SSMI13 (for SSMI-13), SSMI17 (for SSMI-17), and SSMI18 (for SSMI-18). The stations utilised are from the KIT network, SURFRAD network, ARM network and OzFlux network. The validation time period ranges from 1995 – 2018.

The results of the in situ validation show that in general the accuracies of the LST_cci products are better at night than during the day, which is entirely as expected. Furthermore, the microwave data sets tend to have more positive biases than the other data sets, however, they investigate a larger area than the infrared data sets and see thus more heterogeneities around most stations. MODISA, MODIST, ATSR_2 and ATSR_3 have most of the time smaller biases, with SLSTRA tending to have the most negative biases. This latter product is subject to inferior cloud masking, since it uses basic threshold masking whereas the other infrared products are deploying a first version of probabilistic masking. Furthermore, there are large differences found between the biases of LST_cci products with respect to in situ at single stations, showing that the performance of different data sets varies with the land cover type and elevation over which it is investigated.

Intercomparisons of satellite - satellite data pairs are a valuable asset to in situ validation results, especially as not all land covers types and regions are covered by in situ stations. For this project, nine satellite - satellite pairs were globally matched and intercompared, which are namely MOD11A-SEVCCI, MODISA-SEVCCI, ATSOP-SEVCCI, ATSR_3-SEVCCI, MOD11T-SEVCCI, MODIST-SEVCCI, ATSR_3-MOD11T, ATSR_3-MODIST, and MODIST-ATSOP. In these cases, SEVCCI is the LST_cci SEVIRI product, MOD11A is the operational Aqua-MODIS LST product, MOD11T is the operational Terra-MODIS LST product, and ATSOP is the operational AATSR LST product. All intercomparisons were done for the years 2008 – 2010 over different continents, which varied due to the data availability of the data sets. All nine data pairs could be analysed over Africa and Europe. A monthly time series was analysed for all pairs, and additionally the dependence of the differences on elevation, land cover, and satellite angles was investigated.

The results show that the highest positive differences were found for ATSR_3-MOD11T and ATSR_3-SEVCCI data pairs, ATSR_3-MODIST has lower differences, and the most negative ones were found for MOD11T-

SEVCCI, and MOD11A-SEVCCI. MODIST-ATSOP has more negative differences during night, and more positive ones during day. The variability between the data pairs varies over the analysed continents, it is larger over Africa, Australia and South America than over the other continents.

In general, from this first round of validation within LST_cci, it can be concluded that ATSR_2, ATSR_3, MODISA, and MODIST are showing good performance against in situ data. Furthermore, ATSR_3 and MODIST are well correlated. The intercomparison analysis revealed that all LEO IR CCI products are more comparable with the CCI SEVIRI product than the corresponding operational products. While these results about the performances of the products are encouraging, further improvements can still be made to single products or over single regions. Therefore, recommendations for efforts for possible improvements are provided to the algorithm developments teams at the end of the document.

1. Introduction

1.1. Purpose and Scope

Several satellite LST products are developed within the land surface temperature (LST) Climate Change Initiative project (LST_cci), which is part of the European Space Agency (ESA) Climate Change Initiative (CCI). These data sets can be used for a large variety of applications in different fields of climate science.

For ensuring that the users understand these data sets in the best possible way, it is important that information about their quality is available. This can also help to promote the uptake of LST data sets and possible users are informed about differences between the single produced data sets, their global performance as well as their performance over different landscapes and in different regions.

The quality of the data sets is investigated within LST_cci through their validation by an independent validation team. This procedure ensures that the validation results and their interpretations are gained impartial from the producers of the data sets. In this document, the results of the first validation round are presented. The theoretical background for the validation is described separately in in the Product Validation Plan (PVP) [AD-1], which informs in detail about the investigated satellite LST data sets (which are also described in [AD-2]), the used in situ stations and reference data sets for validation, the validation methodology, as well as the used harmonized data formats for storing the data.

There are two different validation approaches used. The first one is the in situ validation, which is the most straight forward approach, where satellite LST data are directly compared to in situ point measurements over several globally distributed stations. For this version of the report, nine LST_cci satellite data sets were validated, which are identified by a 6 character code. They are namely MODISA (for Aqua-MODIS), MODIST (for Terra-MODIS), ATSR_2 (for ATSR-2), ATSR_3 (for AATSR), SLSTRA (for SLSTR-A), SSMI13 (for SSMI-13), SSMI17 (for SSMI-17) and SSMI18 (for SSMI-18). They are analysed over 13 in situ stations belonging to different networks, which are KIT network, SURFRAD network, the ARM network and the OzFlux network. An overview over the single stations, their locations and surfaces can be found in Table 1. This set of stations is distributed over different climatic zones, land covers, elevations and regions worldwide, as detailed in AD-1. The validation time period differs depending on the availability of in situ and satellite data, ranging from 1995 to 2018.

Table 1: Overview of the used in situ stations.

Code	Network	Name	Latitude	Longitude	Elevation	Surface type	Temporal availability
ASM	OzFlux	Alice Springs Mulga Station, Australia	22.28° S	133.25° E	606 m	Woodland (mulga canopy)	2015–2016
SGP	ARM	Southern Great Plains Facility, Oklahoma	36.605° N	97.485° W	318 m	rural (mixture of grassland pasture / wheat fields / bare soil [RD-20])	2003 – now

EVO	KIT	Evora, Portugal	38.540244	-8.003368	230 m	Savannas, woody savanna; 32% tree, 68% grass	2010 – now
DAH_T	KIT	Dahra tree mast, Senegal	15.402336	-15.432744	90 m	Grassland; 96% grass, 4% tree	2010 – 2017
GBB_W	KIT	Gobabeb wind tower, Namibia	-23.550956	15.05138	406 m	Bare ground; 75% gravel, 25% dry grass	2010 – now
KAL_R	KIT	Rust mijn Ziel (RMZ) Farm, Kalahari, Namibia	-23.010532	18.352897	1450 m	Shrub land; 85% grass / soil, 15% tree	2010 - 2011
KAL_H	KIT	Farm Heimat, Kalahari, Namibia	-22.932827	17.992137	1380 m	Shrub land; 37% tree / bush, 63% grass	2011 – 2018
BND	SURFRAD	Bondville, Illinois	40.05155	-88.37325	230 m	Grassland	1995 - now
TBL	SURFRAD	Table Mountain, Boulder, Colorado	40.12557	-105.23775	1689 m	Sparse grassland	1995 - now
DRA	SURFRAD	Desert Rock, Nevada	36.62320	-116.01962	1007 m	Arid shrub land	1998 - now
FPK	SURFRAD	Fort Peck, Montana	48.30798	-105.10177	634 m	Grassland	1995 - now
GCM	SURFRAD	Goodwin Creek, Mississippi	34.2547	-89.8729	98 m	Grassland	1995 - now
PSU	SURFRAD	Penn. State Univ., Pennsylvania	40.72033	-77.93100	376 m	Cropland	1998 - now

In spite of the globally distribution of the in situ stations, they do not cover all important land covers and regions perfectly. Therefore, supplementary satellite – satellite intercomparisons are carried out between LST_cci data sets and external operational and reference LST products over different continents. The relative algorithm performances of the LST_cci data products over different regions worldwide can be investigated with these intercomparisons. For this report, intercomparisons were carried out for the years 2008 – 2010 for nine satellite-satellite pairs, which are summarized in Table 2. Six of these nine data pairs use MSG_SEVIRI as reference satellite data set and they are therefore analysed over the continents Africa and Europe only, as MSG_SEVIRI is a geostationary satellite product that has no global coverage. The three remaining data pairs ENVISAT_AATSR vs TERRA_MOD11, ENVISAT_AATSR vs TERRA_MODIS, and TERRA_MODIS vs ENVISAT_ATSOP are also analysed over Antarctica, Asia, Australia, North America and South America.

Table 2: Summary of the satellite – satellite data pairs used in the intercomparisons.

Satellite 1	Sat 1 6 char code	Satellite 2	Sat 2 6 char code
AQUA MODIS (operational product)	MOD11A	MSG SEVIRI	SEVCCI
AQUA MODIS	MODISA	MSG SEVIRI	SEVCCI
ENVISAT AATSR (operational product)	ATSOP_	MSG SEVIRI	SEVCCI
ENVISAT AATSR	ATSR_3	MSG SEVIRI	SEVCCI
ENVISAT AATSR	ATSR_3	TERRA MODIS (operational product)	MOD11T
ENVISAT AATSR	ATSR_3	TERRA MODIS	MODIST
TERRA MODIS (operational product)	MOD11T	MSG SEVIRI	SEVCCI
TERRA MODIS	MODIST	ENVISAT AATSR (operational product)	ATSOP_
TERRA MODIS	MODIST	MSG SEVIRI	SEVCCI

The data files used within the validation process can be categorized in four different types, which are in situ data files (IS_), satellite extraction data files (SE_), matched satellite – satellite (SS_), and matched satellite – in situ data files (SI_). All four classes have a common data format that is introduced in AD-1. In this way, the validation procedure is harmonized, and can be carried out in the same way for all data sets, which in turn makes the different validation results comparable to each other. This also ensures that the used analysis software can be re-used on additional data sets throughout the project, thus making the validation process faster.

The results for the in situ validation are presented in terms of bias which is the median of the difference of satellite LST minus in situ LST (following [RD-3]) and by the robust standard deviation (RSTD) (see e.g. [RD-4]), which is connected to the precision (median absolute deviation) introduced in RD-3 by a constant factor of 1.48, i.e. RSTD = 1.48 * MAD. Higher accuracy relates here to smaller bias. For the intercomparisons the results are presented in terms of a “difference” between products, which is the difference of satellite 1 LST minus satellite 2 LST. In this case, higher accuracy relates to smaller differences. All biases and differences displayed in this report are on an axis ranging from -10 K to 10 K to make the figures easily comparable to each other.

This document will be updated throughout the project to include further validation results and will be updated accordingly, following future Processing Cycles.

1.2. Structure of the Document

First, a short summary of the introduced satellite data sets is given, followed by an overview of the results of the in situ validations over all satellite data sets and over all stations in Section 3.1. Next, the validation results are described for each station individually in Section 3.2. An overview of the intercomparison results is given in Section 4.1, which are then described in more detail for each continent in Section 4.2. In Section 5, conclusions on the overall results are drawn, and finally recommendations for the producer of the data sets are given in Section 6. In the Appendix (Section 7) additional figures from the intercomparisons are displayed.

1.3. Applicable Documents

Ref Id	Applicable document
AD-1	CCI LST Product Validation Plan (LST-CCI-D4.1-PVIR)
AD-2	CCI LST Product Specification Document (LST-CCI-D1.2-PSD)

1.4. Reference Documents

The following is a list of reference documents with a direct bearing on the content of this report. Where referenced in the text, these are identified as RD-xx, where ‘xx’ is the number in the table below.

Ref Id	Reference document
RD-1	Martin, M.; Göttsche, F.M. ESA DUE GlobTemperature Project: Satellite LST Validation report. Technical report, ESA, 2016. http://www.globtemperature.info/index.php/public-documentation/deliverables-1
RD-2	Martin, M.; Göttsche, F.M.; Ghent, D.; Trent, T.; Dodd, E.; Pires, A.; Trigo, I.; Prigent, C.; Jimenez, C. ESA DUE GlobTemperature Project: Satellite LST Intercomparison Report. Technical report, ESA, 2016. http://www.globtemperature.info/index.php/public-documentation/deliverables-1
RD-3	Guillevic, P.; Göttsche, F.; Nickeson, J.; Hulley, G.; Ghent, D.; Yu, Y.; Trigo, I.; Hook, S.; Sobrino, J.; Remedios, J.; Román, M.; Camacho, F. Land Surface Temperature Product Validation Best Practice Protocol, Version 1.1 2018. https://lpvs.gsfc.nasa.gov/PDF/CEOS_LST_PROTOCOL_Feb2018_v1.1.0_light.pdf
RD-4	Pearson, R.K. Outliers in Process Modeling and Identification. IEEE Transactions On Control Systems Technology 2002, 10, 55–63.
RD-5	Göttsche, F.M.; Hulley, G.C. Validation of six satellite-retrieved land surface emissivity products over two land cover types in a hyper-arid region. Remote Sensing of Environment 2012, 124, 149–158.
RD-6	Wan, Z.; Dozier, J. A Generalized Split-Window Algorithm for Retrieving Land-Surface Temperature from Space. IEEE Transactions on Geoscience and Remote Sensing 1996, 34, 892–905.
RD-7	Aires, F.; Prigent, C.; Rossow, W.; Rothstein, M. A new neural network approach including first guess for retrieval of atmospheric water vapor, cloud liquid water path, surface temperature, and emissivities

Ref Id	Reference document
	over land from satellite microwave observations. Journal of Geophysical Research 2001, 106, 14887–14907.
RD-8	Prata, F. Land surface temperature measurement from space: AATSR algorithm theoretical basis document. Technical report, CSIRO Atmospheric Research, Aspendale, Australia, 2002.
RD-9	Ghent, D. GlobTemperature Project Technical Specification Document. Technical report, ESA, 2016.

1.5. Glossary

Term	Definition
ARM	Atmospheric Radiation Measurement
ATSR	Along Track Scanning Radiometer; the ATSR series of instruments comprises ATSR-1, ATSR-2 and AATSR (ATSR_3)
CCI	Climate Change Initiative
ESA	European Space Agency
GEO	Geostationary orbit
IS	In Situ Files
IR	Infrared
KIT	Karlsruhe Institute of Technology
LCC	Land Cover Class
LEO	Low Earth Orbit
LST	Land Surface Temperature
LST_cci	Land Surface Temperature Climate Change Initiative
MAD	Median Absolute Deviation
MODIS	Moderate Resolution Imaging Spectroradiometer
MSG	Meteosat Second Generation
MW	Microwave
NetCDF	Network Common Data Format
PSD	Product Specification Document
PVIR	Product Validation and Intercomparison Report
PVP	Product Validation Plan
RSTD	Robust Standard Deviation
Sataz	satellite azimuth angle
Satze	satellite zenith angle
SE	Satellite Extraction Files

Term	Definition
SEVIRI	Spinning Enhanced Visible Infra-Red Imager
SH	Southern Hemisphere
SI	Satellite – In situ match ups
SLSTR	Sea and Land Surface Temperature Radiometer
SS	Satellite – Satellite match ups
SSM/I	Special Sensor Microwave – Imager
STD	Standard Deviation
SURFRAD	Surface Radiation Budget Network
ULeic	University of Leicester

2. Satellite Data Sets

The validated CCI satellite and reference data sets are shortly introduced in the following. A more complete overview of the data sets can be found in the PVP [AD-1].

2.1. CCI Satellite Data Sets

Along Track Scanning Radiometer - 2 (ATSR-2 / ATSR_2) and Advanced Along Track Scanning Radiometer (AATSR / ATSR_3)

ATSR-2 is the second, and AATSR the third of a series of instruments (ATSR-1, ATSR-2 and AATSR). ATSR-2 was on board the European Space Agency's (ESA) sun-synchronous, polar orbiting satellite ERS-2 which was launched in April 1995, and AATSR on board ESA's sun-synchronous, polar orbiting satellite Envisat which was launched in March 2002 and stopped operating in April 2012. Both had similar orbit and equator crossing times, which ensures a high level of consistency. The considered data length from ATSR-2 and AATSR is 17 years. The ATSR-2 and AATSR ECV Products are created using the existing GlobTemperature processing chains with any necessary modification.

Moderate Resolution Imaging Spectrometer (MODIS / MODISA and MODIST)

The CCI MODIS products from Aqua (MODISA) and Terra (MODIST) use a generalized split-window (GSW) approach [RD-6] to estimate LST as a linear function of clear-sky TOA brightness temperatures from bands 31 and 32 centred on 11 µm and 12 µm, respectively. Retrieval coefficients are categorised into classes of satellite viewing angle and water vapour. The data is spatially and temporally interpolated onto the ~1 km grid for the given day of the satellite acquisition.

Sea and Land Surface Temperature Radiometer (SLSTR / SLSTRA)

SLSTR is a continuation of the ATSR series. It is based on the principles of AATSR on board the Sentinel satellites 3-A and 3-B, responding to the requirements for an operational and near-real-time monitoring of the Earth surface over a period of 15 to 20 years. Like AATSR a dual view capability is maintained with SLSTR, the nadir swath being 1420 km, and the backward view being 750 km. The spatial resolution of SLSTR is 500 m in the visible and shortwave infrared channels and 1 km in the thermal infrared channels. The baseline retrieval for the operational ESA SLSTR LST product consists of a split-window algorithm with classes of coefficients for each biome-diurnal (day/night) combination.

Special Sensor Microwave / Imager (SSM/I / SSMI_13, SSMI_17, and SSMI_18)

SSM/I sensors have been on board the Defense Meteorological Satellite Program (DMSP) polar satellites since 1987, which observe the Earth twice daily. The local times of their descending and ascending modes are early morning and late afternoon, respectively. There are up to 4 SSM/I instruments in space at the same time with similar overpassing times. A methodology has been developed to estimate LST, along with atmospheric water vapour, cloud liquid water, and surface emissivities over land, from passive microwave imagers [RD-7]. It is based on a neural network inversion, trained on a large data set of simulated radiances, using real atmospheric and surface information over the globe. LST are estimated with a spatial resolution of 0.25° x 0.25.

Spinning Enhanced Visible and Infrared Imager (SEVIRI /SEVCCI)

SEVIRI is the main sensor on board Meteosat Second Generation (MSG), a series of 4 geostationary satellites to be operated by EUMETSAT. SEVIRI was designed to observe the Earth disk with view zenith angles (SZA) ranging from 0º to 80º at a temporal sampling rate of 15 minutes. The first MSG satellite was launched in August 2002, and operational observations are available since January 2004. The High Resolution Visible channel provides measurements with a 1 km sampling distance at sub-satellite point (SSP); for the remaining channels the spatial resolution is 3 km at SSP. The nominal SSP is located at 0° longitude and therefore the MSG disk covers Africa, most of Europe and parts of South America. A SEVIRI LST product is produced by the Land Surface Analysis Satellite Application Facility (LSA SAF). LST is obtained by correcting top-of-atmosphere (TOA) radiances for surface emissivity, atmospheric attenuation along the path and reflection of downward radiation.

2.2. External Satellite Data Sets

Operational MODIS (MYD11 and MOD11 / MOD11A and MOD11T)

The standard operational MODIS LST products MOD11_L2 (Terra) and MYD11_L2 (Aqua) uses a generalized split-window algorithm to retrieve LST of clear-sky pixels from brightness temperatures. This implementation of the algorithm operates with classification-based emissivities. The retrieval coefficients are determined by interpolation on a set of multi-dimensional look-up tables; these are obtained by linear regression of the simulation data generated by radiative transfer over a broad range of surface and atmospheric conditions.

Operational Advanced Along Track Scanning Radiometer (AATSR / ATSOP)

For the standard ESA AATSR LST retrieval, only the nadir view is used. LST are retrieved with a split-window algorithm [RD-8] with 1 km resolution based on the infrared channels at 11 and 12 µm [RD-9].

3. Description and Analysis of In Situ Validation Results

3.1. Overview of Results

First, an overview of the validation results for all satellite data sets over all in situ stations is given. The biases and robust standard deviations (RSTD) for the investigated data sets over each station are shown in Figure 1, and detailed in Table 3 for night-time and in Table 4 for daytime data. When interpreting the results, one has to keep in mind that the time period over which the data is averaged varies between stations and satellite data sets due to their availability. The matched time periods can be seen in Table 5.

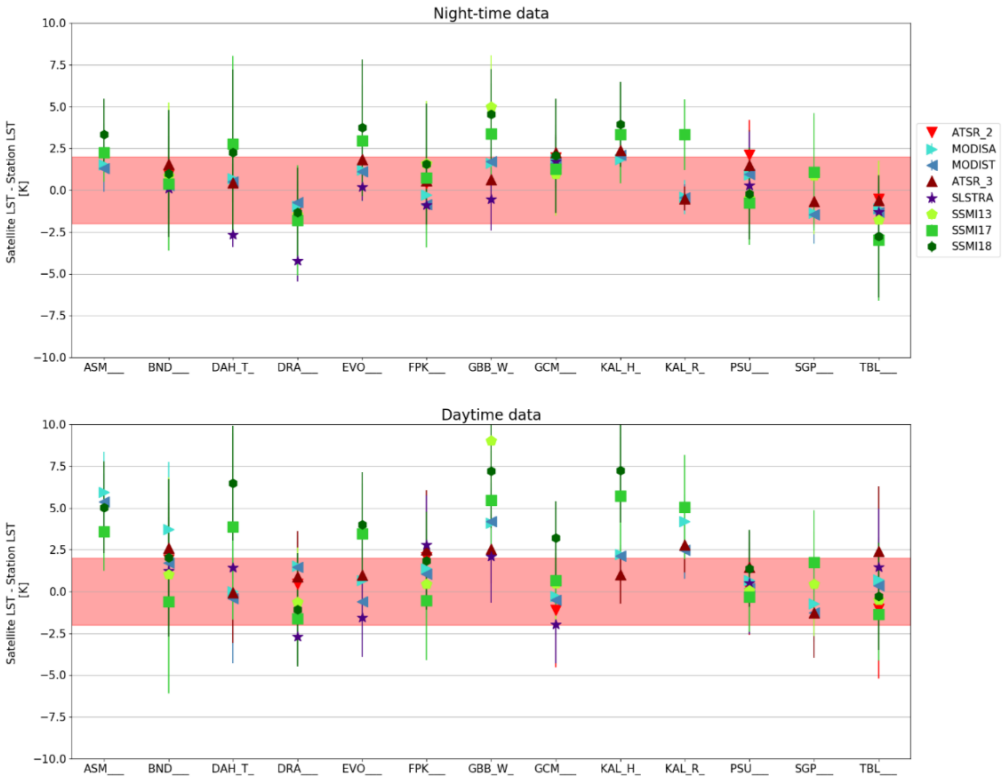

Figure 1: Overview over all validated satellite LST data sets against all stations, for night-time (upper plot) and daytime (lower plot) data. The matched time of the satellite data sets varies, depending on data availability, as indicated in Table 5. The red span marks the bias range of ± 2 K.

In general, the night-time biases are smaller than the daytime biases and have also lower RSTDs. This is expected and mainly caused by the influence of solar radiation during daytime, which results in different surface temperatures observed by the satellite sensors at sunlit and shadowed areas. These differences are often to a lower extend reflected in the point measurements of the in situ sensors. The MW data sets SSMI13, SSMI17, and SSMI18 tend to have the highest biases, and SLSTRA tends to have the lowest biases. The MW data sets investigate a larger area than the IR data sets (see [AD-1]) and capture thus for most stations a more heterogeneous surface than the IR data sets. Thus, the validation results of these data sets cannot be compared directly to the IR data sets. SLSTRA data set often tends to have more negative biases than the other IR data sets, which might be caused by a larger influence of missed cloudy data, as the SLSTRA algorithm uses only a basic cloud mask.

Furthermore, it can be seen in Figure 1 that the magnitude of the biases varies significantly between single stations and also between satellite data sets. For example, ASM___ station has very high daytime biases for all satellite data sets, and over GBB_W_ and DAH_T_ the MW data sets have very high biases. The SLSTRA data set has very low biases over DAH_T_ station at night. These differences can either be caused by the different satellite algorithms, which might represent some surfaces better than others. Or it is due to a different amount of homogeneity in the area around the in situ stations, as larger surface heterogeneities are often not represented by the in situ LST measurement. The reasons for the found biases vary from station to station and will be investigated in detail for each station individually below.

The number of matched data points is shown in Figure 2. The number of matches also varies between satellite data set and station due to the time span that is available for each data sets. The MW data sets have in general a high number of matches, caused by the fact that they can deviate LST also during cloudy time periods contrary to the IR sensors. It is important to notice that the SSMI data points are taken at a local overflight time at around 6:30 AM and 6:30 PM each day, which leads to a varying number in daytime and night-time data. There are more daytime and less night-time data points in summer, when sunset is at a later time and the other way round during winter, when the days are shorter. This might make the statistics of the averaged biases for the time periods with fewer data points less robust. Furthermore, the distinction between night-time and daytime data might be less reasonable for times close to sunset or sunrise.

Both investigated MODIS data sets have as well many data points as they have the longest investigated time period (see Table 5). The low number of SLSTRA data points over DAH_T_ station is caused by the fact that the in situ measurements at this station stopped in January 2017, and the analysed SLSTRA data sets starts in January 2017. Thus, there is only a data overlap of some days.

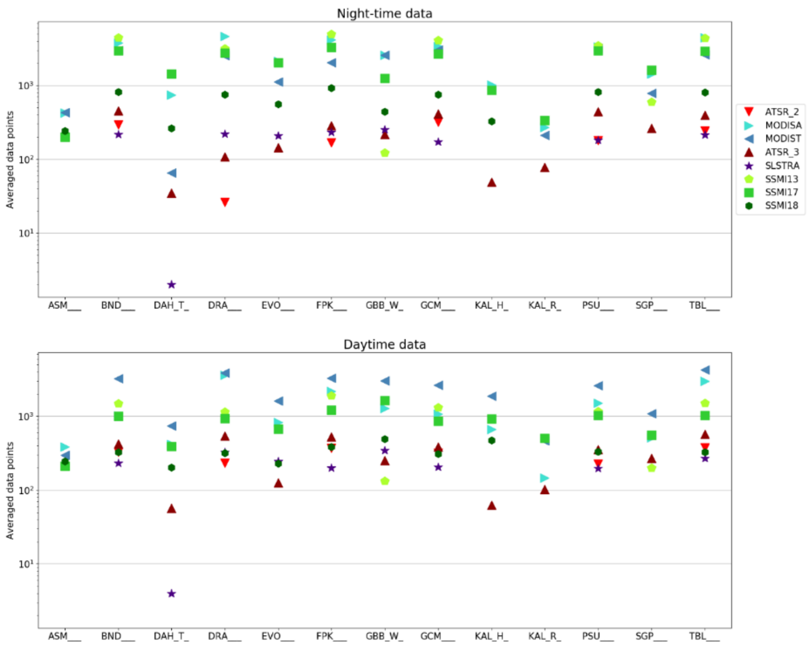

Figure 2: Number of averaged data points over all validated satellite LST data sets and stations, for night-time (upper plot) and daytime (lower plot) data.

Table 3: Median night-time bias) and RSTD in K for the analysed time period

		ASM	BND	DAH_T	DRA	EVO	FPK	GBB_W	GCM	KAL_H	KAL_R	PSU	SGP	TBL
MODISA	bias	1.52	0.39	0.83	-0.94	1.22	-0.30	1.63	1.81	1.84	-0.41	0.91	-1.38	-1.12
	RSTD	1.33	1.70	1.65	1.25	1.90	1.63	1.68	1.51	1.24	1.02	1.76	1.82	1.39
ATSR_3	bias	-	1.54	0.45	-1.37	1.84	0.56	0.64	2.25	2.39	-0.50	1.48	-0.66	-0.59
	RSTD	-	1.66	1.11	0.74	1.01	1.54	1.25	1.07	0.40	0.71	2.11	1.56	1.35
ATSR_2	bias	-	0.92	-	-1.13	-	0.41	-	1.92	-	-	2.11	-	-0.55
	RSTD	-	1.44	-	0.83	-	1.59	-	1.25	-	-	2.08	-	1.36
SLSTRA	bias	-	0.08	-2.68	-4.23	0.19	-0.90	-0.55	1.71	-	-	0.27	-	-1.31
	RSTD	-	1.68	0.73	1.23	0.83	1.47	1.87	1.58	-	-	3.22	-	1.73
MODIST	bias	1.29	0.29	0.51	-0.73	1.01	-0.86	1.71	1.62	2.09	-0.44	0.96	-1.47	-1.34
	RSTD	1.38	1.62	2.16	1.20	1.74	1.79	1.56	1.50	1.30	0.81	1.91	1.70	1.45
SSMI13	bias	-	0.87	-	-1.46	-	1.58	4.99	0.96	-	-	-0.49	0.85	-1.79
	RSTD	-	4.36	-	2.86	-	3.75	3.08	2.48	-	-	2.51	3.47	3.53
SSMI17	bias	2.24	0.39	2.74	-1.80	2.95	0.75	3.36	1.27	3.34	3.32	-0.78	1.09	-2.99
	RSTD	1.72	4.00	5.32	3.31	3.31	4.17	2.98	2.61	2.94	2.11	2.50	3.51	3.62
SSMI18	bias	3.33	0.99	2.26	-1.32	3.74	1.55	4.55	2.05	3.94	-	-0.21	-	-2.76
	RSTD	2.14	3.79	4.95	2.64	4.08	3.61	2.68	3.41	2.55	-	2.74	-	3.66

Table 4: Median daytime bias and RSTD in K for the analysed time period

		ASM	BND	DAH_T	DRA	EVO	FPK	GBB_W	GCM	KAL_H	KAL_R	PSU	SGP	TBL
MODISA	bias	5.93	3.72	0.01	1.51	0.66	1.36	4.11	-0.27	2.22	4.19	0.68	-0.72	0.70
	RSTD	2.43	4.03	2.82	1.94	3.56	2.88	2.06	1.62	1.70	1.57	2.25	2.28	2.34
ATSR_3	bias	-	2.59	-0.06	0.89	0.99	2.52	2.54	0.66	1.02	2.78	1.46	-1.28	2.43
	RSTD	-	2.65	3.01	2.74	2.74	3.56	2.04	1.62	1.73	1.63	2.11	2.70	3.85
ATSR_2	bias	-	1.89	-	0.45	-	2.02	-	-1.11	-	-	0.14	-	-1.05
	RSTD	-	2.82	-	2.50	-	3.97	-	3.44	-	-	2.74	-	4.15
SLSTRA	bias	-	1.25	1.42	-2.70	-1.56	2.79	2.08	-1.96	-	-	0.51	-	1.47
	RSTD	-	3.17	0.62	1.65	2.36	2.97	2.74	2.31	-	-	3.04	-	3.48
MODIST	bias	5.38	1.71	-0.27	1.47	-0.61	1.04	4.17	-0.51	2.13	2.48	0.19	-1.27	0.36
	RSTD	1.65	3.34	3.51	1.87	3.19	2.64	2.28	2.09	1.48	1.72	2.12	2.61	2.89
SSMI13	bias	-	1.01	-	-0.65	-	0.46	9.03	0.48	-	-	0.05	0.44	-0.50
	RSTD	-	5.83	-	3.29	-	2.68	5.26	2.15	-	-	1.88	3.11	2.76
SSMI17	bias	3.58	-0.60	3.45	-1.63	3.47	-0.54	5.47	0.67	5.72	5.05	-0.33	1.75	-1.37
	RSTD	2.36	5.50	6.62	2.64	2.94	3.56	2.90	2.02	3.49	3.11	2.09	3.11	2.75
SSMI18	bias	5.03	2.02	6.48	-1.08	4.01	1.85	7.20	3.20	7.23	-	1.38	-	-0.28
	RSTD	2.76	4.71	3.44	3.38	3.14	2.92	3.41	2.43	3.10	-	2.30	-	3.20

Table 5: Analysed years for the validation of satellite LST data sets over in situ stations

	ASM	BND	DAH_T	DRA	EVO	FPK	GBB_W	GCM	KAL_H	KAL_R	PSU	SGP	TBL
MODISA	2015 - 16	2002 - 18	2009 - 17	2002 - 18	2009 - 18	2002 - 18	2008 - 18	2002 - 18	2011 - 18	2009 - 11	2002 - 18	2007 - 12	2002 - 18
ATSR_3	-	2002 - 12	2009 - 12	2002 - 12	2009 - 12	2009 - 12	2008 - 12	2002 - 12	2011 - 12	2009 - 11	2002 - 12	2007 - 12	2002 - 12
ATSR_2	-	1995 - 2003	-	1998 - 2003	-	1995 - 2003	-	1995 - 2003	-	-	1998 - 2003	-	1995 - 2003
SLSTRA	-	2017 - 18	2017	2017 - 18	2017 - 18	2017 - 18	2017 - 18	2017 - 18	-	-	2017 - 18	-	2017 - 18
MODIST	2015 - 16	2000 - 18	2009 - 17	2000 - 18	2009 - 18	2000 - 18	2008 - 18	2000 - 18	2011 - 18	2009 - 11	2000 - 18	2007 - 12	2000 - 18
SSMI13	-	1995 - 2008	-	1998 - 2008	-	1995 - 2008	2008	1995 - 2008	-	-	1998 - 2008	2007 - 08	1995 - 2008
SSMI17	2015	2009 - 15	2009 - 15	2009 - 15	2009 - 15	2009 - 15	2009 - 15	2009 - 15	2011 - 15	2009 - 11	2009 - 15	2009 - 12	2009 - 15
SSMI18	2016	2016 - 17	2016 - 17	2016 - 17	2016 - 17	2016 - 17	2016 - 17	2016 - 17	2016 - 17	-	2016 - 17	-	2016 - 17

3.2. Results for different stations

The results for the in situ validation over the different stations are presented in the following, more details about the stations and the land surfaces surrounding the stations can be found in the Product Validation Plan [AD-1].

3.2.1. Results over ARM SGP___ Station

Figure 3: *Monthly mean biases (satellite LST - station LST) over SGP___ station. The upper plot represents night-time and the lower daytime data. The red span is the area where the bias is in a ± 2 K range.*

The night-time as well as the daytime biases for the three investigated IR LST data sets (MODISA, MODIST, and ATSR_3) and the MW LST data sets (SSMI13, and SSMI17) are displayed in Figure 3. All data sets show a seasonal cycle, which has higher amplitudes during day. The biases are more positive in the summer months and more negative in the winter months. This is probably caused by the phenological cycle found in the rural area around the station, which is dominated by agricultural fields where wheat and cattle pasture is grown. This cycle leads to changing differences between the in situ and the satellite data sets. The highest absolute biases are seen for the SSMI13 and SSMI17 MW data sets, which observe, as mentioned above, a larger area than the IR sensors.

3.2.2. Results over OzFlux ASM___ Station

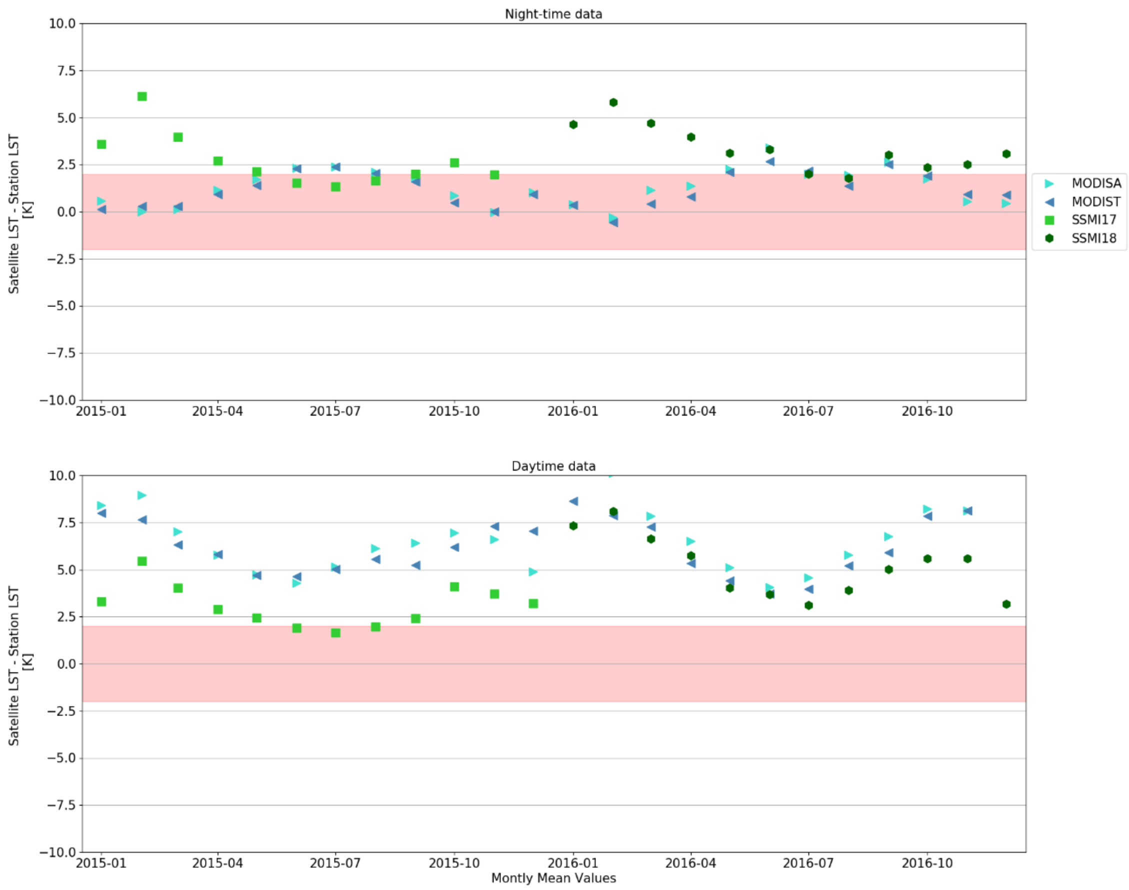

Figure 4: Monthly mean biases (satellite LST – station LST) over ASM___ station. The upper plot represents night-time and the lower daytime data. The red span is the area where the bias is in a ± 2 K range.

The biases for the two investigated IR data sets (MODISA and MODIST) over this station are between 0 K and 2.5 K for the night-time data (Figure 4), which is an acceptable range. However, the biases during day are much higher. They also display a strong yearly cycle with increased values in SH summer above 10 K. The general difference between satellite and in situ daytime data might be caused by the fact that in the region around ASM station the trees stand rather separate from each other, and the red soil beneath them is also seen by the satellite sensors. These different surfaces are probably not adequately captured by the in situ sensor. The further increase in summer might be due to an increased temperature differences on the surfaces between sunlit and shaded areas. Similar high biases during day were already found for validation within the GlobTemperature project [RD-1]. The MW LST data sets display also a night-time seasonal cycle, with increased values in the SH summer months. As mentioned in Section 3.1, the SSMI overflight times are around 6:30 am and 6:30 pm, and thus closer to sunset and sunrise than the IR data sets. This might result in more similar daytime and night-time biases.
Also the robust standard deviation (RSTD) is higher in summer than in winter (Figure 5), which might be due to increased rain fall and clouds during this time of year, leading to larger differences in the LST values. These difficulties to validate the satellite data during day at ASM station is mainly due to the setup of the station and does not reflect the quality of the satellite data. Thus, the daytime data will probably not be considered for validation in the next validation round.

Figure 5: RSTD over ASM___ station. The red span displays the area where RSTD is in a ± 2 K range.

3.2.3. Results over KIT Stations

Results over DAH_T_ Station

Figure 6: Monthly mean biases (satellite LST – station LST) over DAH_T_ station. The upper plot represents night-time and the lower daytime data. The red span is the area where the bias is in a ± 2 K range.

The data gaps in 2012 and 2015 are due to missing in situ data at these times.
The strong seasonal vegetation cycle present at this station [AD-1] is reflected in the observed monthly biases. They increase in the first half of the year and decrease after that. As the rainy season lasts from June to November, the strong negative IR biases for MODIST and ATSR_3 data seen during this time in summer and winter months are probably due to non-flagged cloudy data points observed in daytime and night-time results. Also the number of data points is reduced during the rainy seasons due to the present clouds, which makes the results during these months less robust. Also at this station the results of the SSMI data sets are similar for daytime and night-time results.

Results over EVO___ Station

Figure 7: Monthly mean biases (satellite LST – station LST) over EVO___ station. The upper plot represents night-time and the lower daytime data. The red span is the area where the bias is in a ± 2 K range.

The night-time IR biases are mainly within ± 2K (Figure 7), with increased values for ATSR_3. For all IR daytime biases, a seasonal cycle is seen, with higher values in the summer months. This is caused by the directional effects at this station caused by the trees around the station, resulting in an increased influence of sunlit and shaded areas in summer. The reason for the pronounced negative daytime values for both MODIS data sets as well as for SLSTRA in the first half of 2017 is unclear and needs further investigation.

Results over GBB_W_ Station

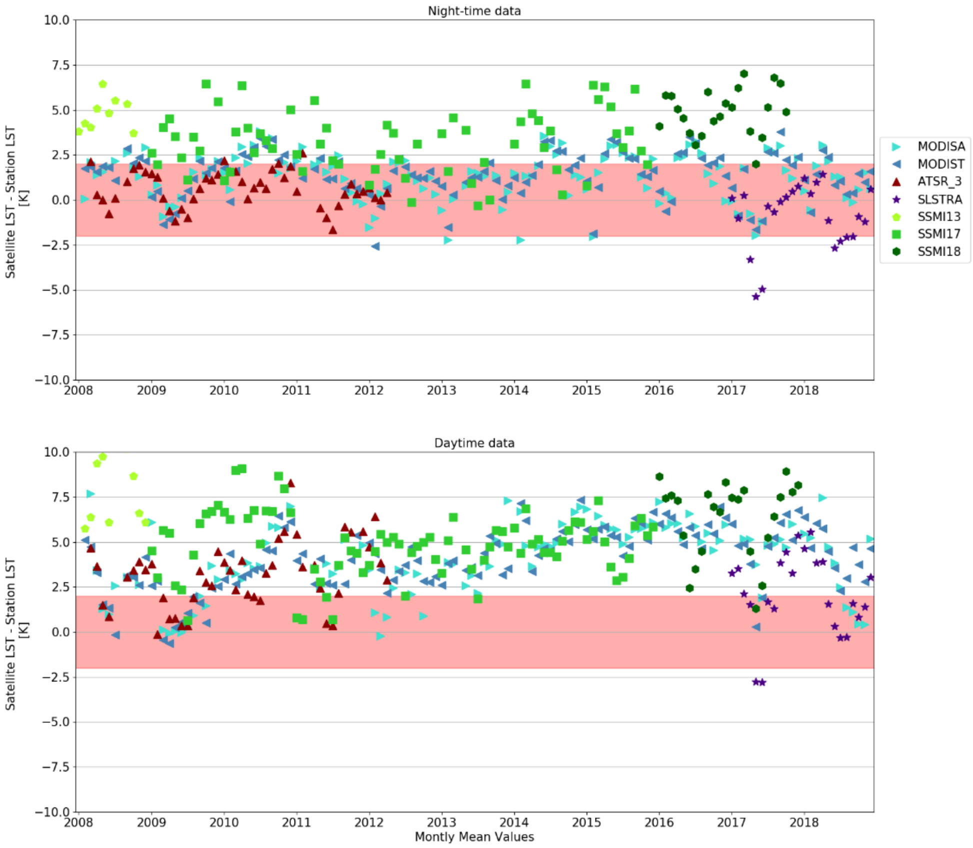

Figure 8: Monthly mean biases (satellite LST – station LST) over GBB_W_ station. The upper plot represents night-time and the lower daytime data. The red span is the area where the bias is in a ± 2 K range.

The night-time IR biases are for all sensors in an acceptable range, whereas the daytime biases are worse for most months. The station is a well-known and good characterised in situ station located in a hyper-arid and very homogeneous surrounding of the gravel-plains of the Namib Desert. As these biases cannot be explained by surface heterogeneities, they might be due to differences in the emissivities used for the calculation of the satellite and in situ LST values. The in situ LST is calculated with a constant emissivity of 0.94 [RD-5] that was determined by combining in situ measurements and laboratory emissivity spectra of soil samples. Thus, this high daytime biases might be caused by the satellite LST algorithms that might use a different emissivity at this region. The SSMI MW data sets display similar increased biases for daytime and night-time data.

Results over KAL_R_ / KAL_H_ Stations

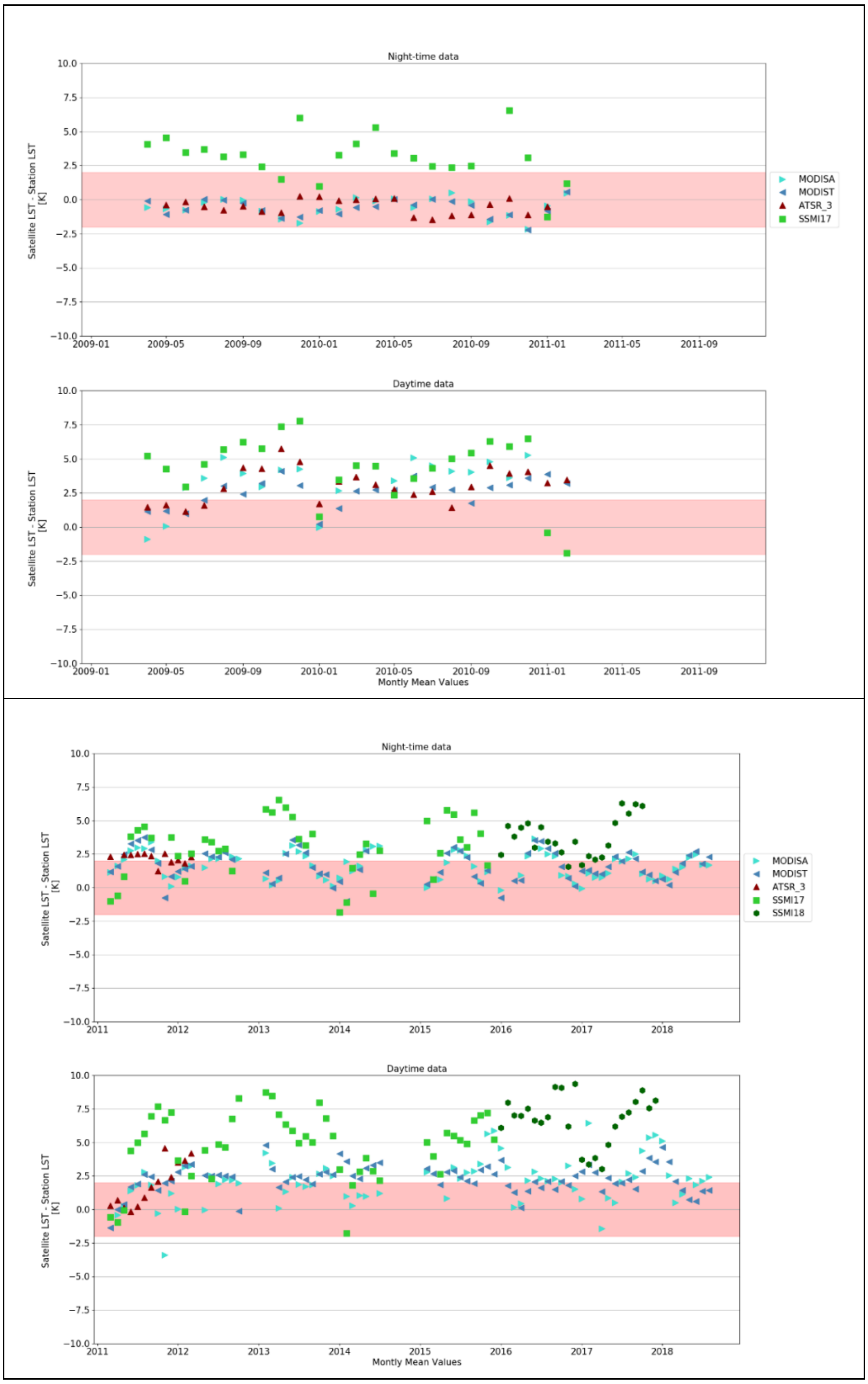

Figure 9: Monthly mean biases (satellite LST – station LST) over KAL_R_ (upper) and KAL_H_ (lower) stations. The upper plot represents night-time and the lower daytime data. The red span is the area where the bias is in a ± 2 K range.

The station in the Kalahari semi-desert was located at farm "Rust mijn Ziel" (KAL_R_) until February 2011 and at farm "Heimat" (KAL_H_) afterwards. KAL_H_ has more bushes and less large trees than KAL_R_, which might explain the smaller daytime IR biases at KAL_H_ station due to a lesser influence of sunlit and shaded areas. Increased night-time biases at KAL_H_ are found for the SH winter months. During winter, the number of IR data points increases as during summer there are two rainy seasons observed in the region [AD-1]. Thus, the lower biases in summer might be due to a larger influence of missed clouds then.

3.2.4. Results over SURFRAD stations

Results over BND___ Station

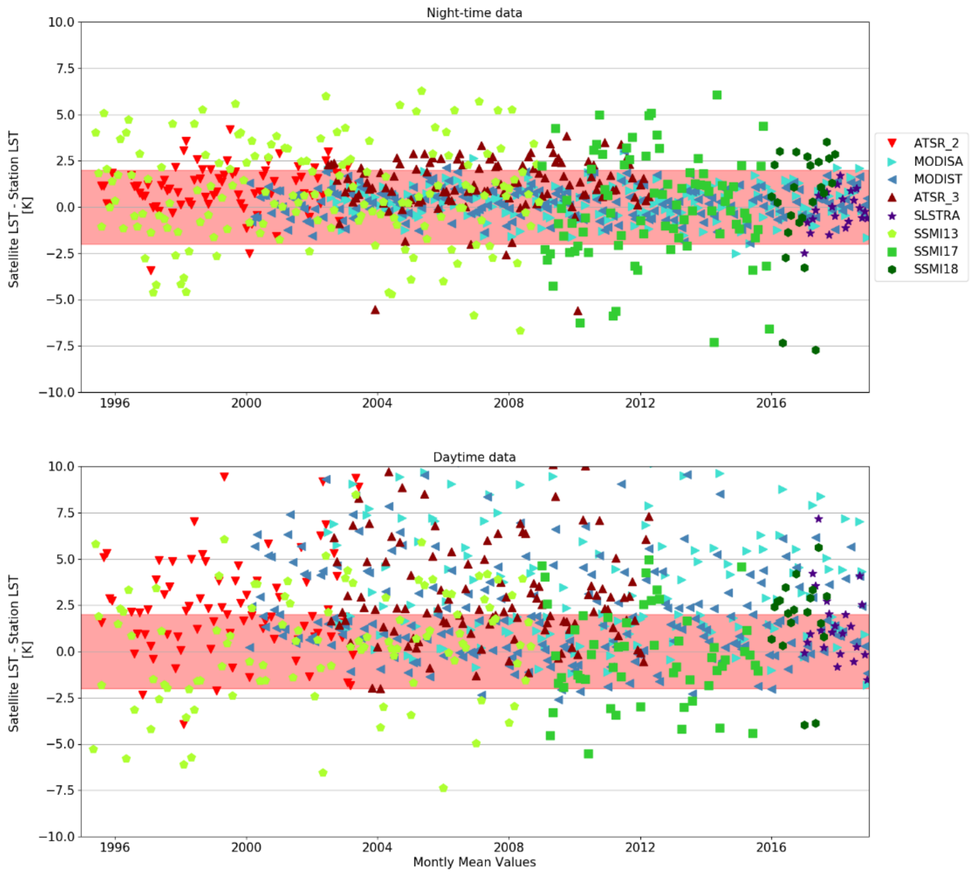

Figure 10: Monthly mean biases (satellite LST – station LST) over BND___ station. The upper plot represents night-time and the lower daytime data. The red span is the area where the bias is in a ± 2 K range.

For the IR data sets, the night-time biases are most of the time within ± 2 K, whereas the daytime values display a strong seasonal cycle. This seasonal cycle was already seen for validations over this station within the GlobTemperature project [RD-1], and it was then concluded that this is mainly due to the harvesting cycle seen in the agricultural area around the station. Thus, for the next Validation Cycle within the project, the BND___ daytime data might be removed as the biases are mainly reflecting the missing homogeneity around the station and cannot be attributed to the quality of the satellite data sets.

Results over DRA___ Station

Figure 11: Monthly mean biases (satellite LST – station LST) over DRA___ station. The upper plot represents night-time and the lower daytime data. The red span is the area where the bias is in a ± 2 K range.

The night-time biases for the IR validation of ATSR_2, ATSR_3, MODISA and MODIST lie most of the months within ± 2 K. However, the daytime biases display a strong seasonal cycle, with increased biases in the summer months. As DRA___ station is located within a valley and surrounded by mountains, these biases might be due to different observed sunlit and shadowy areas throughout the year at daytime, which was already observed and described in the GlobTemperature project validation [RD-1]. The negative SLSTRA biases for night-time and daytime data are probably due to missed cloudy data over this station, as the SLSLTRA algorithm uses for now only the basic operational cloud mask due to a lack of temporal interpolation in the accompanying meteorological fields before January 2020, which prevents the use of the probabilistic cloud mask. This will be improved in future versions of the data set in which offline processing of the temporal interpolation will be performed to allow the implementation of the probabilistic cloud mask. This cloud mask was the one which performed most optimal in the GlobTemperature Cloud Clearing Round Robin.

Results over GCM___ Station

Figure 12: Monthly mean biases (satellite LST – station LST) over GCM___ station. The upper plot represents night-time and the lower daytime data. The red span is the area where the bias is in a ± 2 K range.

At this station, the daytime IR biases tend to be lower than the night-time biases, which is unexpected, as during daytime usually the influence of the solar radiation increases the biases. However, this phenomenon was already seen during the GlobTemperature IR validation at this station, where it was concluded that it is probably caused by the observed area around the station. The area consists of a mixture of grassland and woods. This mixture might stay warmer during night than the grass observed by the in situ sensor, which experiences a stronger cooling than the tree crown temperature, which stays usually closer to air temperature [RD-1].

Results over FPK___ Station

Figure 13: Monthly mean biases (satellite LST – station LST) over FPK___ station. The upper plot represents night-time and the lower daytime data. The red span is the area where the bias is in a ± 2 K range.

The night-time IR biases are well within ± 2 K most of the time, whereas for the daytime biases a yearly cycle is seen with increased values in the summer months. FPK___ station is protected by a small fence from the grassland surrounding it, where bison herds graze [RD-1]. This fence might lead to a difference in the length or colour of the grass inside and outside the fence in the summer months, which is reflected in the increased difference in satellite and in situ LST in summer.

Results over PSU___ Station

Figure 14: Monthly mean biases (satellite LST – station LST) over PSU___ station. The upper plot represents night-time and the lower daytime data. The red span is the area where the bias is in a ± 2 K range.

As the area around the station is very heterogeneous and consists of different land covers including populated areas, only one pixel was used for validation of the IR satellite LST data sets. The night-time data is well within ± 2 K for most IR satellite data sets, only ATSR_2 has higher biases, which was already seen within the GlobTemperature validation over this station [RD-1]. The night-time biases of the MW sensors tend to be lower than that of the IR sensors. However, the heterogeneous area around the station is reflected stronger in the larger area observed by the MW sensors, which cannot be reduced, which influences the MW biases.

Results over TBL___ Station

Figure 15: Monthly mean biases (satellite LST – station LST) over TBL___ station. The upper plot represents night-time and the lower daytime data. The red span is the area where the bias is in a ± 2 K range.

This station is located on the edge of a mountain, and only one pixel representing the land cover around the station best was chosen to validate the IR LST data sets to avoid the influence of the mountain edges. The biases are in a good range during night-time, but during day especially both ATSR data sets show increased biases.

The larger negative biases for the MW LST data sets are probably caused by the larger observed area, including a mountain ridge west of the station.

4. Description and Analysis of Intercomparison Results

4.1. Overview of Results

Nine satellite – satellite data pairs were intercompared globally, and the results were analysed for different continents for the years 2008 - 2010.

Six of the satellite – satellite pairs were analysed over Africa (Afr) and Europe (Eur) only, as they were intercompared against SEVIRI data, which are not globally available. This data pairs are namely MOD11A-SEVCCI, MODISA-SEVCCI, ATSOP-SEVCCI, ATSR_3-SEVCCI, MOD11T-SEVCCI, and MODIST-SEVCCI, where SEVCCI is the LST_cci SEVIRI product, ATSOP the operational ATSR_3 product, MOD11A the operational Aqua-MODIS LST product, and MOD11T the operational Terra-MODIS LST product. Three other data pairs, were both intercompared satellite data sets are globally available were additionally intercompared over Antarctica (Ant), Asia (Asi), Australia (Aus), North America (NAm), and South America (SAm). These data pairs are ATSR_3-MOD11T, ATSR_3-MODIST, and MODIST-ATSOP.

All data is analysed divided into daytime and night-time data, and analysed seasonally. The seasons are named “DJF” (December, January, February) for NH winter, “MAM” (March, April, May) for NH spring, “JJA” (June, July, August) for NH summer, and “SON” (September, October, November) for NH autumn. The differences were investigated for different aspects:

- Time series of monthly differences
- Differences for different satellite angles
- Differences for different land cover classes
- Differences for different elevation heights
- Number of averaged data points per pixel

An overview of the seasonal differences over the different continents is given in Figure 16 for daytime and in Figure 17 for night-time data. The differences are also described in Table 6 for the results over Africa and Europe, and in Table 7 for the results over the other continents. All these data are averaged over a large time span and a large region, and many regional or temporal differences might overlie and average out each other. Thus, these results can only give a first indication about the differences between data sets but should also be considered carefully and cannot replace the more detailed analysis carried out for the single continents below.

For the daytime data, ATSR_3-MOD11T has often the highest differences, and ATSR_3-MODIST often has smaller differences close to 0 K. Over Africa and Europe, where all data pairs are analysed, it can be seen that MOD11A-SEVCCI and MOD11T-SEVCCI have more negative differences than the other data pairs. This indicates, that the MOD11A and MOD11T algorithms tends to have lower LST values than the LST_cci MODIS algorithm, where the differences are more positive. A larger spread between the analysed data pairs is seen for the continents Africa, Australia, and South America. For the night-time data, again ATSR_3-MOD11T has high differences, and ATSR_3-MOD11T lower differences. There are larger differences for MODIST-ATSOP in the season “MAM”, however, during this season there are only few matches for this data pair (and none in “JJA”), thus, these results may be due to a low number of averaged matches.

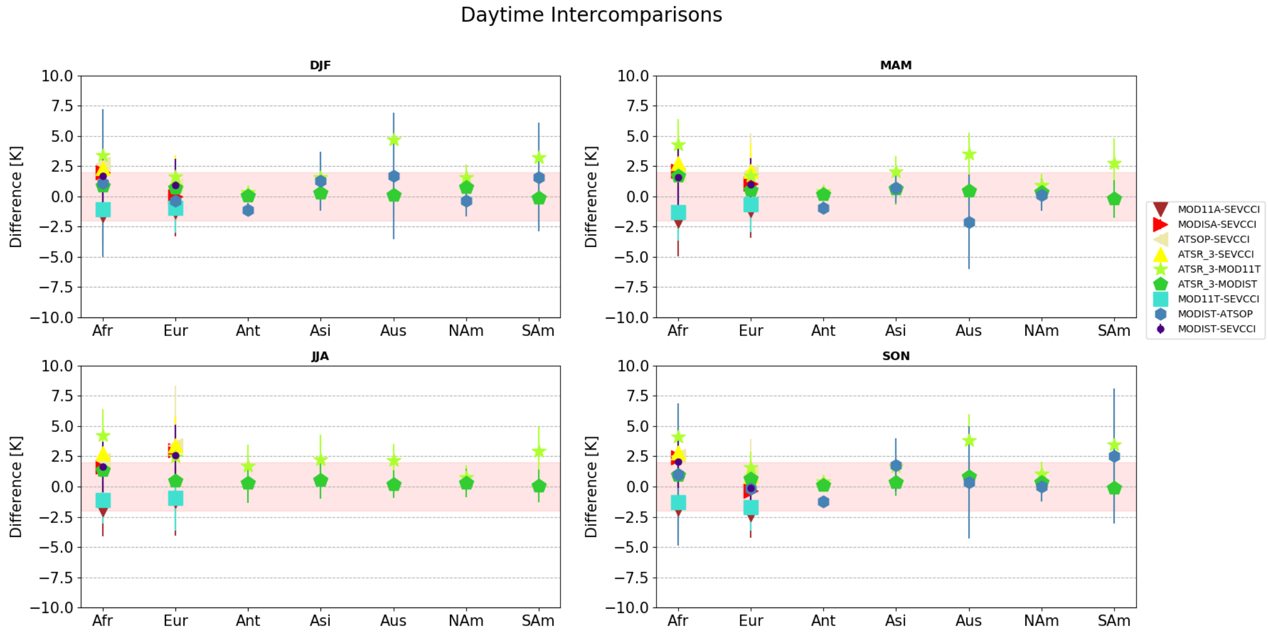

Figure 16: Overview of the daytime differences over the four seasons for all nine intercompared satellite-satellite pairs. The red span marks the difference range of ± 2 K.

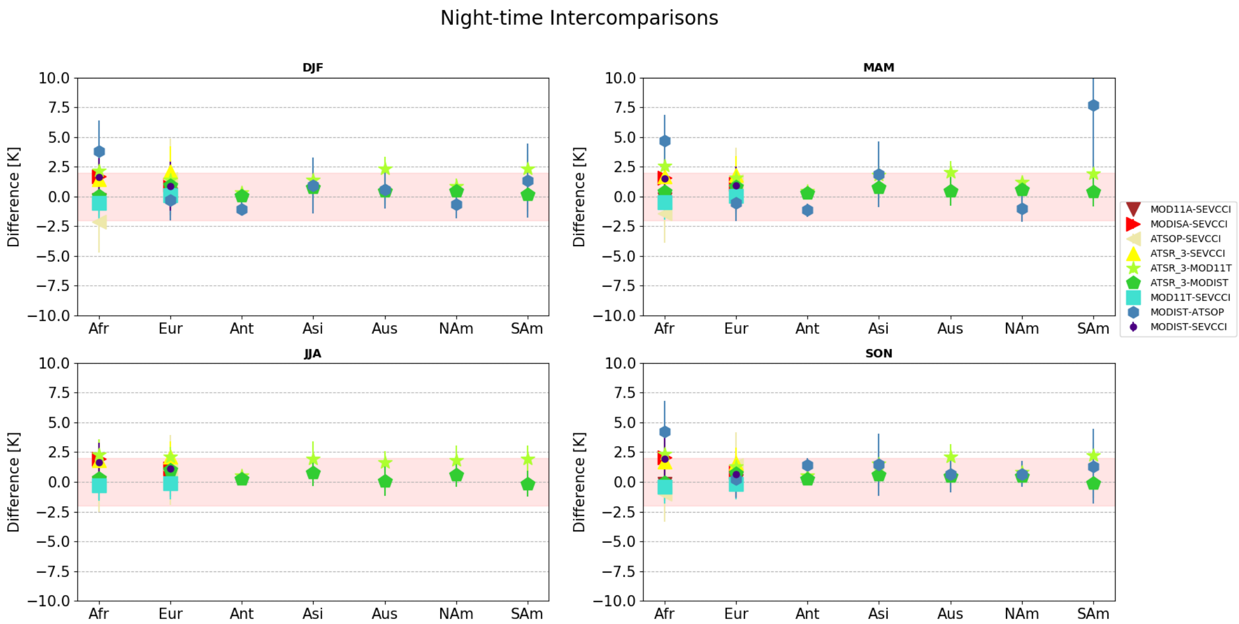

Figure 17: Overview of the night-time differences over the four seasons for all nine intercompared satellite-satellite pairs. The red span marks the difference range of ± 2 K.

Table 6: Overview of seasonal results of the median differences of the analysed satellite-satellite pairs over the continents Africa and Europe, where data from all satellite - satellite pairs are available. Results are presented in terms of difference (diff) and RSTD

Region	Product 1	Product 2		DJF Day	DJF Night	MAM Day	MAM Night	JJA Day	JJA Night	SON Day	SON Night
Africa	MOD11A	SEVCCI	diff	-1.56	-0.31	-2.00	-0.26	-1.87	-0.14	-1.82	-0.16
			RSTD	2.42	1.41	2.95	1.45	2.27	1.33	2.51	1.41
	MODISA	SEVCCI	diff	1.97	1.71	2.09	1.59	1.62	1.91	2.38	2.07
			RSTD	2.09	1.50	2.45	1.56	2.59	1.70	2.42	1.75
	ATSOP_	SEVCCI	diff	2.69	-2.12	1.83	-1.40	2.15	-0.28	2.54	-0.99
			RSTD	3.68	2.59	3.32	2.48	3.29	2.24	3.85	2.34
	ATSR_3	SEVCCI	diff	2.35	1.45	2.77	1.71	2.79	1.85	2.85	1.69
			RSTD	1.42	1.04	1.63	1.16	1.87	1.20	1.53	1.08
	ATSR_3	MOD11T	diff	3.41	2.16	4.28	2.57	4.24	2.28	4.11	2.34
			RSTD	1.96	1.26	2.13	1.35	2.15	1.29	2.00	1.13
	ATSR_3	MODIST	diff	0.88	0.03	1.71	0.40	1.34	0.32	0.94	-0.06
			RSTD	1.84	1.25	2.24	1.17	1.81	0.99	1.76	1.25
	MOD11T	SEVCCI	diff	-1.09	-0.52	-1.28	-0.49	-1.13	-0.31	-1.27	-0.44
			RSTD	2.13	1.44	2.37	1.44	1.94	1.29	2.12	1.38
	MODIST	ATSOP_	diff	1.09	3.82	-	4.66	-	-	0.99	4.25
			RSTD	6.12	2.55	-	2.22	-	-	5.90	2.58
	MODIST	SEVCCI	diff	1.69	1.65	1.57	1.53	1.63	1.67	2.03	1.92
			RSTD	2.18	1.56	2.33	1.51	2.09	1.60	2.15	1.78
Europe	MOD11A	SEVCCI	diff	-1.23	0.15	-1.12	0.19	-1.18	0.13	-2.32	0.04
			RSTD	2.08	1.72	2.30	1.44	2.85	1.39	1.91	1.26
	MODISA	SEVCCI	diff	0.00	1.00	1.02	1.03	2.97	1.12	-0.35	0.81
			RSTD	2.09	2.02	2.34	1.54	2.88	1.39	2.02	1.50
	ATSOP_	SEVCCI	diff	0.86	1.47	2.02	1.25	3.43	0.98	0.99	1.41
			RSTD	2.52	3.40	3.17	2.83	4.89	2.95	2.94	2.74
	ATSR_3	SEVCCI	diff	1.25	2.12	2.10	1.82	3.41	2.09	0.90	1.60
			RSTD	2.16	2.08	2.30	1.60	2.40	1.29	1.90	1.29
	ATSR_3	MOD11T	diff	1.65	1.39	1.70	1.57	2.46	2.10	1.59	1.31
			RSTD	1.10	0.98	1.30	0.90	1.90	0.86	1.29	0.83
	ATSR_3	MODIST	diff	0.69	0.90	0.54	0.81	0.44	0.97	0.65	0.72
			RSTD	0.82	0.90	0.99	0.83	1.26	0.87	0.87	0.83
	MOD11T	SEVCCI	diff	-0.97	0.10	-0.68	0.03	-0.92	-0.14	-1.72	-0.16
			RSTD	2.05	1.72	2.27	1.44	2.71	1.36	1.91	1.29
	MODIST	ATSOP_	diff	-0.38	-0.31	-	-0.57	-	-	-0.16	0.26
			RSTD	1.38	1.69	-	1.50	-	-	1.33	1.59
	MODIST	SEVCCI	diff	0.90	0.89	0.96	0.93	2.57	1.12	-0.13	0.63
			RSTD	2.18	2.06	2.22	1.59	2.52	1.47	1.91	1.48

Seasonal Median (K)

Table 7: Overview of seasonal results of the median differences of the analysed satellite-satellite pairs over the continents where only LEO – LEO matches are available

Region	Product 1	Product 2		Seasonal Median (K)							
				DJF		MAM		JJA		SON	
				Day	Night	Day	Night	Day	Night	Day	Night
Antarctica	ATSR_3	MOD11T	diff	0.34	0.31	0.38	0.48	1.68	0.53	0.43	0.50
			RSTD	0.19	0.30	0.36	0.36	1.76	0.39	0.30	0.34
	ATSR_3	MODIST	diff	0.04	0.04	0.17	0.28	0.31	0.24	0.14	0.22
			RSTD	0.39	0.43	0.44	0.43	1.69	0.43	0.44	0.42
	MODIST	ATSOP_	diff	-1.12	-1.06	-0.95	-1.15	-	-	-1.25	1.40
			RSTD	0.56	0.55	0.52	0.55	-	-	0.50	0.59
Asia	ATSR_3	MOD11T	diff	1.57	1.37	2.04	1.83	2.26	1.96	1.67	1.52
			RSTD	1.26	1.01	1.28	1.29	2.02	1.47	1.60	1.14
	ATSR_3	MODIST	diff	0.30	0.72	0.63	0.75	0.53	0.75	0.34	0.56
			RSTD	1.16	0.86	1.29	0.96	1.53	1.10	1.11	0.93
	MODIST	ATSOP_	diff	1.25	0.93	0.69	1.87	-	-	1.78	1.44
			RSTD	2.46	2.36	1.20	2.77	-	-	2.22	2.64
Australia	ATSR_3	MOD11T	diff	4.70	2.33	3.49	2.02	2.19	1.63	3.82	2.13
			RSTD	2.13	0.99	1.78	0.98	1.32	0.96	2.15	1.05
	ATSR_3	MODIST	diff	0.13	0.47	0.44	0.43	0.20	0.05	0.82	0.48
			RSTD	1.85	1.13	1.22	1.19	1.14	1.22	1.38	1.13
	MODIST	ATSOP_	diff	1.69	0.56	-2.13	-	-	-	0.35	0.65
			RSTD	5.23	1.57	3.91	-	-	-	4.63	1.56
NAmerica	ATSR_3	MOD11T	diff	1.58	0.87	0.91	1.22	0.75	1.81	1.03	0.81
			RSTD	1.07	0.67	0.98	0.09	1.02	1.22	1.05	0.65

	ATSR_3	MODIST	diff	0.72	0.47	0.35	0.59	0.28	0.56	0.35	0.44
			RSTD	0.90	0.70	0.96	0.87	1.17	0.99	0.83	0.67
	MODIST	ATSOP_	diff	-0.35	-0.65	0.12	-1.03	-	-	0.01	0.67
			RSTD	1.31	1.17	1.33	1.11	-	-	1.25	1.11
SAmerica	ATSR_3	MOD11T	diff	3.22	2.35	2.75	1.94	2.96	1.94	3.47	2.22
			RSTD	2.31	1.19	2.03	1.22	1.97	1.10	2.59	1.08
	ATSR_3	MODIST	diff	-0.16	0.16	-0.22	0.37	0.05	-0.15	-0.12	-0.13
			RSTD	2.21	1.42	1.56	1.19	1.36	1.08	1.94	1.25
	MODIST	ATSOP_	diff	1.59	1.34	-	7.69	-	-	2.52	1.31
			RSTD	4.49	3.14	-	5.98	-	-	5.60	3.16

4.2. Results for different Continents

The results of the intercomparison analysis are displayed in the following for each continent separately. For clarity, not all analysed figures are presented in this section, however, they can all be found in the Appendix (Section 7).

4.2.1. Results over Africa

The monthly differences over the investigated time span is shown in Figure 18 for all investigated satellite – satellite pairs, as well as the number of monthly averaged data points. The highest number of data points is found for the MODIS data sets against SEVCCI data. A significant jump to more data points can be seen in mid-2008. MOD11A-SEVCCI and MOD11T-SEVCCI daytime differences are more negative than MODISA-SEVCCI and MODIST-SEVCCI differences, as already mentioned in Section 4.1. ATSR_3-SEVCCI is more comparable than ATSR_3-MODIST and ATSR_3-MOD11T. ATSR_3-MOD11T is more comparable than ATSR_3-MODIST, which also shows that MOD11T has lower LST values than the MODIST algorithm. ATSOP-SEVCCI shows a stronger seasonal cycle both for daytime and night-time data than the other satellite-satellite data pairs.

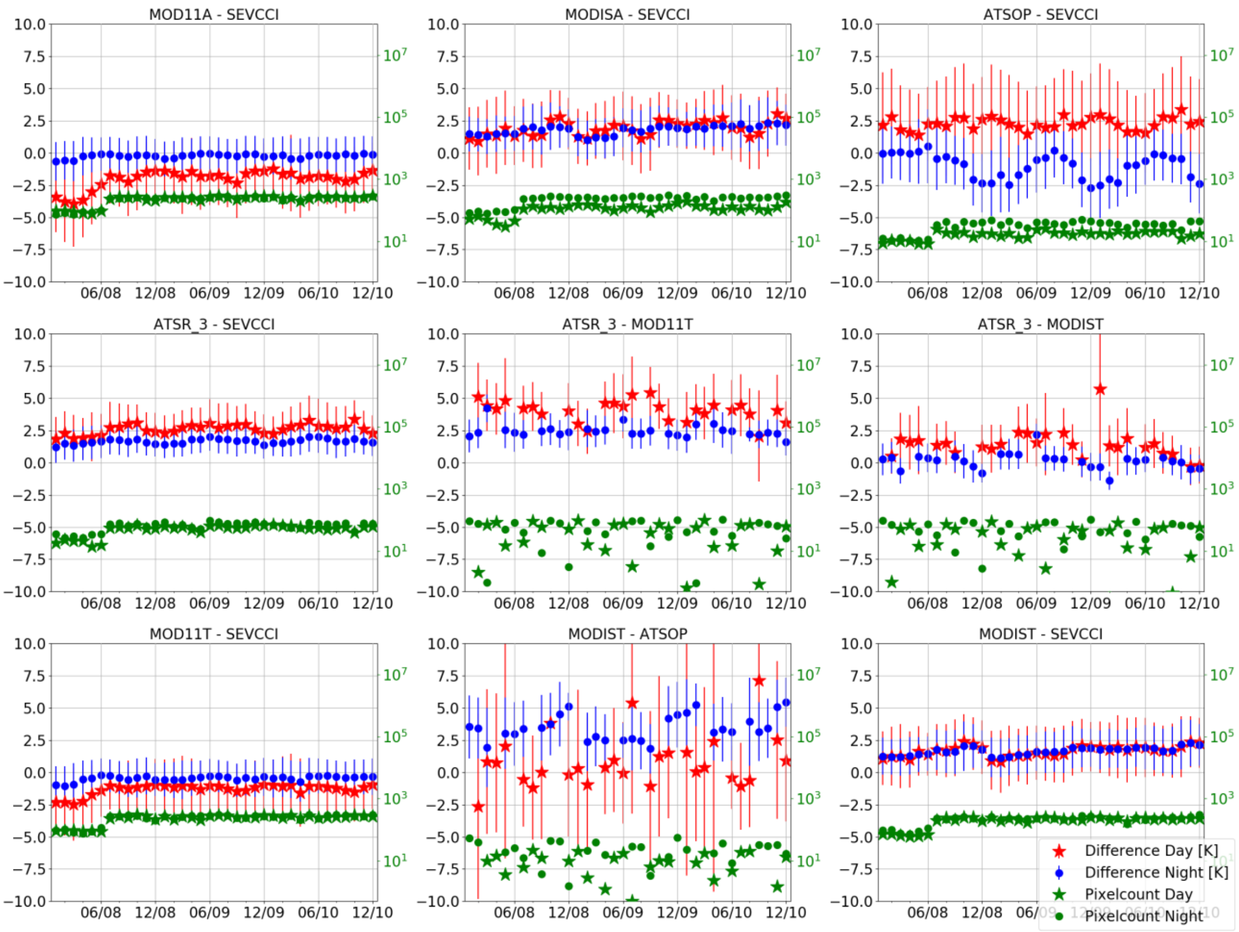

Figure 18: Monthly time series for all investigated satellite – satellite data sets over Africa. Red stars represent the daytime data, blue dots the night-time data, the green stars and dots on the right axis display the averaged pixel numbers for daytime and night-time, respectively.

When comparing the results of the different intercomparison pairs over such large areas as continents, it has to be considered that the number and distribution of the averaged pixels might vary between different pairs. And thus, the analysis of different regions and land covers might influence the results. Therefore, the distribution of the averaged pixels was also investigated. The results show that for all satellite- satellite pairs, fewer data points were found in the centre of Africa. For the comparison of ATSR_3-SEVCCI, the available data points were distributed in "stripes" over the continent (see Figure 19 for the seasonal number of averaged night-time data points for ATSR_3-SEVCCI). The intercomparison of MODIST-ATSOP had in general only few data points, none in "MAM" and "JJA" for daytime data, and none in "JJA" for night-time data. This low number of averaged data points can influence the statistics of the results, and outliers can have a stronger influence on the differences.

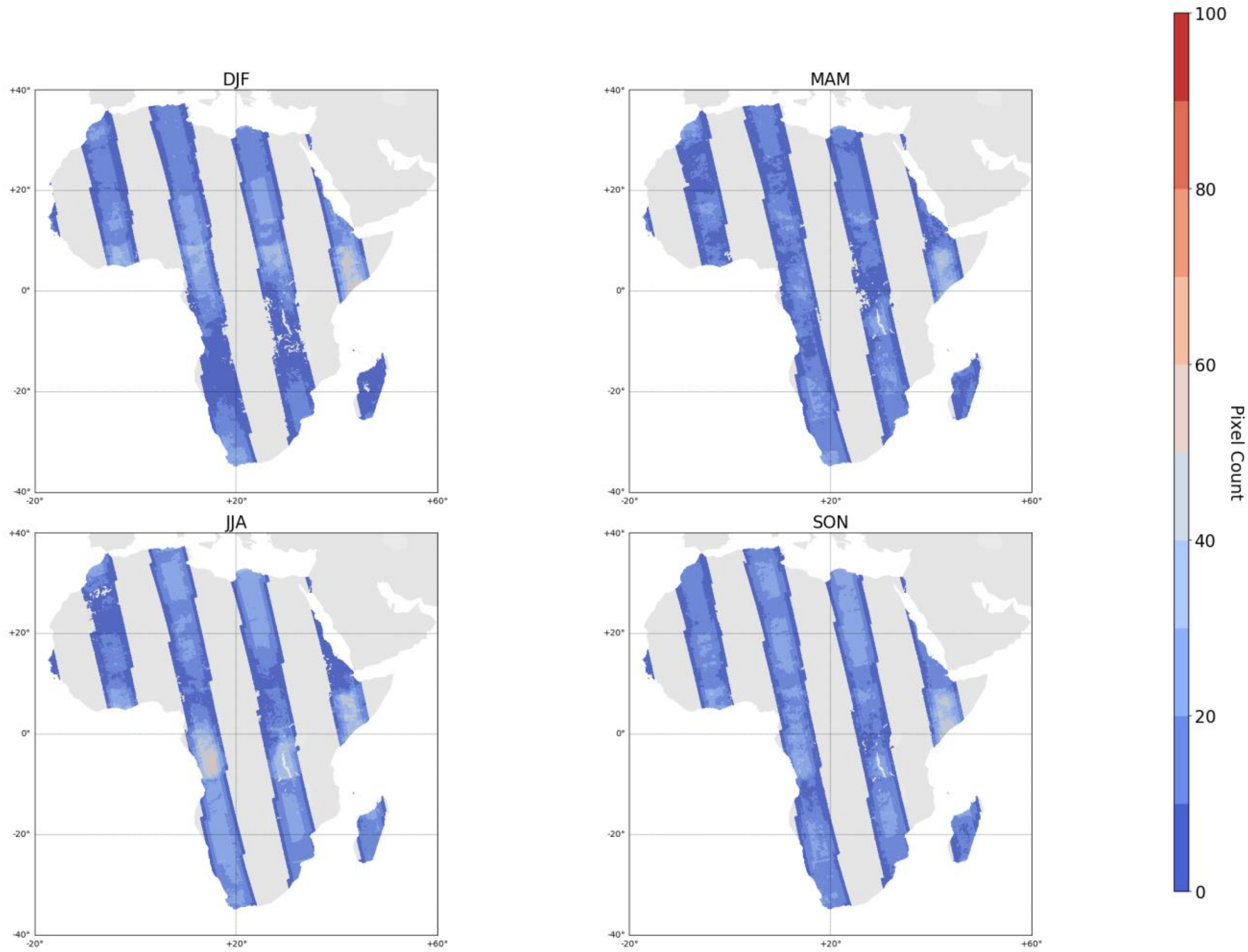

Figure 19: Number of seasonal night-time averaged data points per pixel for ATSR_3-SEVCCI differences over Africa

The analysis of the differences for different elevation classes showed that most pixels have an elevation between 200 – 500 m. No significant differences between the different elevation classes were found.

The analysis of the land cover classes displayed that most pixels have a land cover of vegetation/cropland (class 4 of the ALB2 land cover classification), grassland (class 14 of the ALB2 land cover classification), or bare soil Entisols (class 21 of the ALB2 land cover classification). No significant differences between them could be seen.

The influence of the satellite angles on the results was investigated by calculating the differences for different ranges of the satellite zenith angle (satze) multiplied by the sign of the satellite azimuth angle (sataz). These results gave no large differences for all continents for ATSR_3 and ATSOP satellite angles, as the satze for these data sets ranges from -20° to +20° only (Figure 20 for ATSR_3-SEVCCI differences). The intercomparisons of MODIS data sets against SEVCCI showed an increase in the number of pixel counts for MODIS values of satze*sign(sataz) between -65° to – 55 ° and from 55° to 65° (Figure 21 for MODIST-SEVCCI differences). The daytime differences increase substantially for larger MODIS satze values, due to an increased influence of differences in seen sunlit and shadowy areas. This increase has an asymmetric shape. It is stronger for MODIST and MOD11T for negative sataz values, and stronger for positive sataz values for MODISA and MOD11A. This is caused by the local overflight time of the satellites. When the sataz is negative, it means that the satellite is viewing the scene from west to east, and the other way round when the sataz is positive. As the local overpass time is in the morning for Terra-MODIS, the sun is shining from the east then and casting more shadows to the west. It is the other way round for Aqua-MODIS, which has a local overpass time in the afternoon.

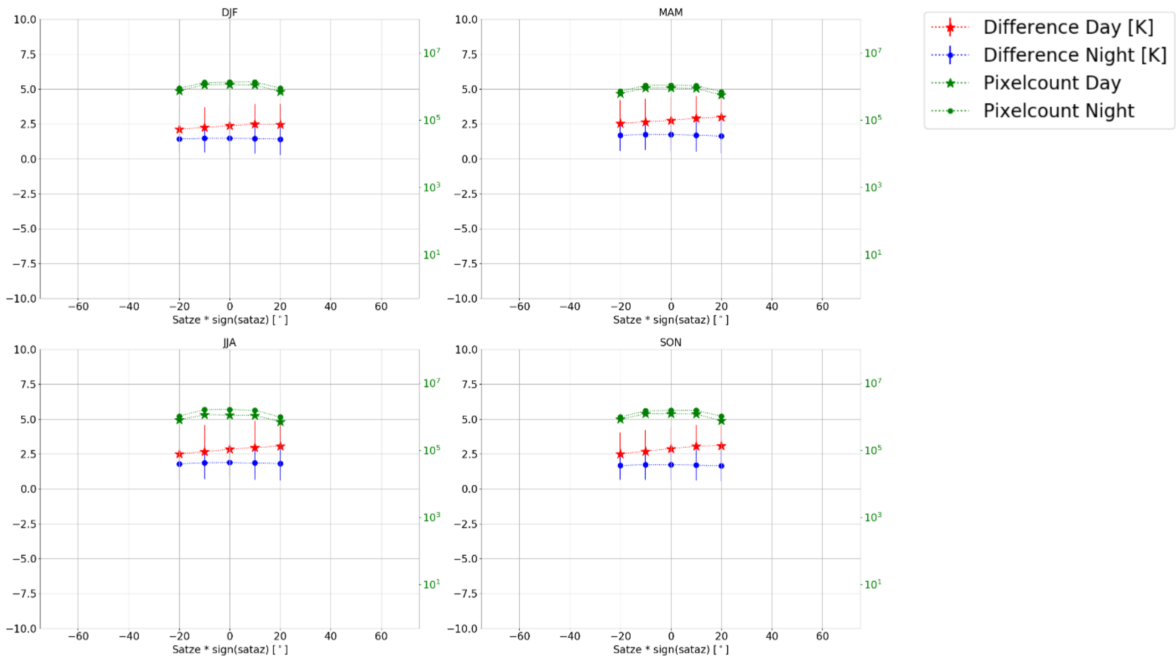

Figure 20: Seasonal differences between ATSR3-SEVCCI LST data for different satze*sign(sataz) values of ATSR_3; red stars represent the daytime data, blue dots the night-time data, and the green stars and dots on the right axis display the averaged pixel numbers for daytime and night-time data, respectively

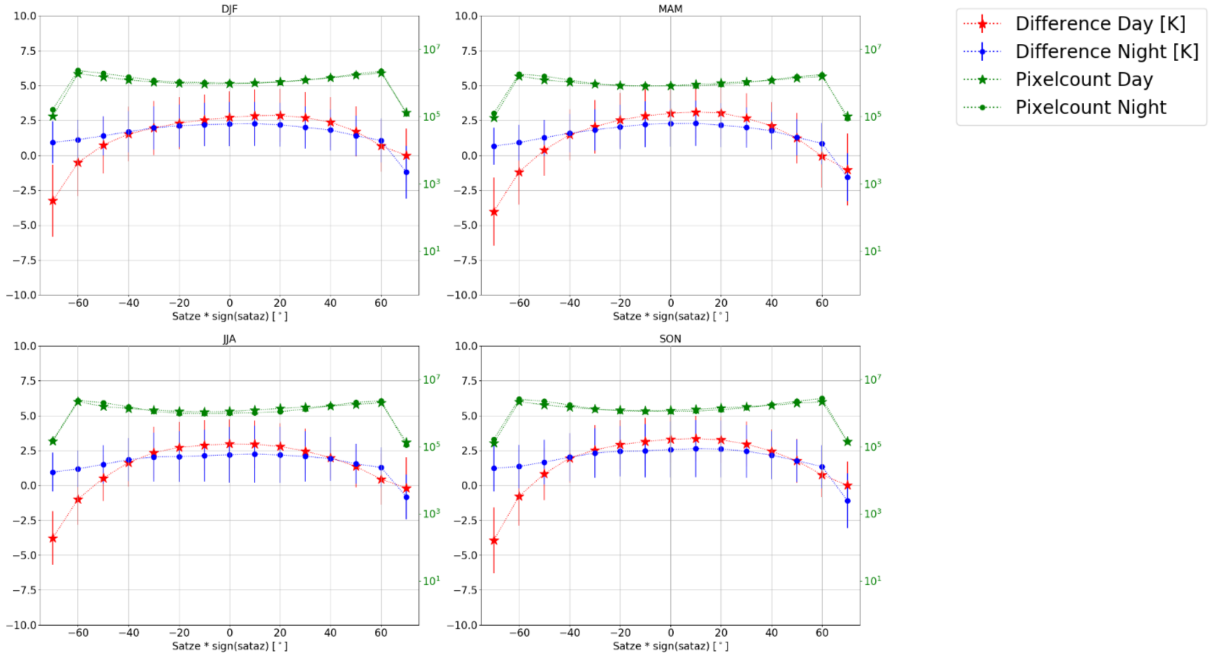

Figure 21: Seasonal differences between MODIST and SEVCCI LST data for different satze*sign(sataz) of MODIST; red stars represent the daytime data, blue dots the night-time data, and the green stars and dots on the right axis display the averaged pixel numbers for daytime and night-time data, respectively

4.2.2. Results over Antarctica

The time series of the three analysed satellite – satellite data sets (Figure 22) reveals that the differences are small over Antarctica, and mainly below 2 K for all three intercomparisons. ATSR_3-MOD11T and ATSR_3-MODIST have positive differences, whereas MODIST-ATSOP has more negative differences. The number of analysed pixels shows a seasonal cycle for daytime and night-time data due to the polar summer and winter.

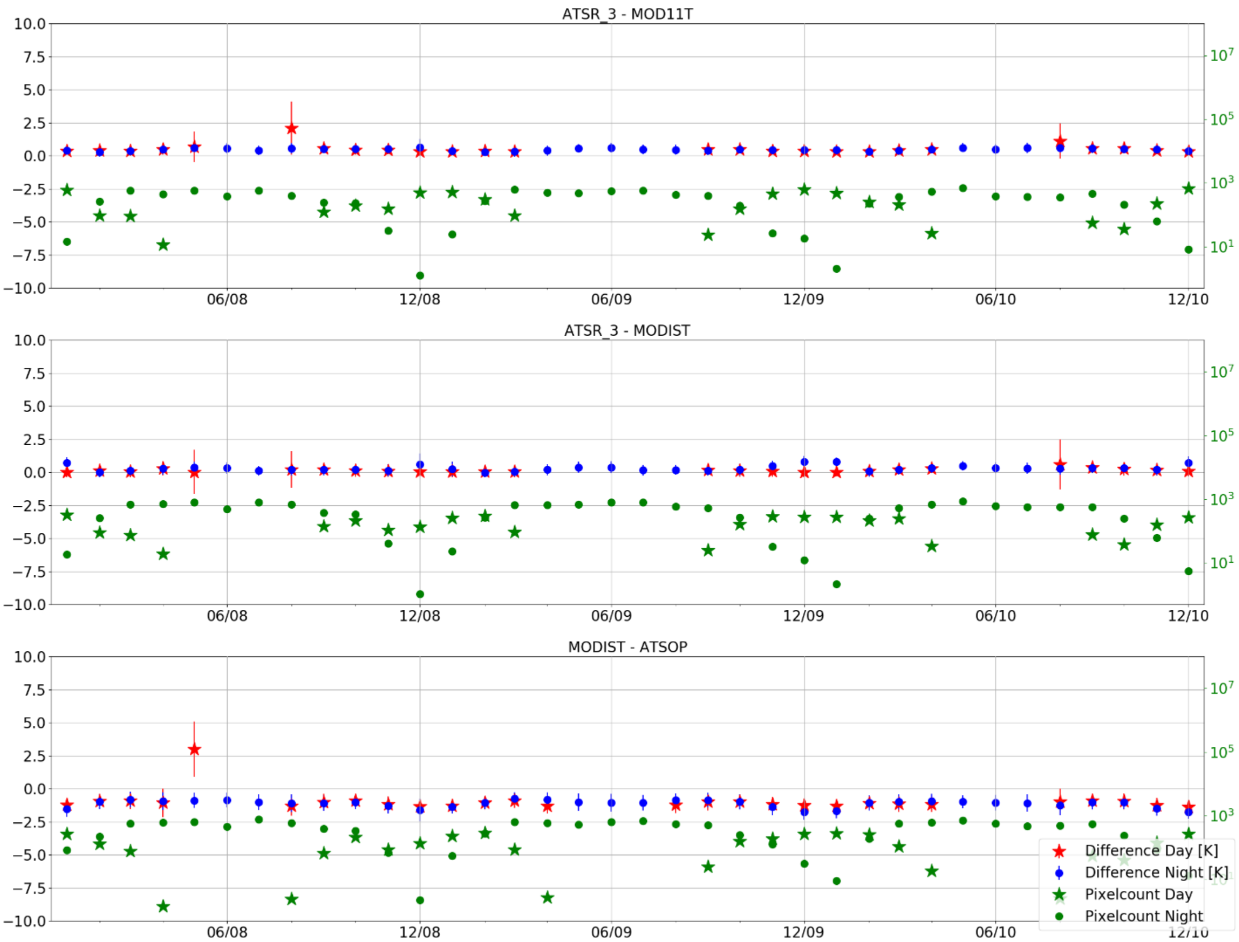

Figure 22: Monthly time series for all investigated satellite – satellite data sets over Antarctica. Red stars represent the daytime data, blue dots the night-time data, the green stars and dots on the right axis display the averaged pixel numbers for daytime and night-time, respectively.

The analysis of the distribution of averaged data points showed that most analysed pixels are in the South of Antarctica. The distribution between daytime and night-time data shifts, as mentioned above, due to the polar seasons. The number of averaged pixels for ATSR_3-MODIST daytime data is displayed in Figure 23.

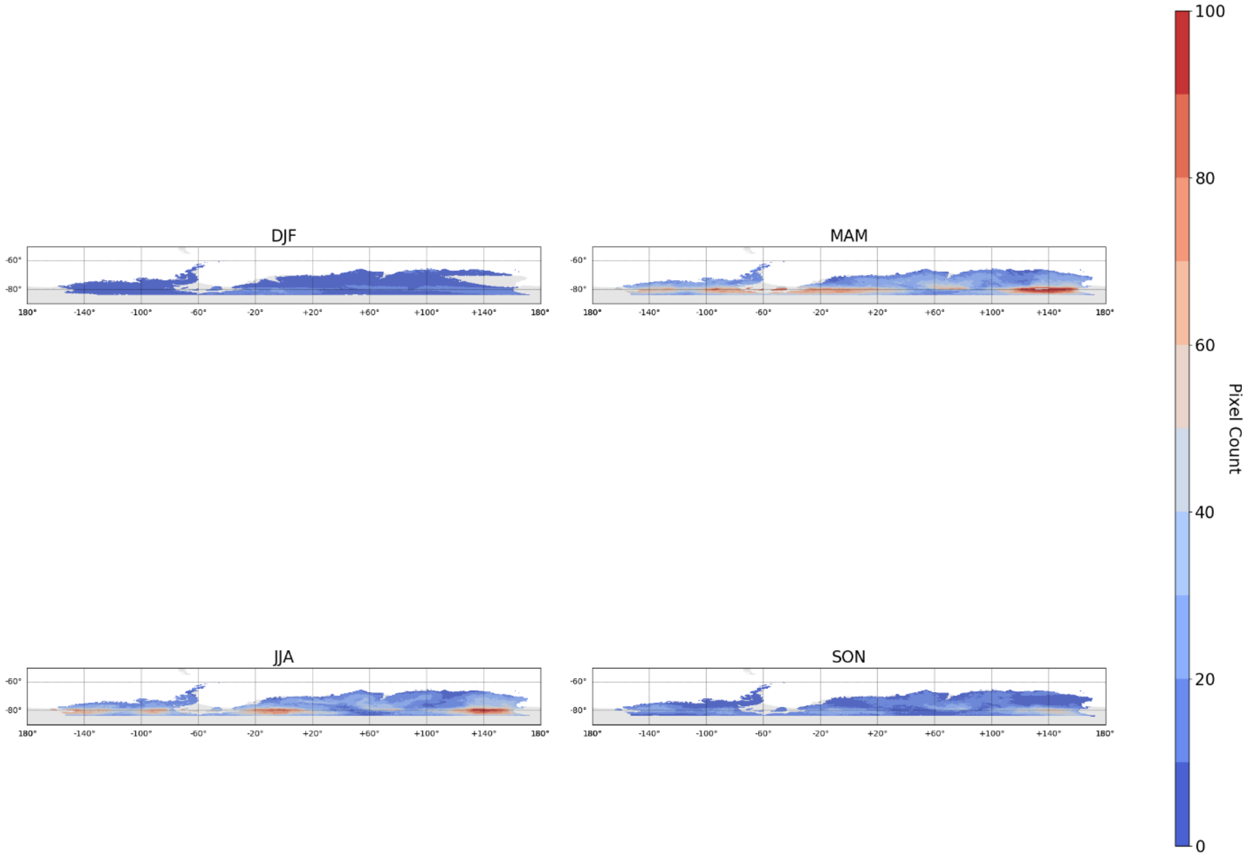

Figure 23: Number of seasonal night-time averaged data points per pixel for ATSR_3-MOD11T differences over Antarctica

The analysis of the different elevation classes revealed that most pixels are located in a height above 2000 m, but no significant differences are found between different classes.

As all pixels over Antarctica are classified in the land cover class "Permanent Snow and Ice" (class 27 of the ALB2 land cover classification), the analysis over different land cover classes did give no additional insights to the validation.

The influence of the satellite angles showed no significant differences for ATSR_3 and ATSOP satellite angles, for MODIST it was found that most data points have a satellite zenith angle between 25° to 35°. The differences for different satellite angles is not significant, the differences only increase for MODIST satellite angles > 45° (Figure 24).

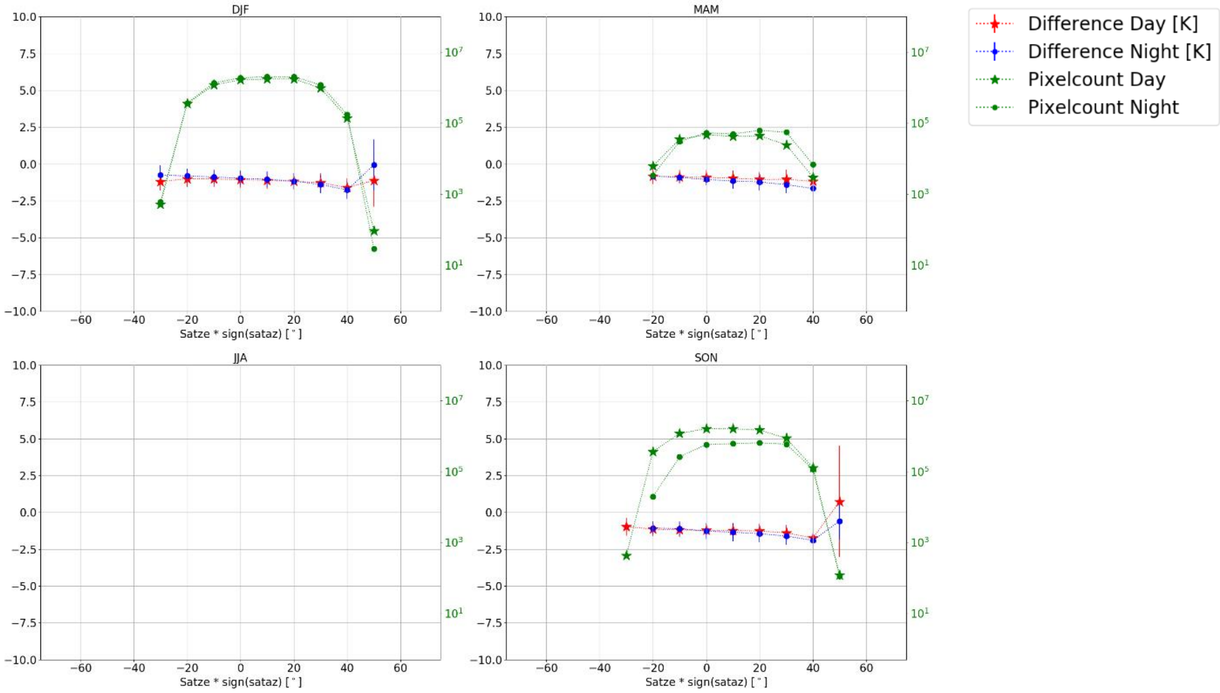

Figure 24: Seasonal LST differences between MODIST and ATSOP LST data for different satze*sign(sataz) of MODIST; red stars represent the daytime data, blue dots the night-time data, and the green stars and dots on the right axis display the averaged pixel numbers for daytime and night-time data, respectively

4.2.3. Results over Asia

The time series of the three analysed satellite – satellite data sets over Asia can be seen in Figure 25. A yearly cycle is found in all data sets, which is less pronounced for the ATSR_3-MODIST data set. The found differences between daytime and night-time differences are small.

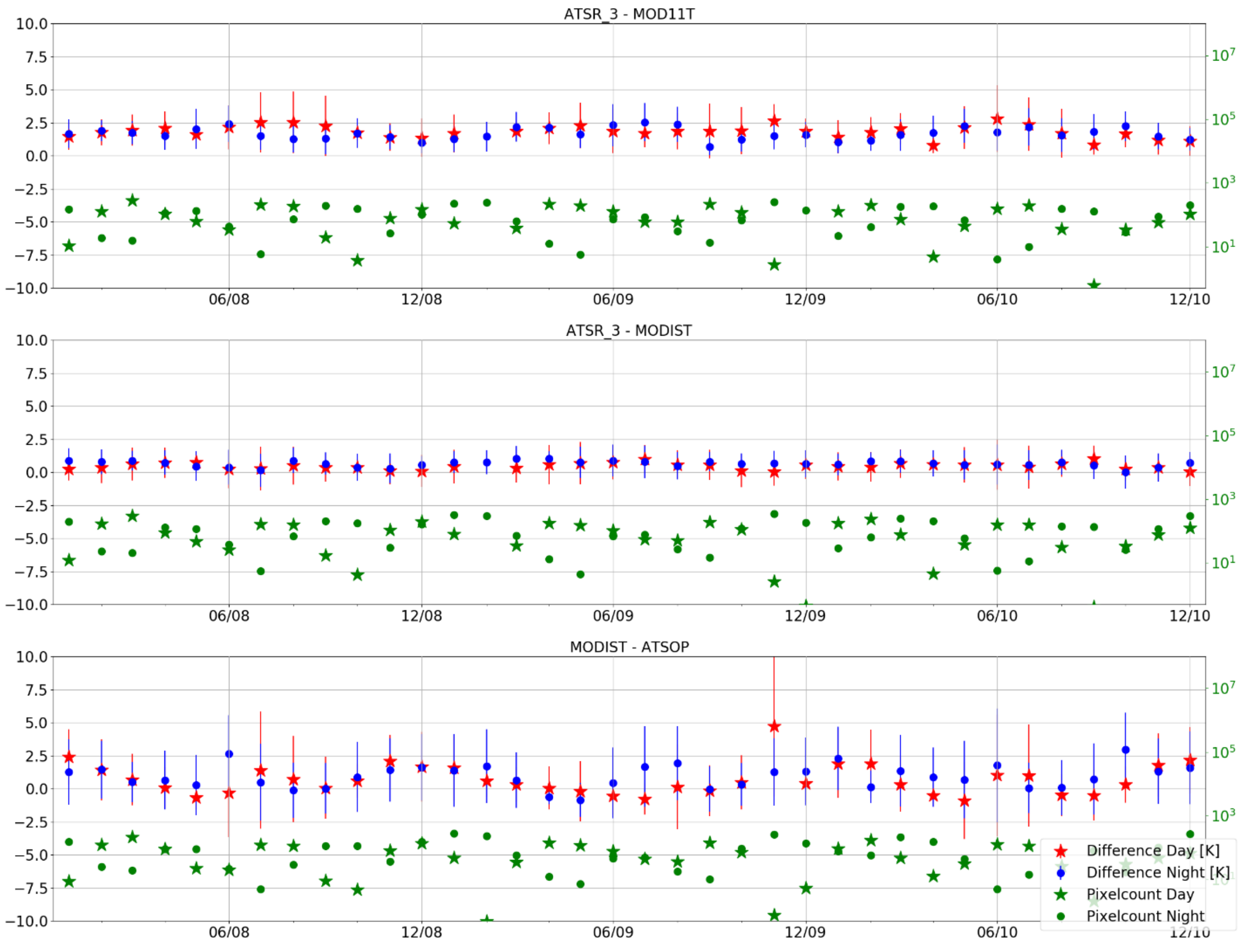

Figure 25: Monthly time series for all investigated satellite – satellite data sets over Asia. Red stars represent the daytime data, blue dots the night-time data, the green stars and dots on the right axis display the averaged pixel numbers for daytime and night-time, respectively.

The distribution of the pixel counts shows that the whole continent is covered for all three data sets, with more data points further in the north (see Figure 26 for ATSR_3-MOD11T daytime pixel counts). For MODIST-ATSOP there is nearly no data in spring (“MAM”) and no data in summer (“JJA”) for daytime and night-time results, as already seen over the other continents.

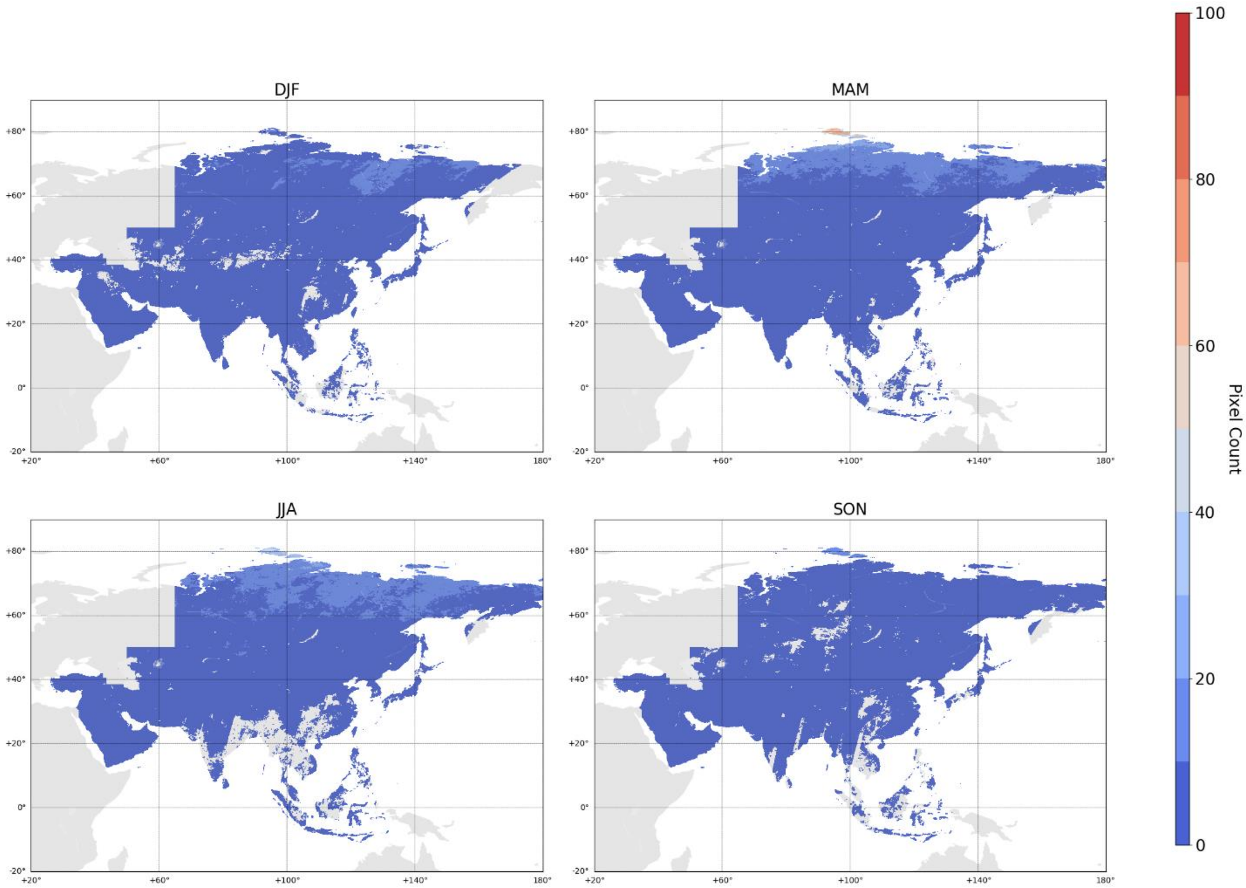

Figure 26: Number of seasonal daytime averaged data points per pixel for ATSR_3-MOD11T data over Asia

The analysis of the different elevation classes showed that most pixels have an elevation between 50 m – 200 m or between 200 m – 500 m. No significant differences between the single classes was found.

The main land cover classes found for the intercomparisons over Asia are “Open needleleaved deciduous or evergreen forest” (class 9 of the ALB2 land cover classification) and “sparse vegetation” (class 15 of the ALB2 land cover classification). All analysed data pairs showed more positive and higher differences for class 15 than for class 9, although not always to a significant degree (Figure 27 for MODIST-ATSR_3 daytime differences). Sparse vegetation is mainly found in the North of Asia, whereas class 9 is found in the centre of the continent.

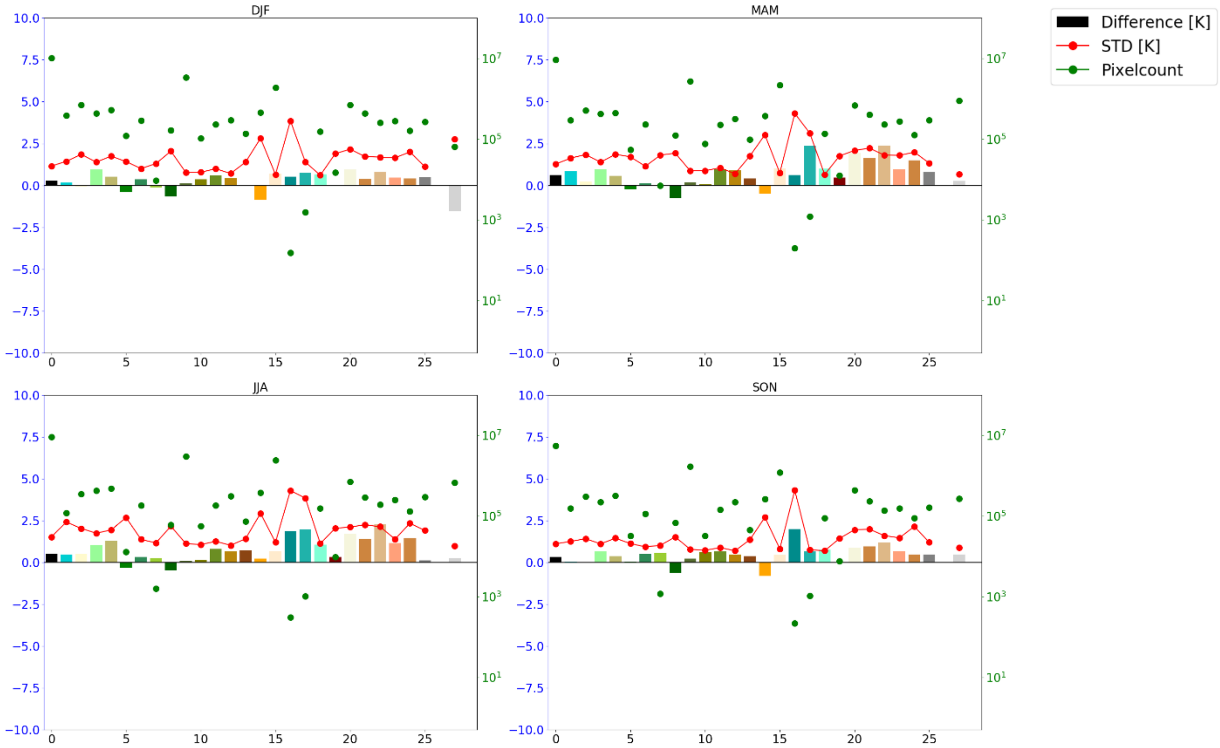

Figure 27: Seasonal daytime differences for different land cover classes for ATSR3-MODIST over Asia; the bars are the median differences, red points the RSTD and the green points on the right axis show the number of averaged data points

The analysis of the differences with respect to different satellite angles showed again no significant differences for the ATSR intercomparisons, but for MODIST-ATSOP the value of MODIST satze*sign(sataz) increased significantly for large satze values (>65°) (see Figure 28).

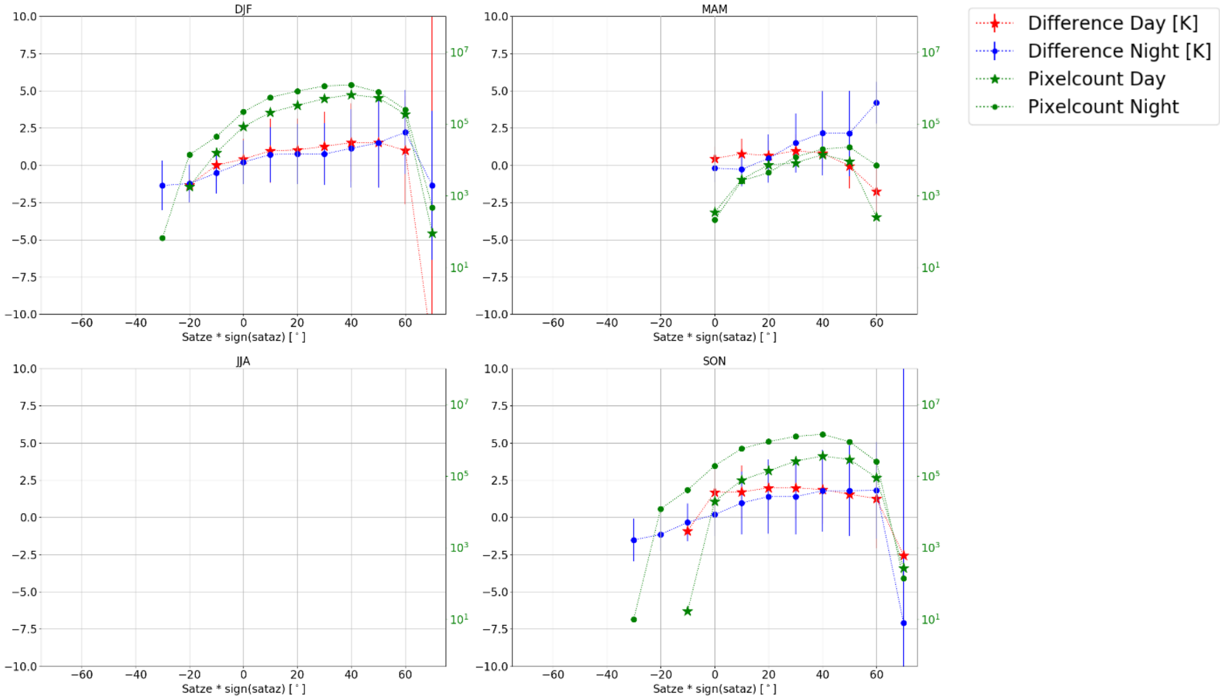

Figure 28: Seasonal LST differences between MODIST and ATSOP LST data for different satze*sign(sataz) of MODIST; red stars represent the daytime data, blue dots the night-time data, and the green stars and dots on the right axis display the averaged pixel numbers for daytime and night-time data, respectively

4.2.4. Results over Australia

The results of the time series analysis of the differences over Australia are shown in Figure 29. It can be seen that the differences are mainly positive for all three intercompared data pairs, with higher daytime differences in SH summer months, when the influence of the solar radiation increases the difference in temperature between sunlit and shadowy areas. ATSR_3-MOD11T has in general higher differences than ATSR_3-MODIST, and also higher robust standard deviations, as already seen before.

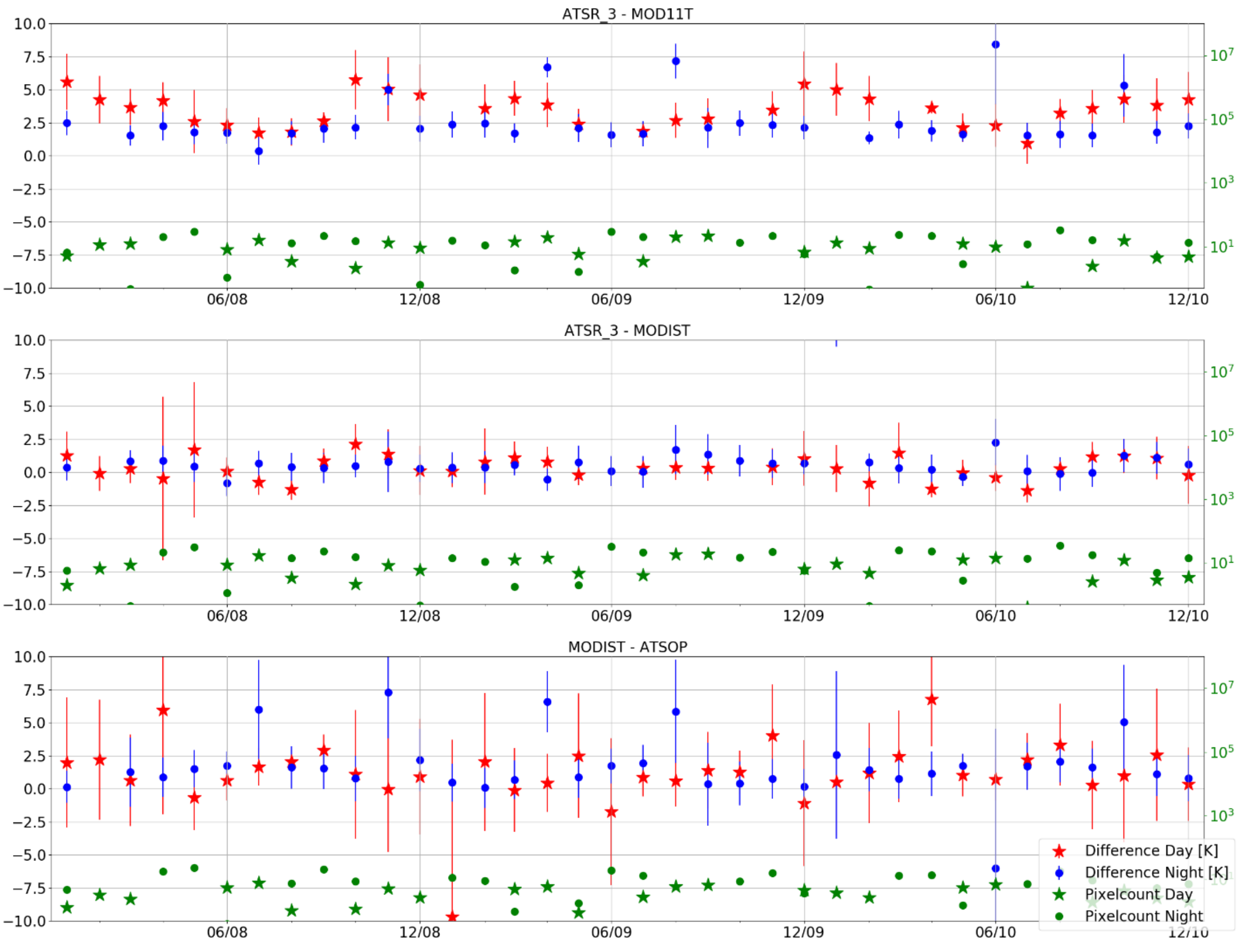

Figure 29: Monthly time series for all investigated satellite – satellite data sets over Australia. Red stars represent the daytime data, blue dots the night-time data, the green stars and dots on the right axis display the averaged pixel numbers for daytime and night-time, respectively.

The number of averaged data points per pixel is < 10 per pixel for all satellite – satellite intercomparisons. More data points are seen during night, where also the whole continent is covered by the intercomparisons for ATSR_3-MODIST and ATSR_3-MOD11T. In contrast, the centre of Australia is not covered for these data pairs during day (Figure 30 for ATSR_3-MOD11T intercomparisons). MODIST-ATSOP has no data coverage for SH autumn ("MAM") and SH winter ("JJA") for night-time, and only few data points for SH autumn during day, similar as found over the other continents.

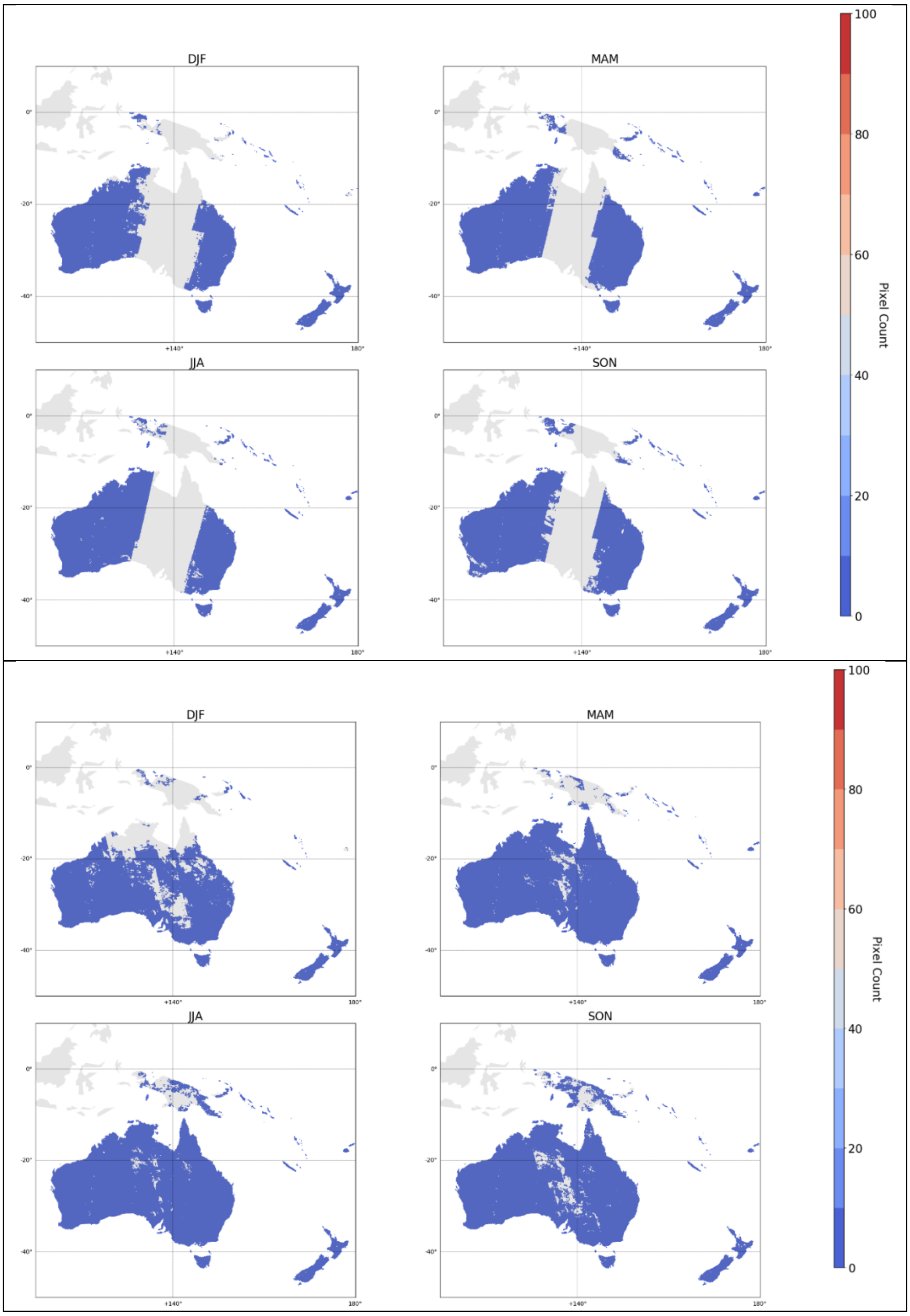

Figure 30: Seasonal distribution of the number of daytime (upper) and night-time (lower) averaged data points per pixel for ATSR_3-MOD11T data over Australia

The analysis of the differences for different elevation classes showed that most analysed pixels have an elevation between 200 m – 500 m, for ATSR3-MOD11T the highest absolute differences for this elevation class were found in Australian summer (Figure 32), in accordance with what the time series analysis showed.

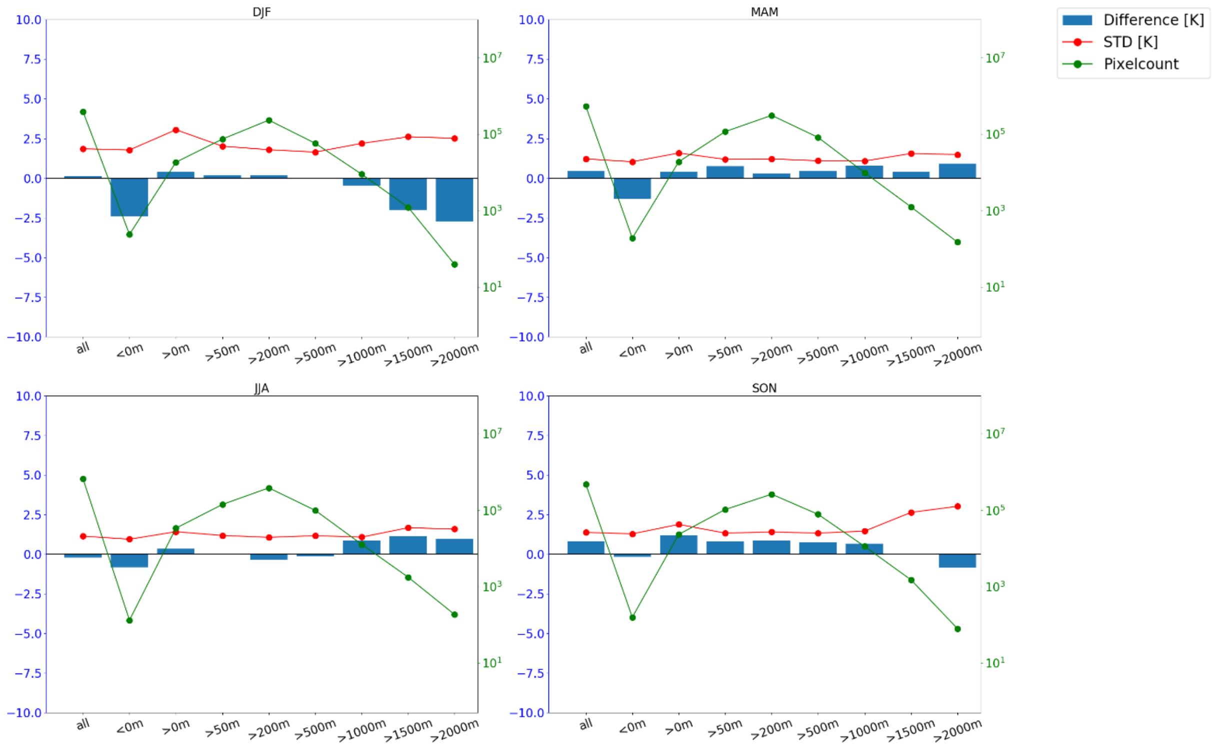

Figure 31: Seasonal daytime differences for different elevation classes for ATSR3-MODIST over Australia; blue bars are the median differences, red points the RSTD and the green points on the right axis show the number of averaged data points

The main land cover class found over Australia is "sparse vegetation" (class 15 of the ALB2 land cover classification), which covers the centre of Australia (Figure 32 for daytime results of ATSR_3-MOD11T differences).

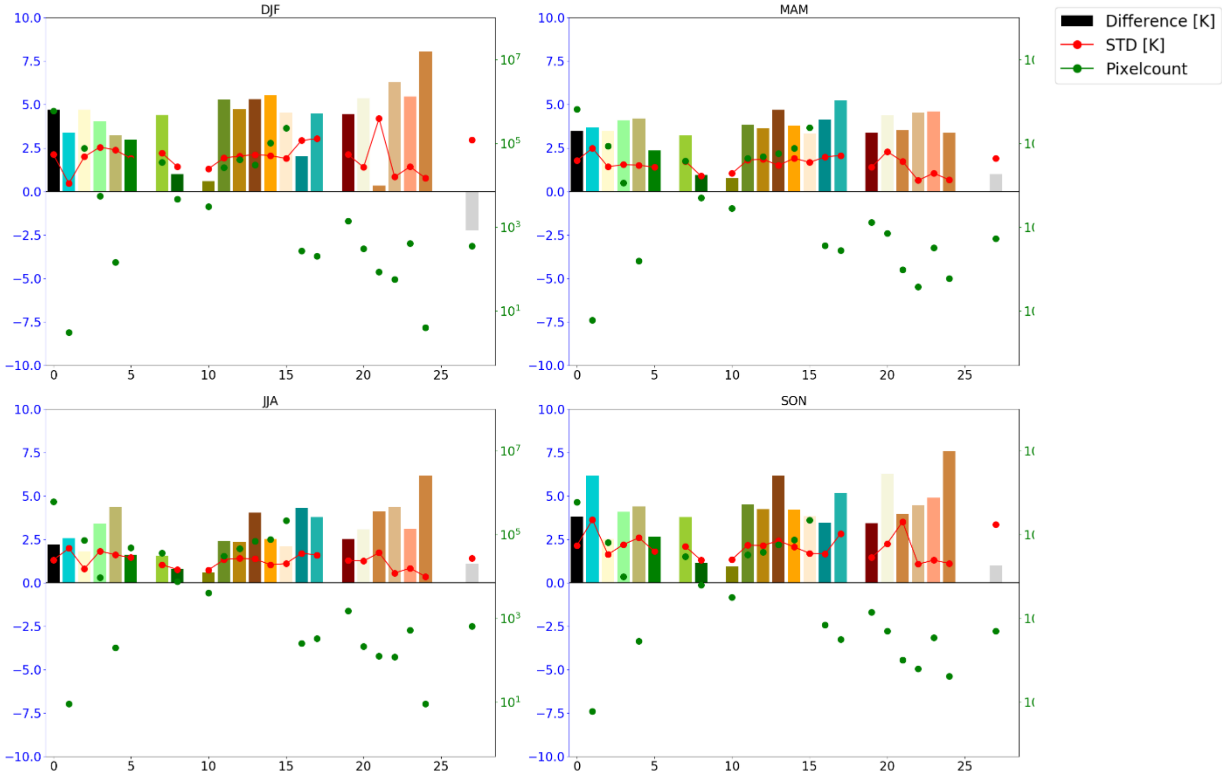

Figure 32: Seasonal daytime differences for different land cover classes for ATSR3-MOD11T over Australia; the bars are the median differences, red points the RSTD and the green points on the right axis show the number of averaged data points

The comparison of the differences against the satellite angles showed that for the intercomparisons of ATSR_3-MOD11T and ATSR_3-MODIST the differences were lower for more negative values of satze*sign(sataz) and increased for positive values of satze*sign(sataz) (Figure 33 for ATSR_3-MODIST). This increase was more pronounced than found over the other continents. The local overpass time for the ATSR_3 satellite is in the morning, thus, when the ATSR_3 satellite azimuth angle is negative, it is looking on the scene from the West whereas the sun is shining from the East, which leads to a larger influence of shadows for these azimuth angles.

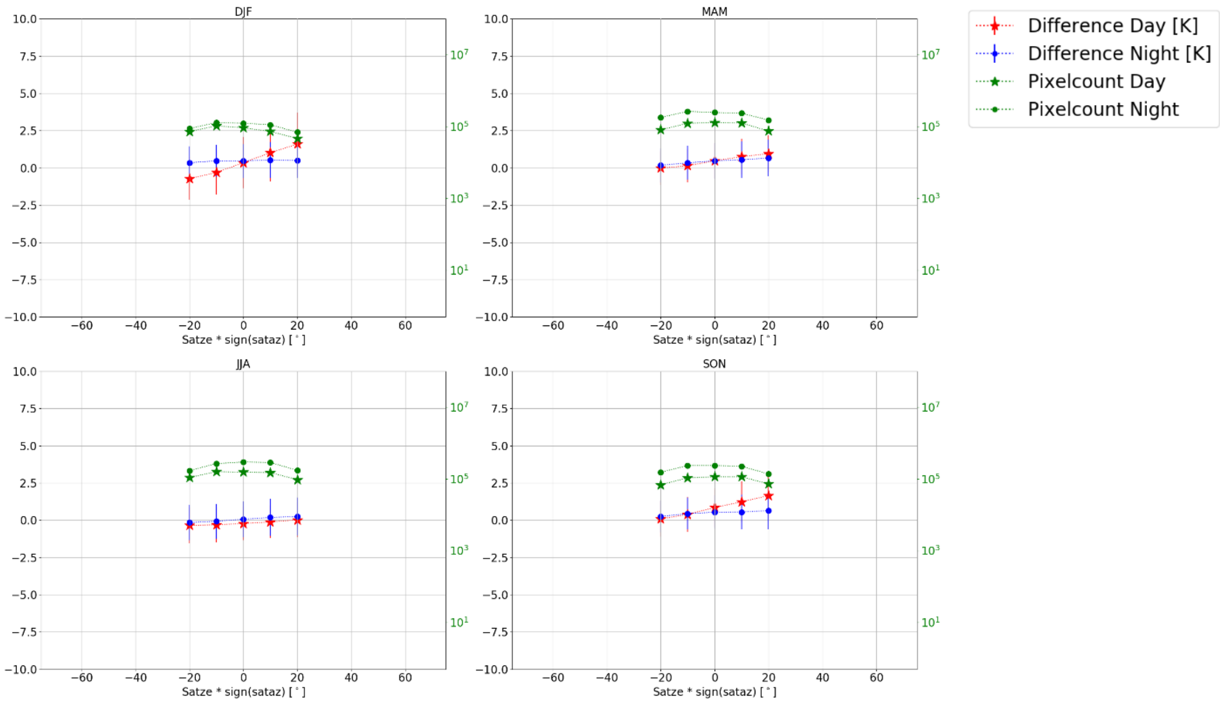

Figure 33: Seasonal LST differences between ATSR_3 and MODIST LST data for different satze*sign(sataz) of ATSR_3; red stars represent the daytime data, blue dots the night-time data, and the green stars and dots on the right axis display the averaged pixel numbers for daytime and night-time data, respectively

4.2.5. Results over Europe

The time series for all nine analysed satellite – satellite intercomparisons over Europe are displayed in Figure 34. MOD11A-SEVCCI and MOD11T-SEVCCI have the most pronounced negative differences, whereas MODISA-SEVCCI has positive daytime differences in winter and negative daytime differences in summer. Increased daytime differences during summer were also found for ATSOP-SEVCCI, ATSR_3-SEVCCI and MODIST-SEVCCI during summer. The smallest differences are found for ATSR_3-MODIST. The intercomparison of LEO data sets vs SEVCCI gave in general higher differences than the intercomparison of LEO vs LEO data sets.

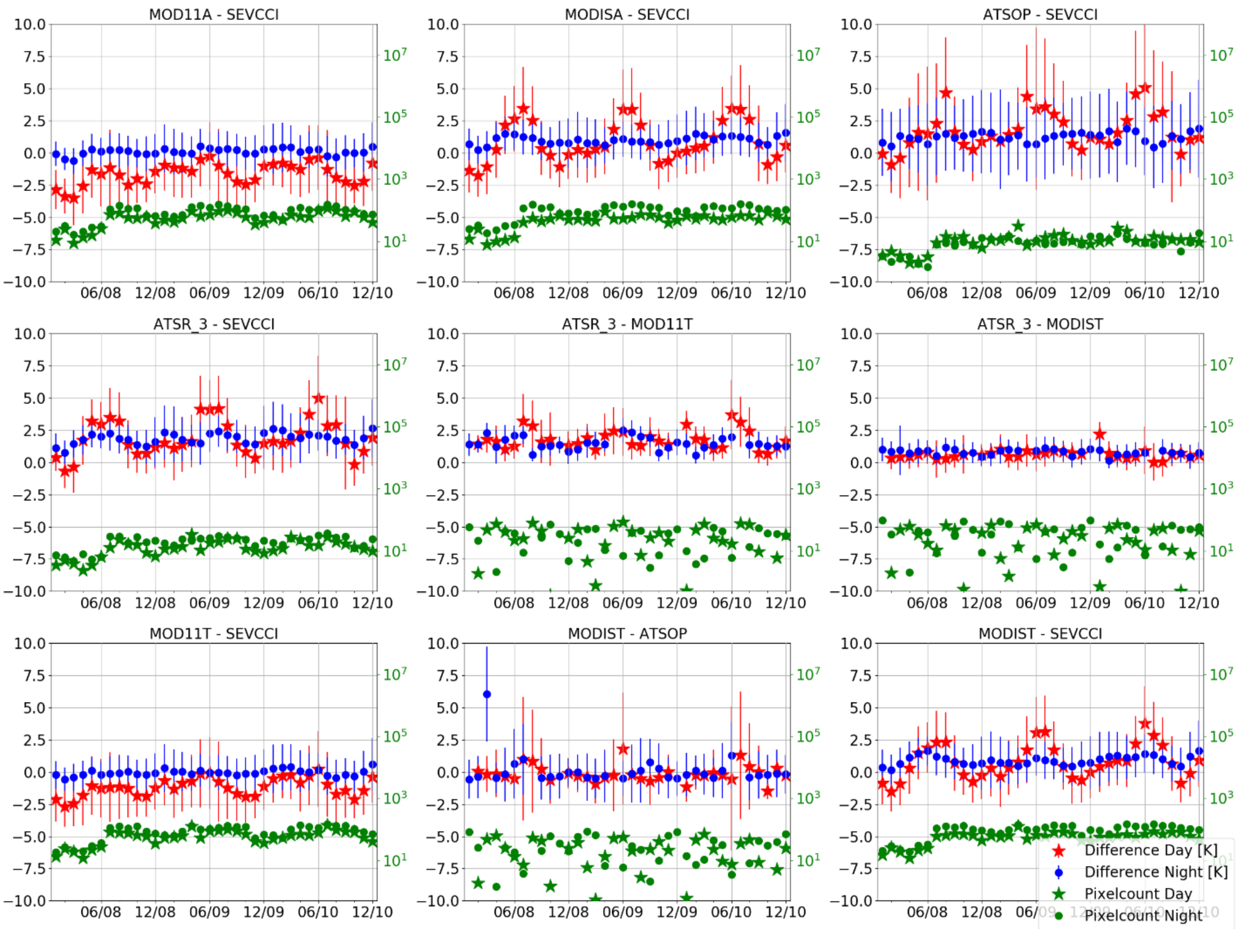

Figure 34: Monthly time series for all investigated satellite – satellite data sets over Europe. Red stars represent the daytime data, blue dots the night-time data, the green stars and dots on the right axis display the averaged pixel numbers for daytime and night-time, respectively.

The number and distribution of the averaged data points per pixel showed that most data points were found for the MODIS-SEVCCI intercomparisons (see Figure 35 for the analysis of MODIST-SEVCCI daytime data), and that the intercomparisons of ATSR_3-SEVCCI covered the continent only partly in “stripes”. Furthermore, for MODIST-ATSOP no data points were available in spring and summer, as has already been found over the other continents.

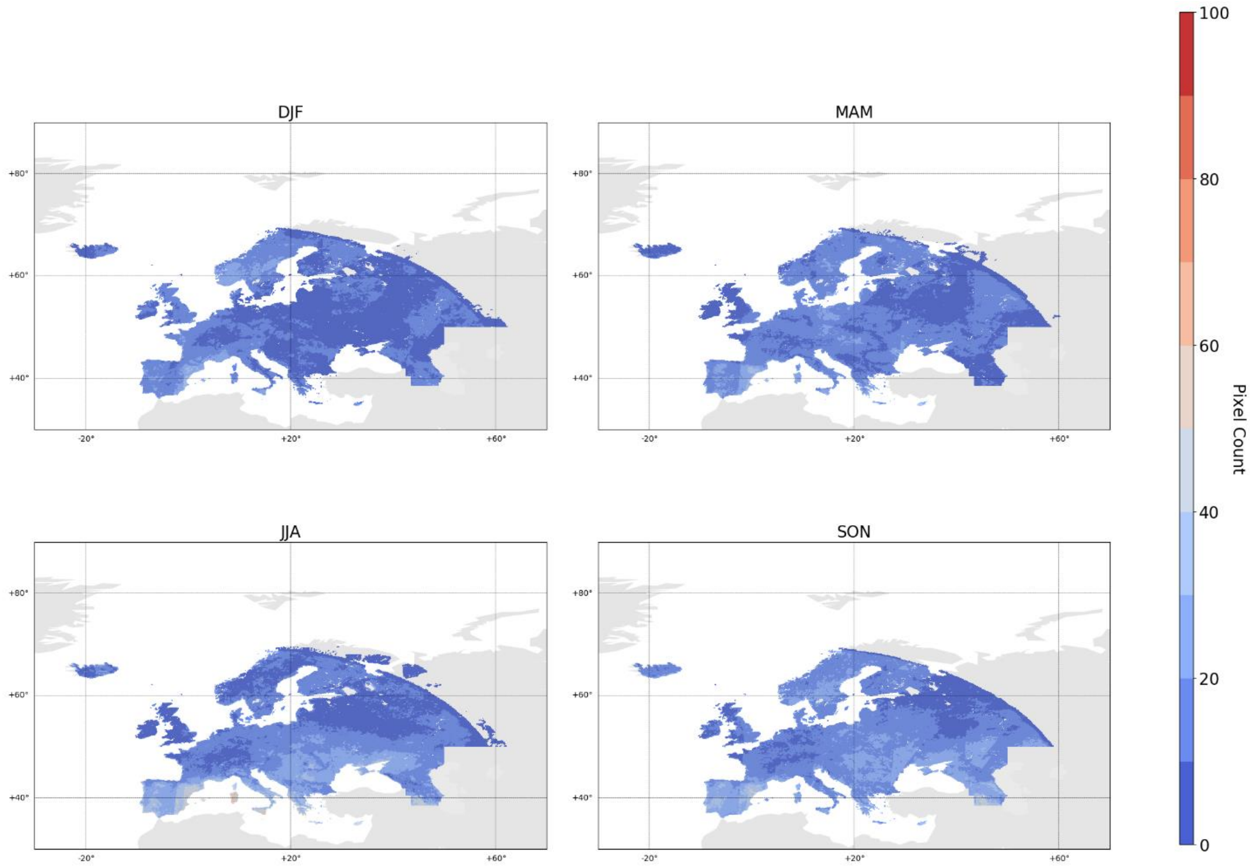

Figure 35: Number of seasonal daytime averaged data points per pixel for MODIST-SEVCCI data over Europe

The analysis of the differences for different elevation classes showed that most pixels fall into an elevation class of 50 m – 200 m. No significant differences between single elevation classes was found.

The main land cover classes found over Europe are "Closed broadleaved deciduous forest" (class 6 of the ALB2 land cover classification), "Open needleleaved deciduous or evergreen forest" (class 9 of the ALB2 land cover classification) and "sparse vegetation" (class 15 of the ALB2 land cover classification). The land cover classes for MODISA-SEVCCI daytime differences are shown in Figure 36. Sparse vegetation covers the north of the continent, whereas the forest is distributed throughout the continent. Also here the results show that differences for "sparse vegetation" tend to be more positive than for the other two main classes.

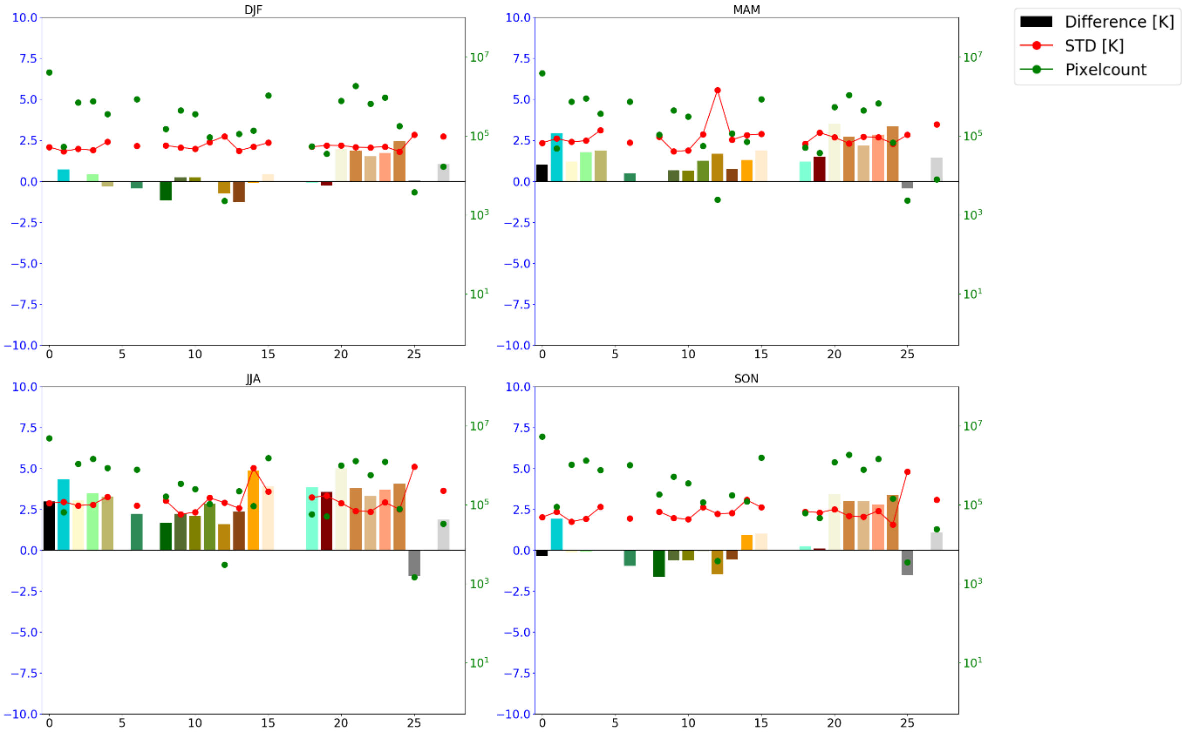

Figure 36: Seasonal daytime differences for different land cover classes for MODISA-SEVCCI over Europe; the bars are the median differences, red points the RSTD and the green points on the right axis show the number of averaged data points

The analysis of the differences with respect to different classes of satze*sign(sataz) showed again the asymmetric distribution of data points for the MODIS data sets against SEVCCI, that were already found over Asia. This is less pronounced here for autumn and winter season (Figure 37 for MODISA-SEVCCI differences), when the influence of the solar radiation might be smaller.

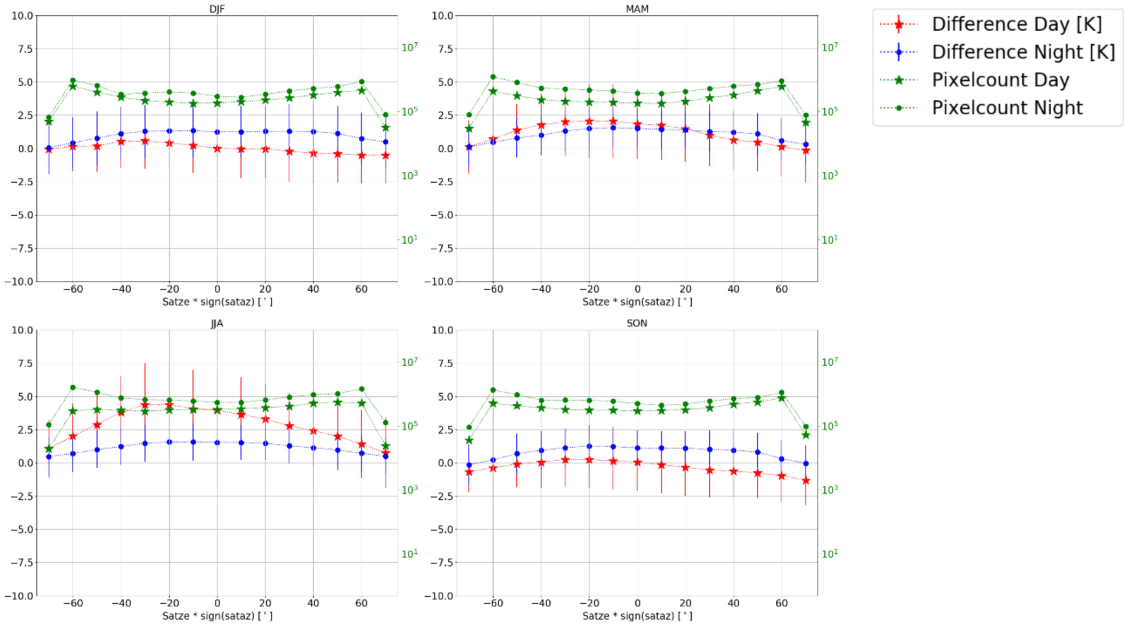

Figure 37: Seasonal LST differences between MODISA -SEVCCI LST data for different satze*sign(sataz) of MODISA; red stars represent the daytime data, blue dots the night-time data, and the green stars and dots on the right axis display the averaged pixel numbers for daytime and night-time data, respectively

4.2.6. Results over North America

The results of the time series analysis over North America is shown in Figure 38. The differences are positive for ATSR_3-MOD11T and ATSR_3-MODIST, and negative for MODIST-ATSOP. They are not very large for all data sets and mainly below 2 K. A yearly cycle is seen in the monthly differences as well, however, it is not very pronounced.

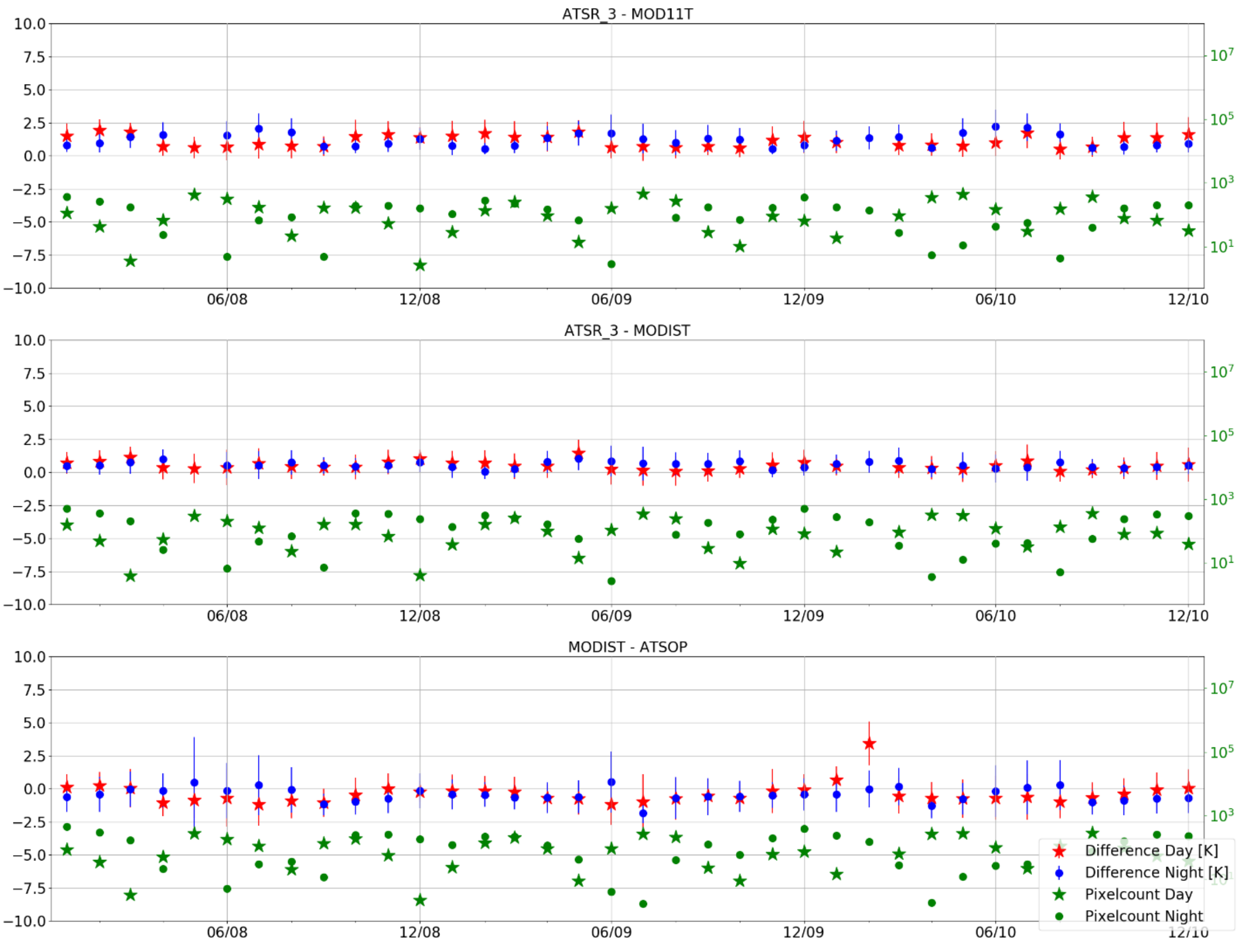

Figure 38: Monthly time series for all investigated satellite – satellite data sets over North America. Red stars represent the daytime data, blue dots the night-time data, the green stars and dots on the right axis display the averaged pixel numbers for daytime and night-time, respectively.

Over this continent, the number of averaged data points varied substantially between daytime and night-time data for all satellite pairs. There were many data points (> 100) during night, and the number was lower during day (<20) (Figure 39 for the data distribution for ATSR_3-MODIST data pair). However, these differences mainly concern the North of the continent, where the number of overpasses increases due to the proximity of the pole.

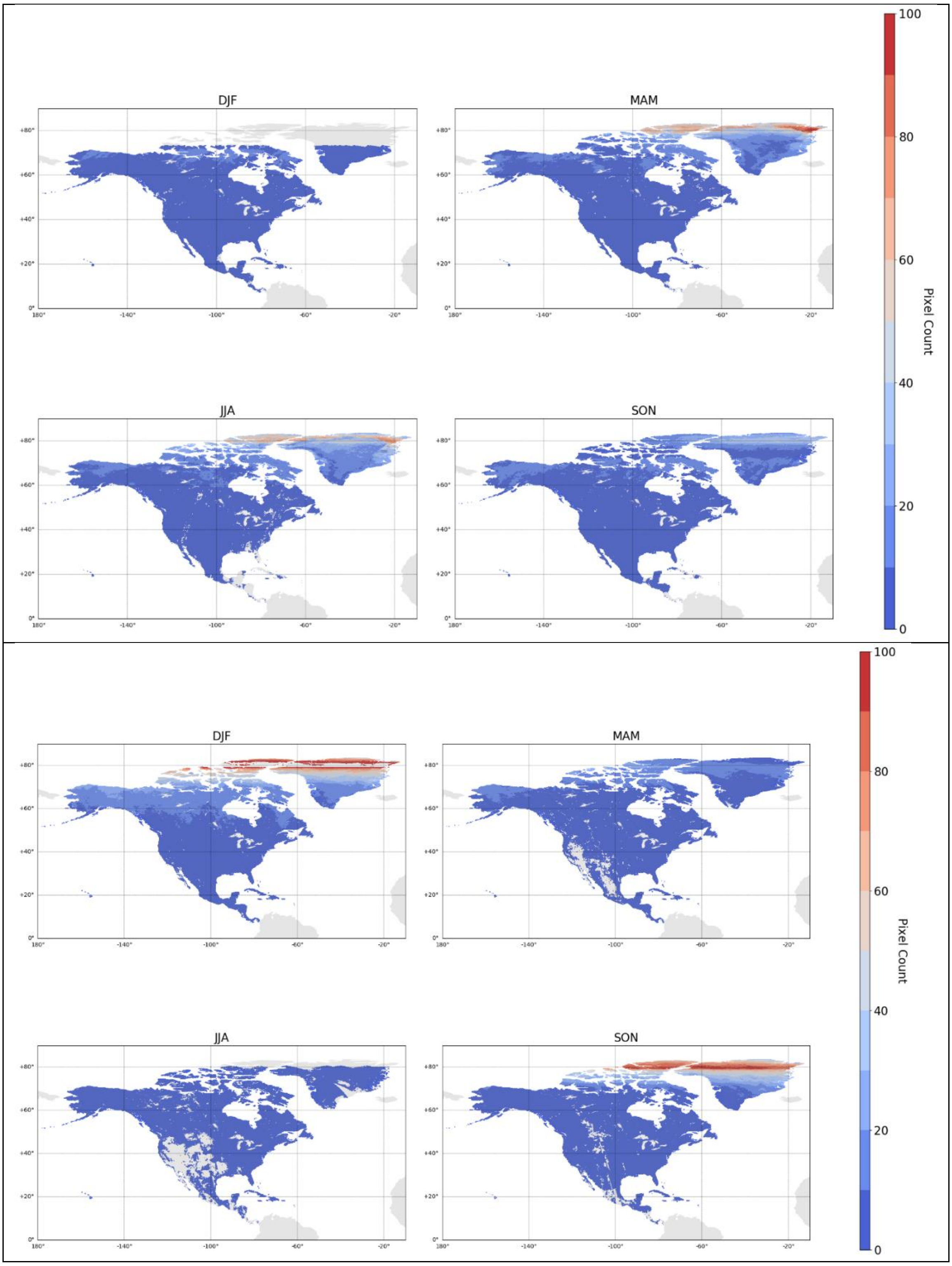

Figure 39: Number of seasonal daytime (upper) and night-time (lower) averaged data points per pixel for ATSR_3-MODIST data over North America

The analysis of the differences for different elevation classes showed that most analysed pixels have an elevation of 200 – 500 m. No significant differences between the single classes were found for night-time data, whereas during day higher elevation classes have smaller differences and also smaller RSTD. This was unexpected, as usually during day, for higher elevation the influence of shadowy and sunlit areas is increased and thus the differences and the RSTD increase (see Figure 40 for daytime differences of ATSR_3-MODIST).

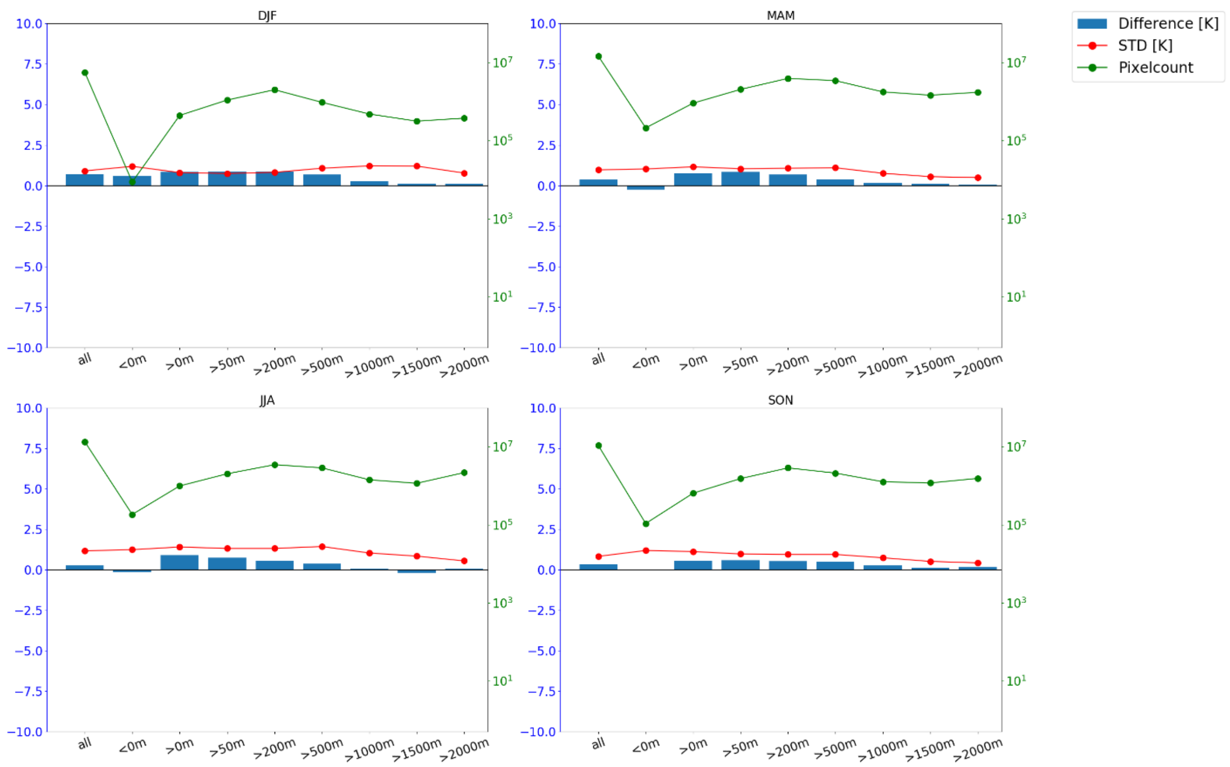

Figure 40: Seasonal daytime differences for different elevation classes for ATSR_3-MODIST over North America; blue bars are the median differences, red points the RSTD and the green points on the right axis show the number of averaged data points

The analysis of the different land cover classes showed that most data points fall in the land cover class of “sparse vegetation” (class 15 of the ALB2 land cover classification), which is mainly found in the north of North America, where, as described above, most data points are located (Figure 41 for differences over different land cover classes for ATSR_3-MOD11T).

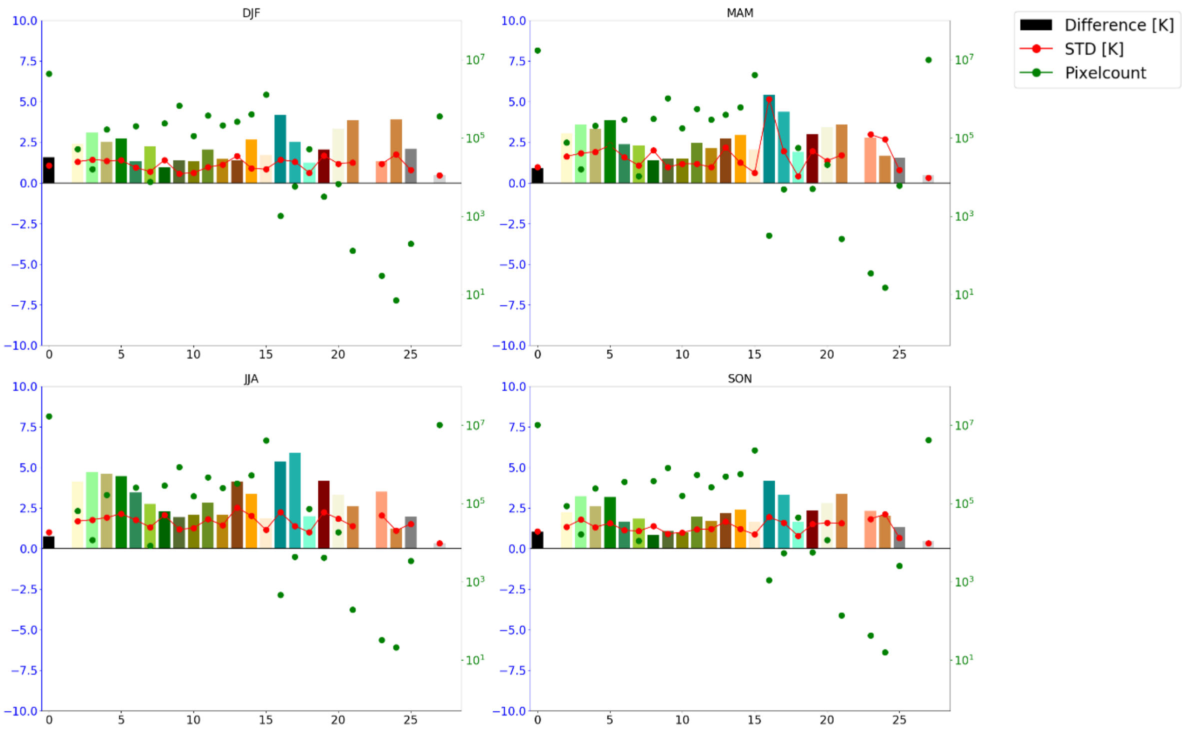

Figure 41: Seasonal daytime differences for different land cover classes for ATSR_3-MOD11T over North America; the bars are the median differences, red points the RSTD and the green points on the right axis show the number of averaged data points

The analysis of the satellite angles gave, as seen for the other continents described above, that for MODIST satellite angles, the differences and RSTD increase for larger zenith angles.

4.2.7. Results over South America

The results of the time series analysis over South America is displayed in Figure 42. ATSR_3-MOD11T has higher, i.e. more positive differences than ATSR_3-MODIST, as already found before.

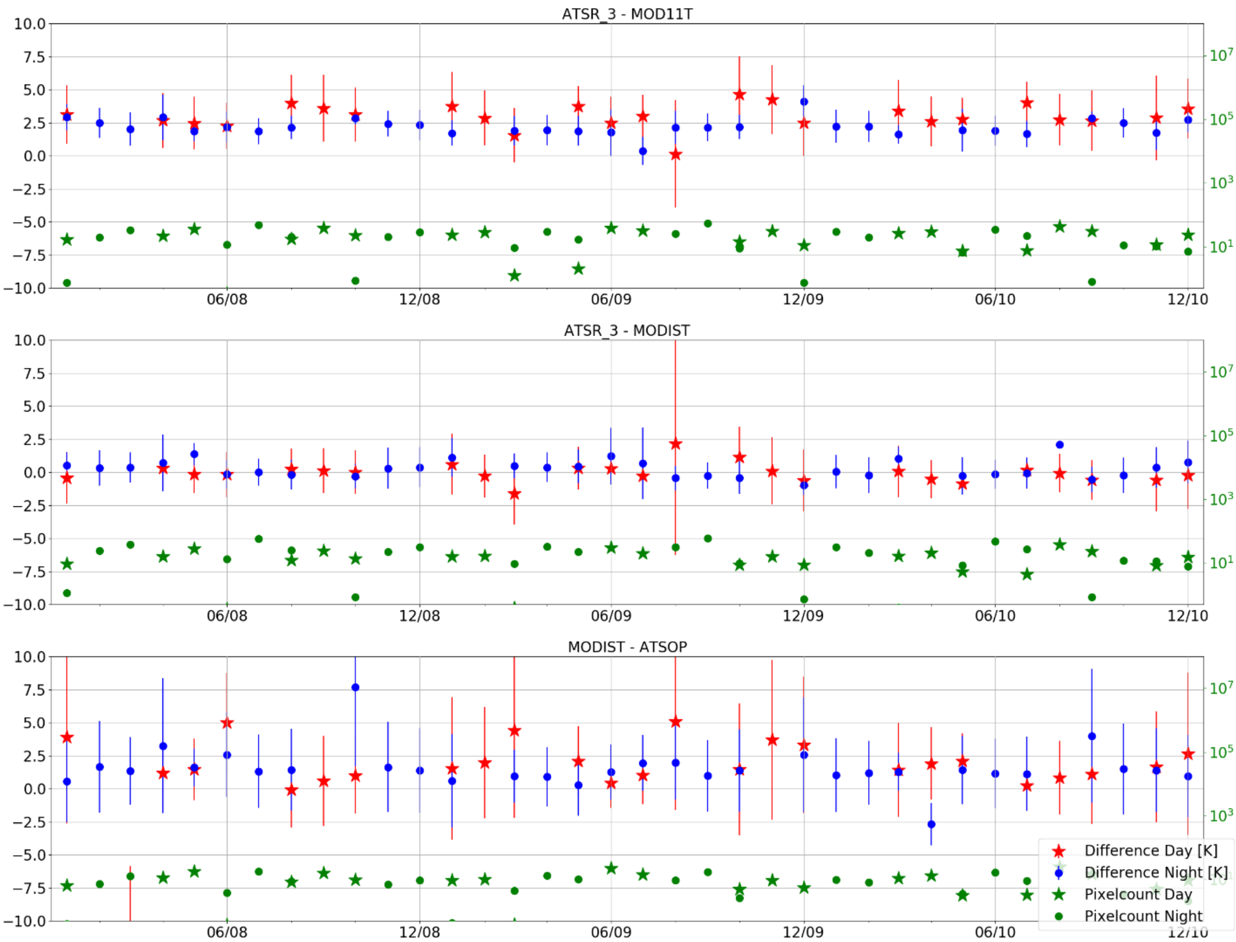

Figure 42: Monthly time series for all investigated satellite – satellite data sets over South America. Red stars represent the daytime data, blue dots the night-time data, the green stars and dots on the right axis display the averaged pixel numbers for daytime and night-time, respectively.

The number and distribution of the averaged data points per pixel showed that more data points lie in the South of the continent, whereas the north is not totally covered. Figure 43 displays the daytime pixel count for ATSR_3-MODIST data pair.

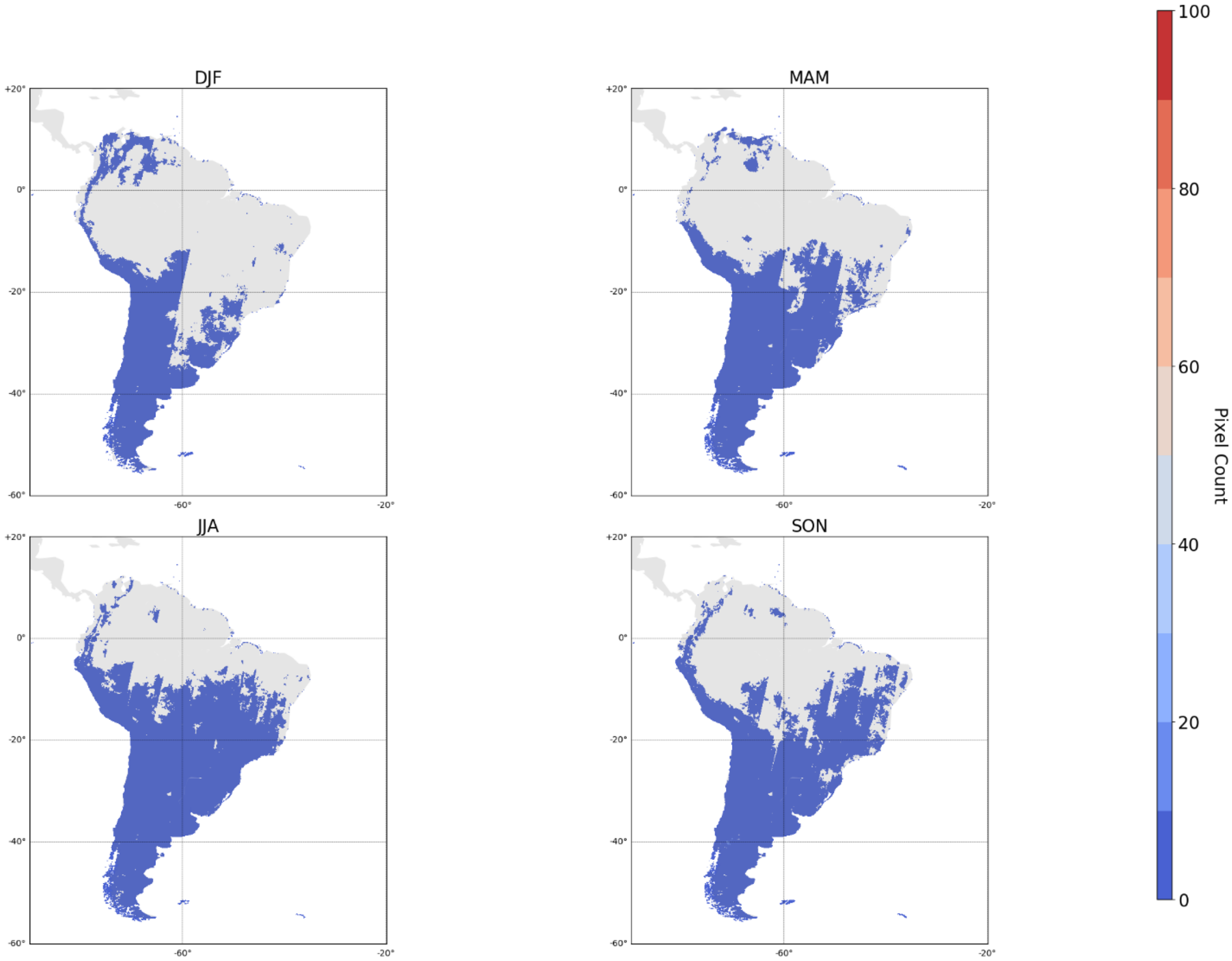

Figure 43: Number of seasonal daytime averaged data points per pixel for ATSR_3-MODIST data over South America

It was found with the analysis of the differences for different elevation classes that most pixels have an elevation between 200 to 500 m or above 2.000 m. These high elevations are mainly found at the mountain ridge at the West of the continent. The differences for these two dominant elevation classes differ, they are smaller for elevation > 2.000 m for ATSR_3-MODIS, and larger for MODIST-ATSOP. The RSTD for all intercomparison pairs increases significantly for elevations > 2.000 m (Figure 44 for differences for different land cover classes for ATSR_3-MOD11T).

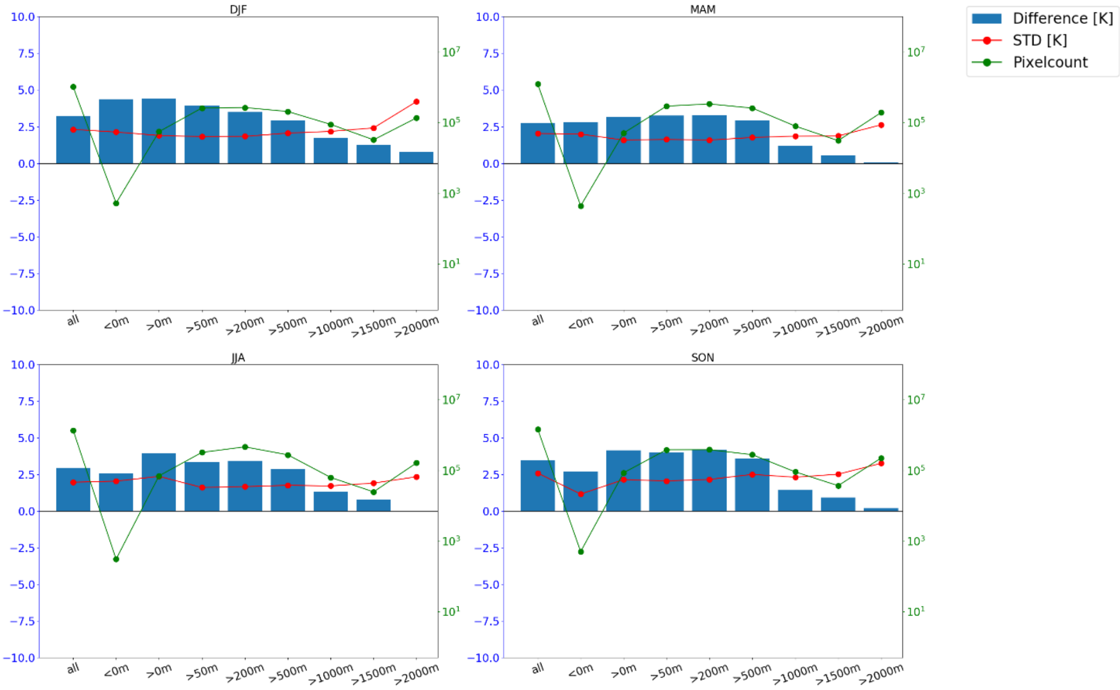

Figure 44: Seasonal daytime differences for different elevation classes for ATSR_3-MOD11T over South America; blue bars are the median differences, red points the RSTD and the green points on the right axis show the number of averaged data points

The main land cover classes found in the analysis over South America were “Closed to open shrubland” (class 13 of the ALB2 land cover classification), followed by „sparse vegetation” (class 15 of the ALB2 land cover classification) and “Closed to open broadleaved evergreen and / or semi deciduous forest” (class 5 of the ALB2 land cover classification). For the two intercomparison of ATSR_3-MODIS (see Figure 45 for daytime differences for ATSR_3-MODIST), class 13 has more positive differences than class 15, for MODIST-ASTOP is this the other way round. This might be connected to the results of the elevation classes, as class 13 is found along the mountain ridge in the West, where also the elevation is highest.

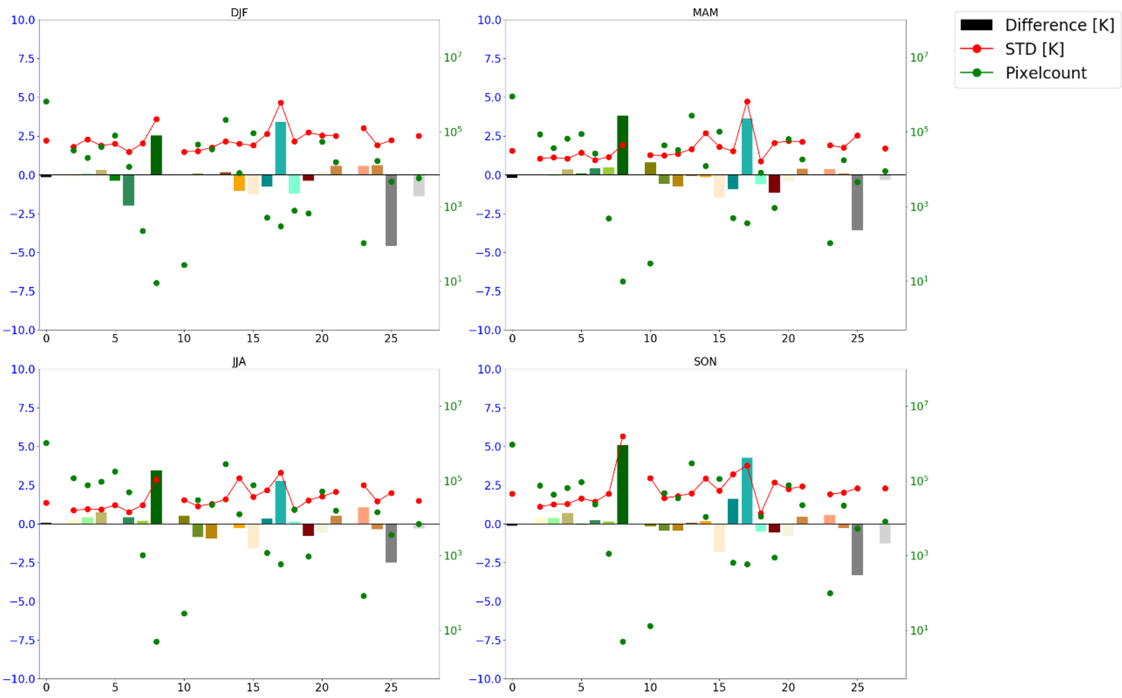

Figure 45: Seasonal daytime differences for different land cover classes for ATSR_3-MODIST over South America; the bars are the median differences, red points the RSTD and the green points on the right axis show the number of averaged data points

The analysis of the different satellite angles showed an increase with increasing satellite zenith angles as has been found for the other continents before.

5. Conclusions

In this work the results of the validation of the satellite LST data sets developed within the LST_cci project are presented. The validation is done in two parts, first is an in situ validation against point measurements at different, globally distributed stations. Second is the intercomparison of the LST_cci data sets with operational and reference data sets over different continents.

For the in situ validation, five IR satellite LST data sets (ATSR_2, ATSR_3, SLSTRA, MODISA, MODIST) and three MW LST data sets (SSMI13, SSMI17, and SSMI18) have been compared with in situ data from 13 stations including stations from the KIT network, SURFRAD network, an ARM stations and an OzFlux station over the time period from 1995 - 2018. The investigated time period varied depending on the data availability of the satellite as well as the in situ data set.

The results are presented in terms of product accuracy and robust standard deviation (RSTD) for both validation types: i) in terms of bias (satellite LST – in situ LST) for the in situ validation; and ii) differences (satellite 1 LST – satellite 2 LST) for the intercomparisons. The results of the in situ validation show that in general the accuracies of the LST_cci products are better at night than during the day, as the influence of sunlit and shadow areas during day can increase the point-to-area differences between the satellite scale LST and the in situ point measurements. The highest positive biases were found for the three MW data sets, however, these data sets also view a larger area than the IR satellite sensors, and see therefore at most stations larger heterogeneities than the IR sensors leading to larger biases. Furthermore, for the MW data sets the differences between daytime and night-time biases are smaller, as the local overflight time is close to sunset and sunrise. The most negative biases were found for the SLSTRA data set, where only data from two years could be analysed. The accuracy of MODISA, MODIST, ATSR_2 and ATSR_3 are generally good, with MODISA and MODIST often similar across sites.

It was also found that the biases as well as the RSTD varies significantly between the stations, which indicates that the satellite algorithms perform differently over different land covers, elevations and regions. For example, the ASM___ station in Australia showed very high daytime biases for all investigated LST data sets, and BND___ station had very high RSTD, indicating that the differences in satellite and in situ LST is larger. These differences were further investigated by analysing the time series of biases over each station individually.

For the second part of the presented validation, nine satellite vs. satellite pairs were intercompared, being MOD11A-SEVCCI, MODISA-SEVCCI, ATSOP-SEVCCI, ATSR_3-SEVCCI, MOD11T-SEVCCI, and MODIST-SEVCCI, ATSR_3-MOD11T, ATSR_3-MODIST, and MODIST-ATSOP. They were matched globally, and the analysis was performed for each continent. The intercomparisons against SEVCCI were carried out over Africa and Europe, as the SEVIRI instrument is flown on a geostationary satellite, and not available globally. For the three other data pairs, intercomparisons over Antarctica, Asia, Australia, North America and South America were also analysed. All intercomparisons were carried out for a time period of 2008 – 2010 to coincide with the SEVCCI data availability in Processing Cycle 1. Monthly time series of differences are analysed, and additional information of the intercomparisons were obtained from investigating further the dependence of the differences on the elevation, land cover classes, satellite angles, and number of averaged data points.

It was found that for daytime data, ATSR_3-MODIST performed better than ATSR_3-MOD11T. MOD11A-SEVCCI and MOD11T-SEVCCI have the most negative differences, which reveals that MOD11T has in general lower LST values than MODIST. ATSR_3-SEVCCI tends to have more positive differences, with MODIST-ATSOP showing more negative differences during day. Over the continents Africa, Australia, and

South America a larger spread in the differences was found than over the other continents. The satellite vs. satellite pair MODIST-ATSOP has often only few data points in the season “MAM” (March April May) and “JJA” (June July August). The results over the single continents showed that the additional analysis for elevation angles, land cover classes and satellite angles can give valuable further insights into the differences.

Overall, from the in situ validation it can be concluded that in this first round of validation within LST_cci, ATSR_2, ATSR_3, MODISA, and MODIST perform well, especially during night. Furthermore, ATSR_3 and MODIST seem to be well correlated even though their retrieval algorithms are different. The additional intercomparisons revealed that the LEO IR LST_cci products are more comparable with the SEVIRI LST_cci product than the corresponding operational products are with SEVIRI LST_cci, with differences generally < 2K which is within the corresponding uncertainty range of the SEVCCI product.

6. Recommendations for the next Processing Cycle

In this section, important points that should be considered when developing a LST data set are summarized for producers of LST data sets. They are drawn from the validation work within LST_cci presented in this report, where the comparisons of several LST data sets with in situ data sets as well as with other operational satellite data sets are presented.

First of all, it is very helpful if all important information on the data set is presented with the data set itself in form of comprehensive meta data, which easily be done using the netCDF data format.

In this work, we found that different LST data set perform differently over different land cover classes, over different regions, elevation heights or in different climatic zones. Thus, it is best to validate the developed data sets over many different stations or in different regions to better understand their performance. Results of the validation analysis should be presented in a statistical meaningful way, i.e. using the median instead of the mean and robust standard deviation instead of standard deviation so as to provide more sensible results without single, large outliers having undue influence.

It is also advisable to validate the produced data sets for different time periods or over a long time period dependent on data availability to see if there are drifts or step changes in the LST data over time.

Comparisons of the developed data sets with other data sets, either in direct intercomparisons, or by comparing differences from different satellite data sets with the same in situ data, can give further insights in the performance of the data set. One can distinguish where the differences to other data sets are large, and where they give similar results, and investigate this further.

It is also helpful to compare the developed data sets with other LST data sets that are derived from the same satellite instrument but with a different algorithm. This analysis can show how large the influence of algorithm formulation is on the resulting LST product.

Additional analysis of biases or differences and RSTD with respect to different viewing angles, topography and land covers can further help to understand the developed data sets over special regions.

Finally, if large negative biases between the satellite and in situ LST data are found in the validation, this might be due to missed clouds in the satellite data set and should be investigated further by the data providers.

7. Appendix

7.1. Africa

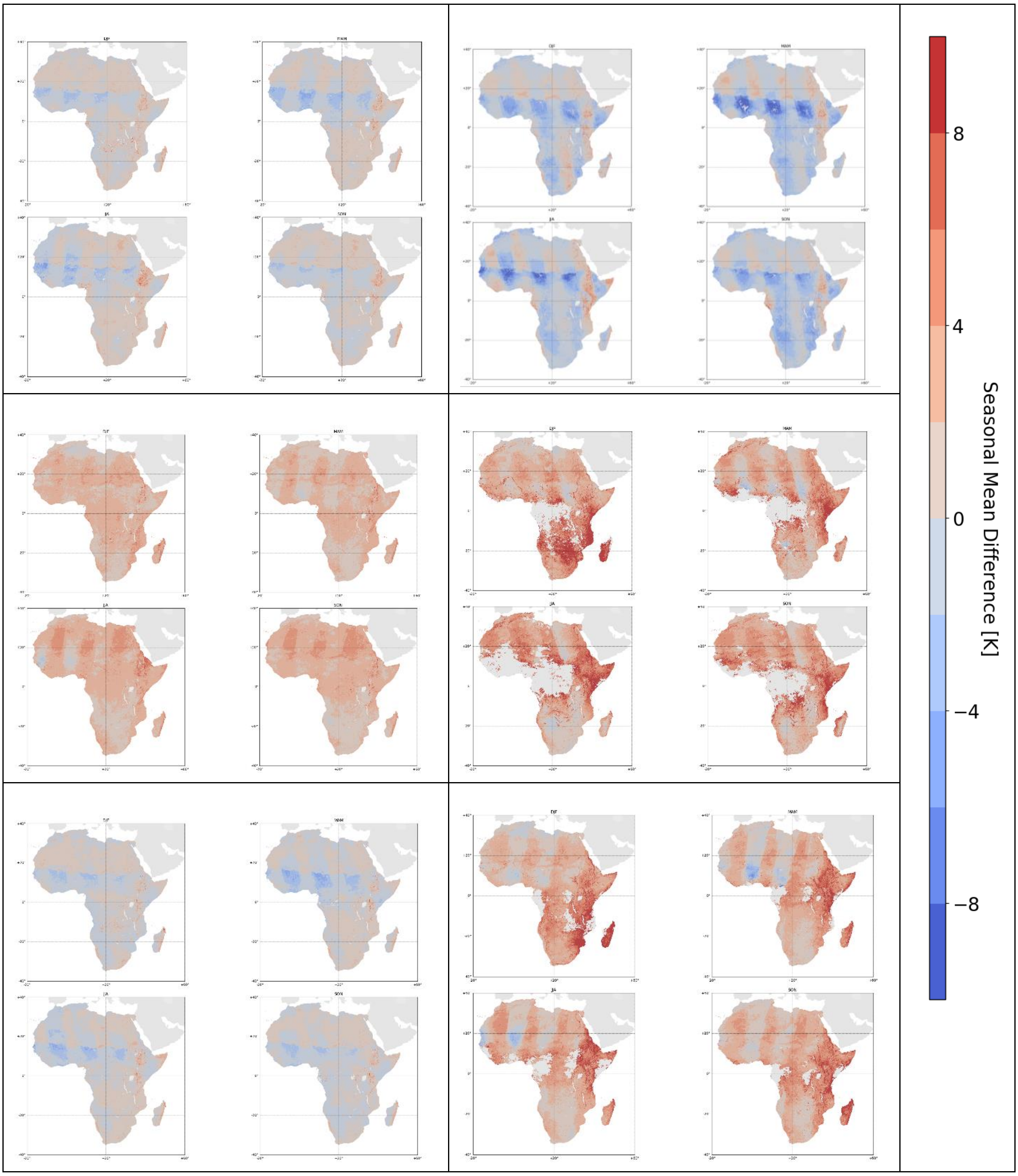

Figure 46: Seasonal mean differences of LST_satellite 1 – LST_satellite 2 in K; left row displays night-time and right row daytime data. Upper plots are for MOD11A-SEVCCI, middle plots for MODISA-SEVCCI, and lower plots for MOD11T-SEVCCI.

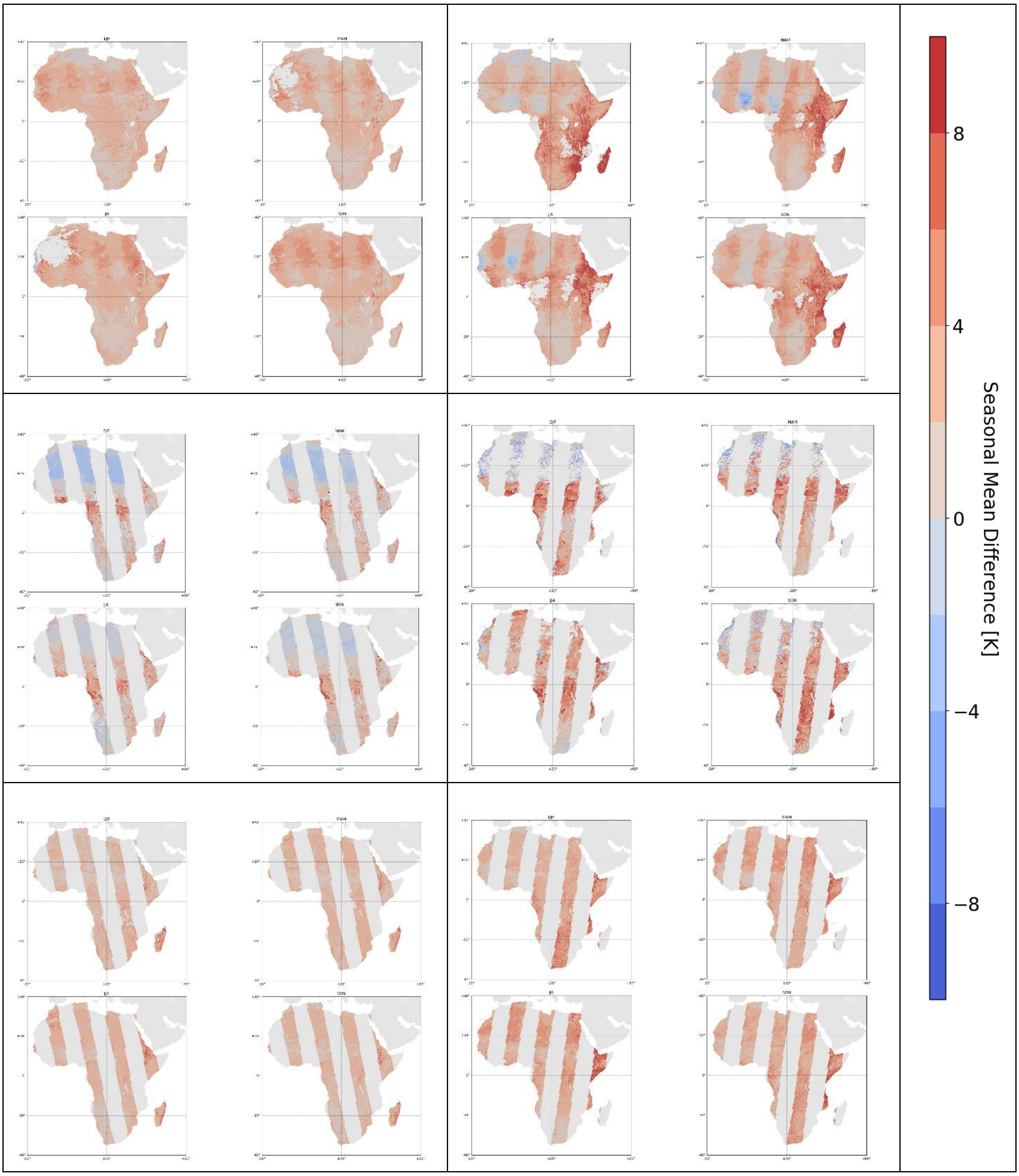

Figure 47: Seasonal mean differences of LST_satellite 1 – LST_satellite 2 in K; left row displays night-time and right row daytime data. Upper plots are for MODIST-SEVCCI, middle plots for ATSOP-SEVCCI, and lower plots for ATSR_3-SEVCCI.

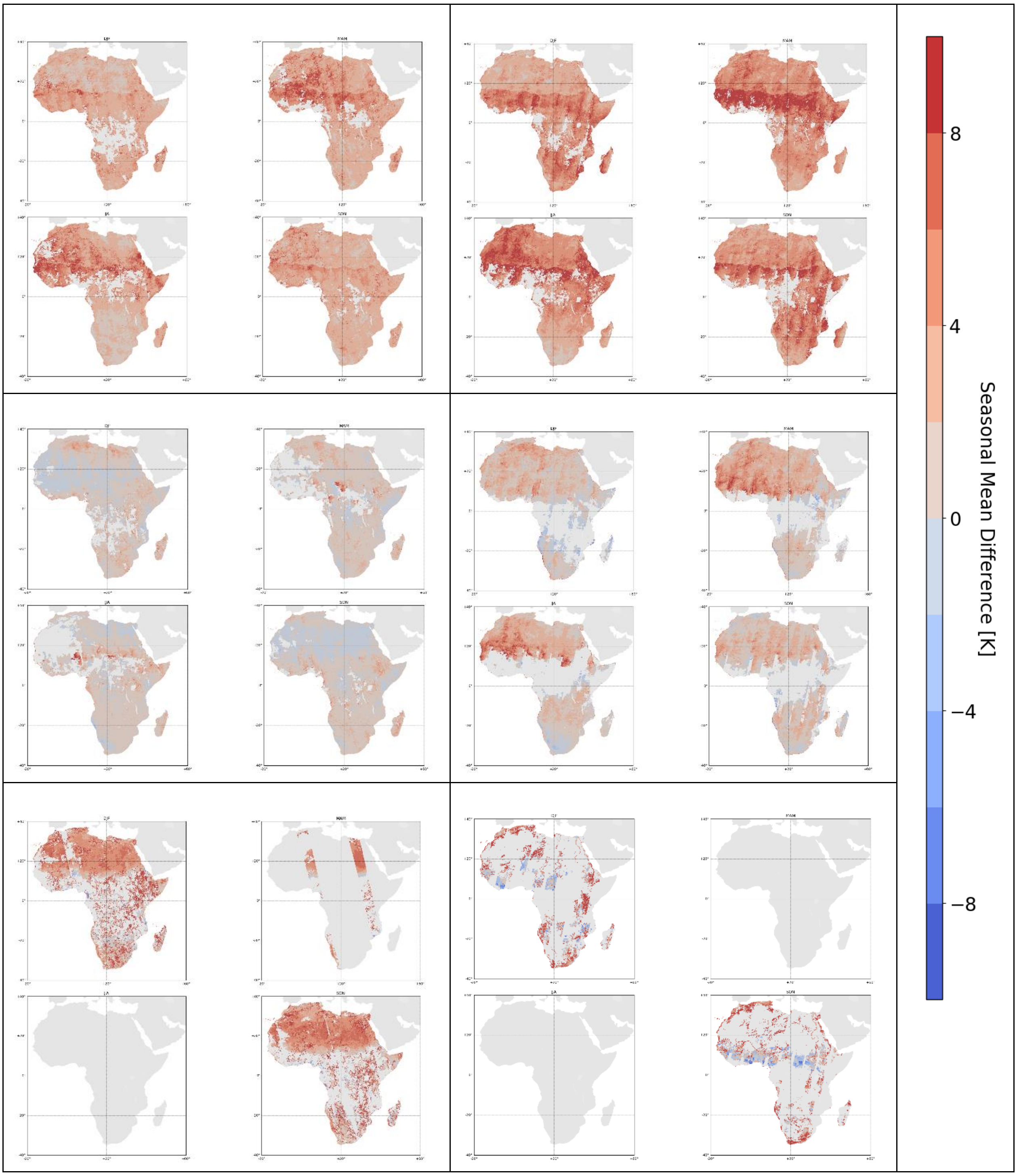

Figure 48: Seasonal mean differences of LST_satellite 1 – LST_satellite 2 in K; left row displays night-time and right row daytime data. Upper plots are for ATSR_3-MOD11T, middle plots for ATSR_3-MODIST, and lower plots for MODIST-ATSOP.

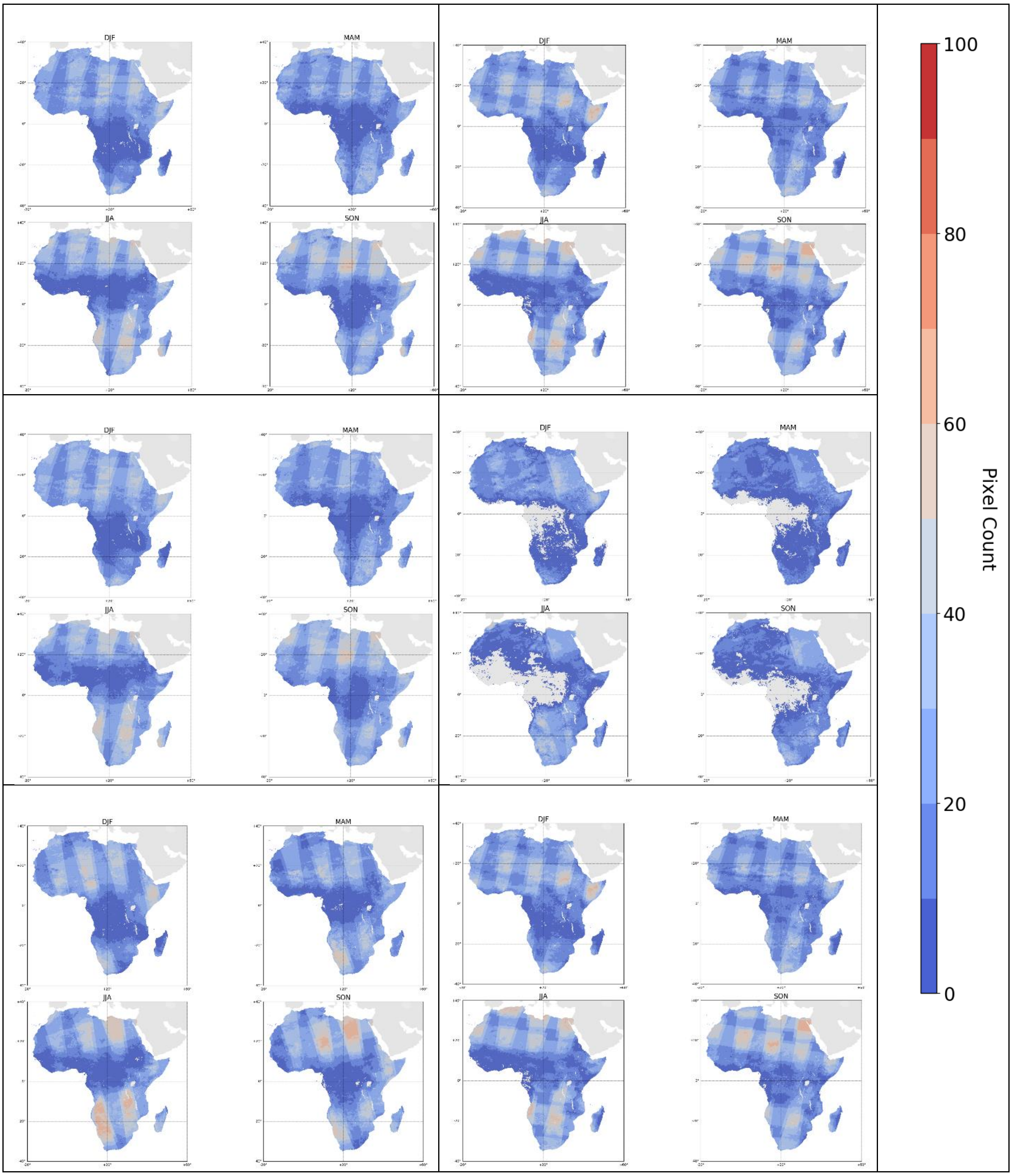

Figure 49: Number of seasonal averaged data points per pixel; left row displays night-time and right row daytime data. Upper plots are for MOD11A-SEVCCI, middle plots for MODISA-SEVCCI, and lower plots for MOD11T-SEVCCI.

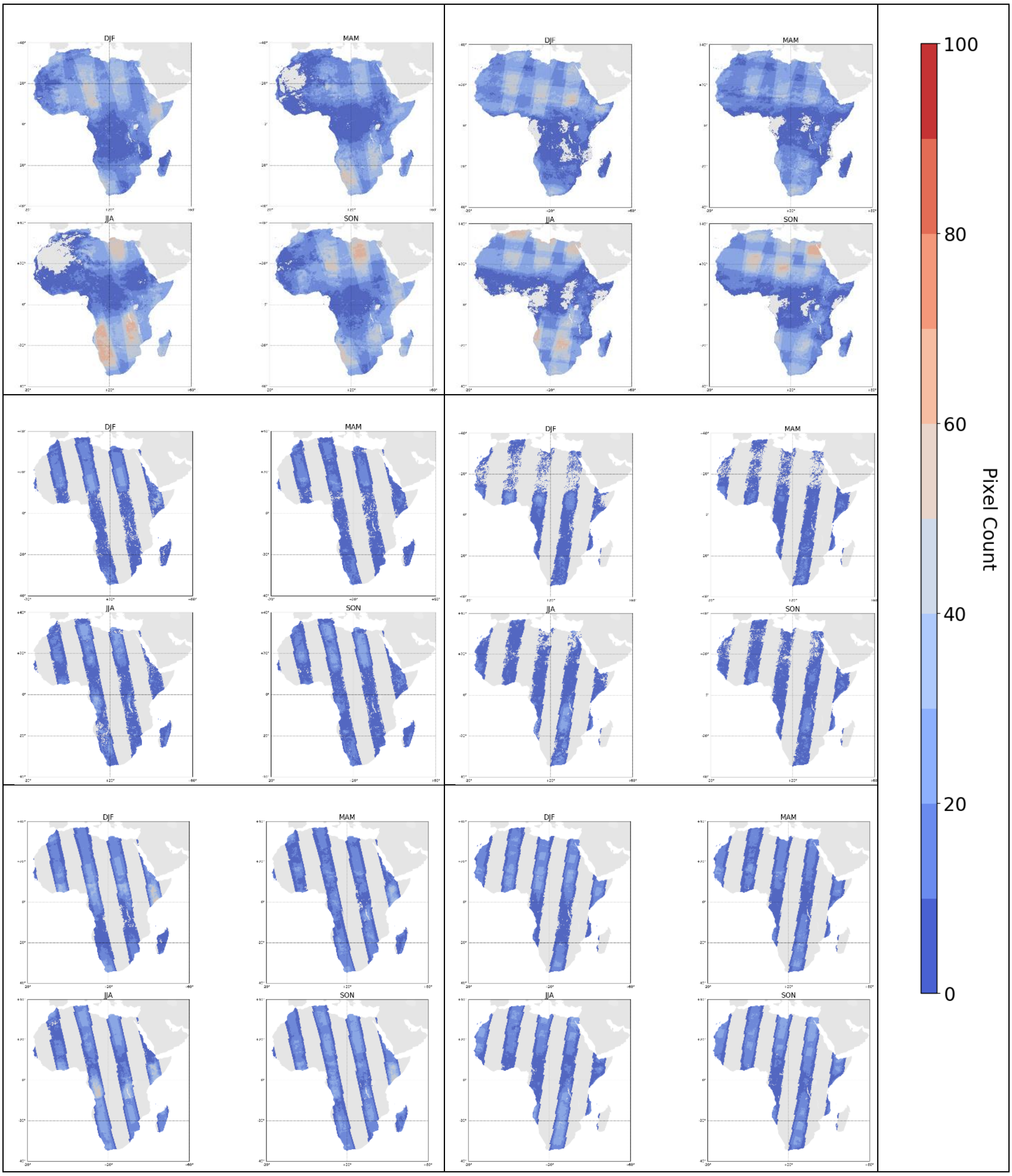

Figure 50: Number of seasonal averaged data points per pixel; left row displays night-time and right row daytime data. Upper plots are for MODIST-SEVCCI, middle plots for ATSOP-SEVCCI, and lower plots for ATSR_3-SEVCCI.

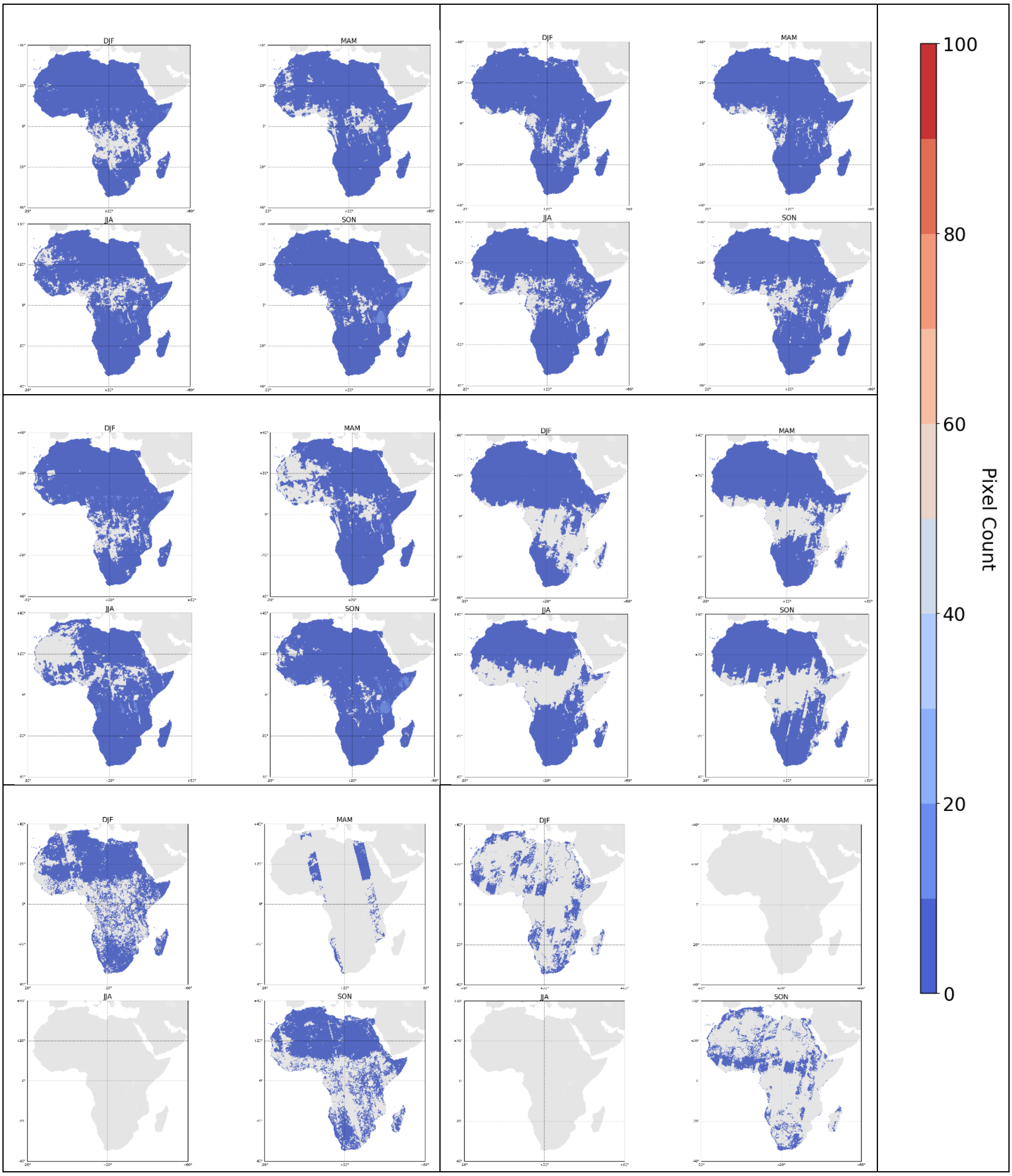

Figure 51: Number of seasonal averaged data points per pixel; left row displays night-time and right row daytime data. Upper plots are for ATSR_3-MOD11T, middle plots for ATSR_3-MODIST, and lower plots for MODIST-ATSOP.

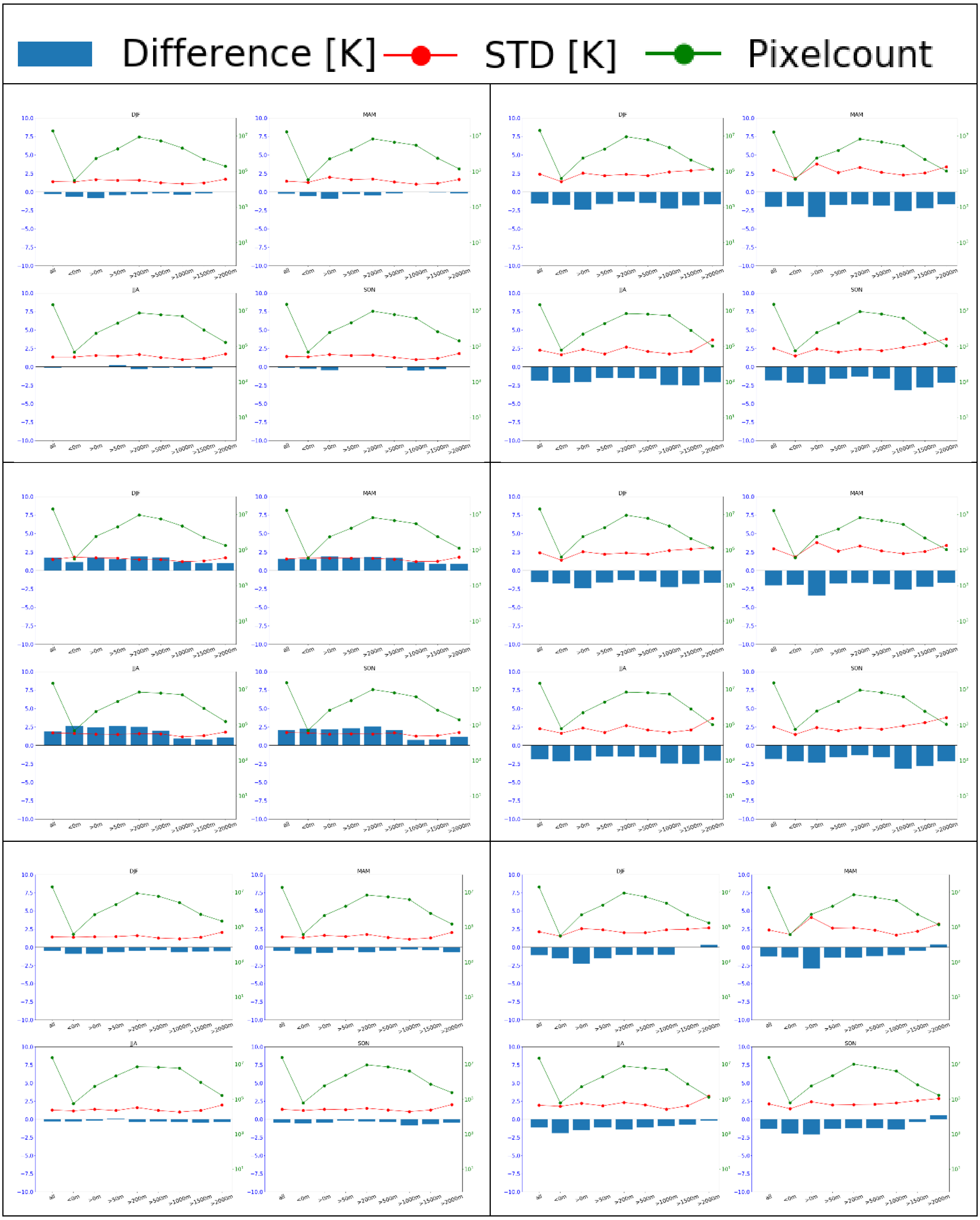

Figure 52: Seasonal differences for different elevation classes; blue bars are the median differences, red points the RSTD and the green points on the right axis show the number of averaged data points Left row displays night-time and right row daytime data. Upper plots are for MOD11A-SEVCCI, middle plots for MODISA-SEVCCI, and lower plots for MOD11T-SEVCCI.

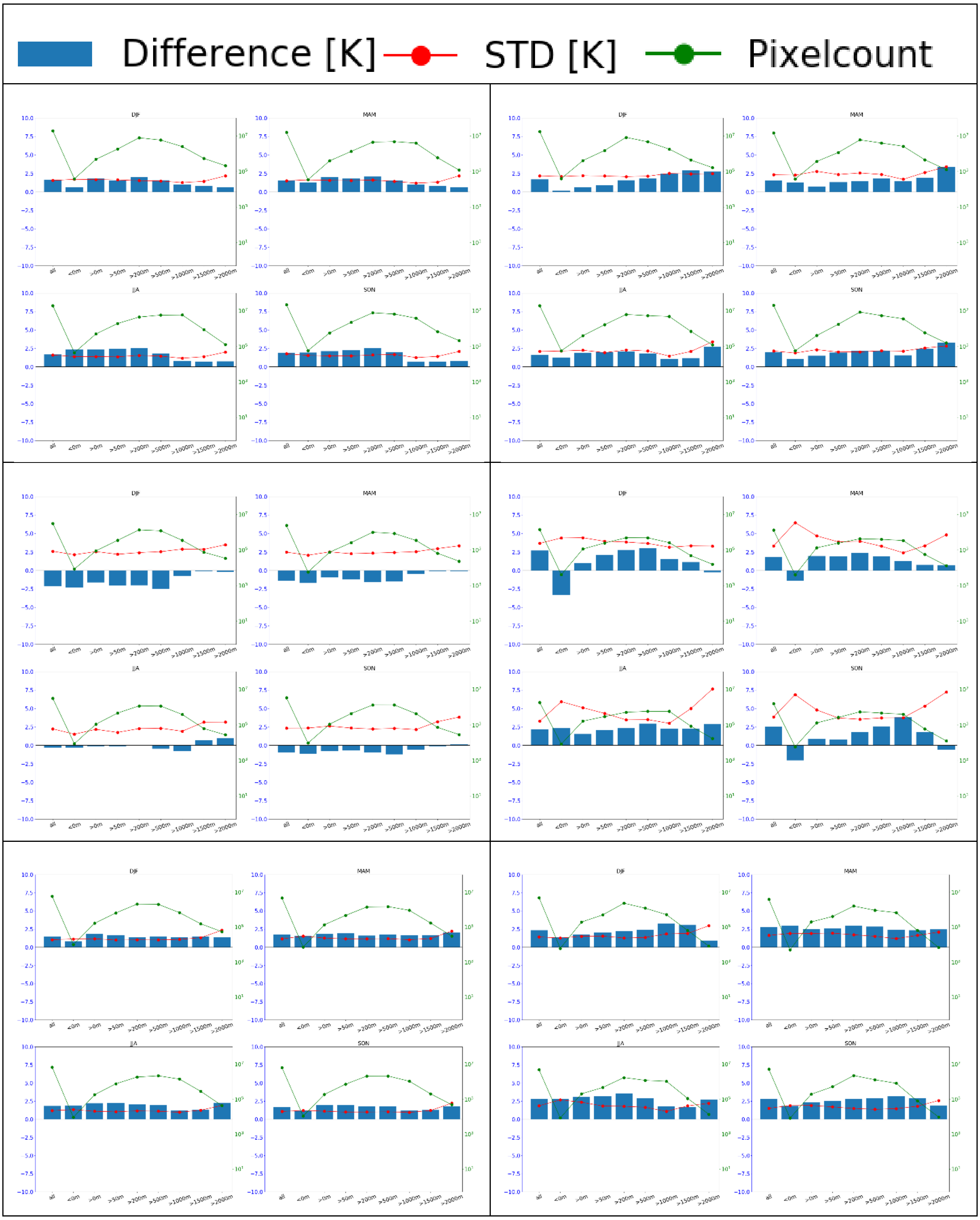

Figure 53: Seasonal differences for different elevation classes; blue bars are the median differences, red points the RSTD and the green points on the right axis show the number of averaged data points Left row displays night-time and right row daytime data. Upper plots are for MODIST-SEVCCI, middle plots for ATSOP-SEVCCI, and lower plots for ATSR_3-SEVCCI.

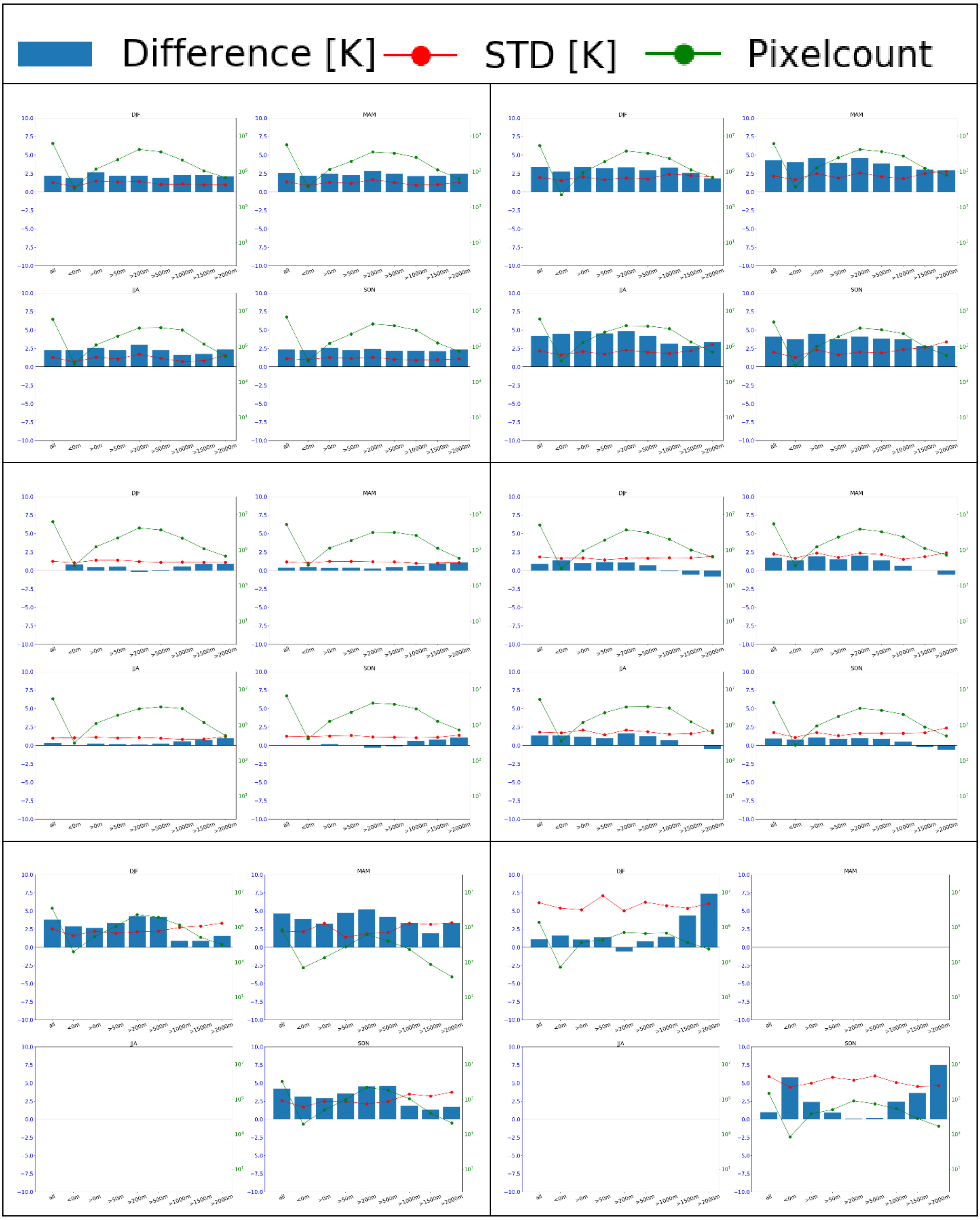

Figure 54: Seasonal differences for different elevation classes; blue bars are the median differences, red points the RSTD and the green points on the right axis show the number of averaged data points Left row displays night-time and right row daytime data. Upper plots are for ATSR_3-MOD11T, middle plots for ATSR_3-MODIST, and lower plots for MODIST-ATSOP.

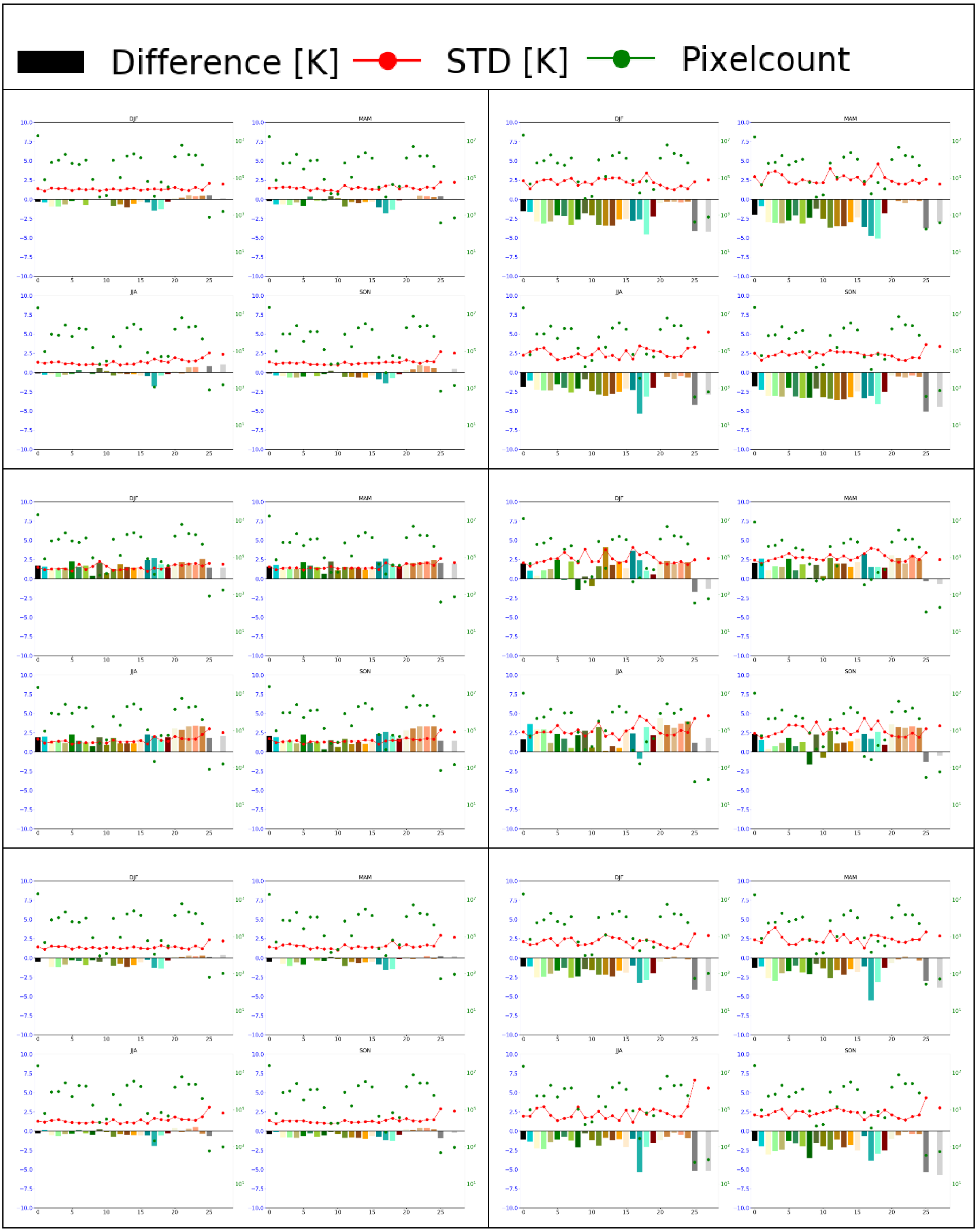

Figure 55: Seasonal differences for different land cover classes; coloured bars are the differences, red points the RSTD and the green points on the right axis show the number of averaged data points. Left row displays night-time and right row daytime data. Upper plots are for MOD11A-SEVCCI, middle plots for MODISA-SEVCCI, and lower plots for MOD11T-SEVCCI.

Figure 56: Seasonal differences for different land cover classes; coloured bars are the differences, red points the RSTD and the green points on the right axis show the number of averaged data points. Left row displays night-time and right row daytime data. Upper plots are for MODIST-SEVCCI, middle plots for ATSOP-SEVCCI, and lower plots for ATSR_3-SEVCCI.

Figure 57: Seasonal differences for different land cover classes; coloured bars are the differences, red points the RSTD and the green points on the right axis show the number of averaged data points. Left row displays night-time and right row daytime data. Upper plots are for ATSR_3-MOD11T, middle plots for ATSR_3-MODIST, and lower plots for MODIST-ATSOP.

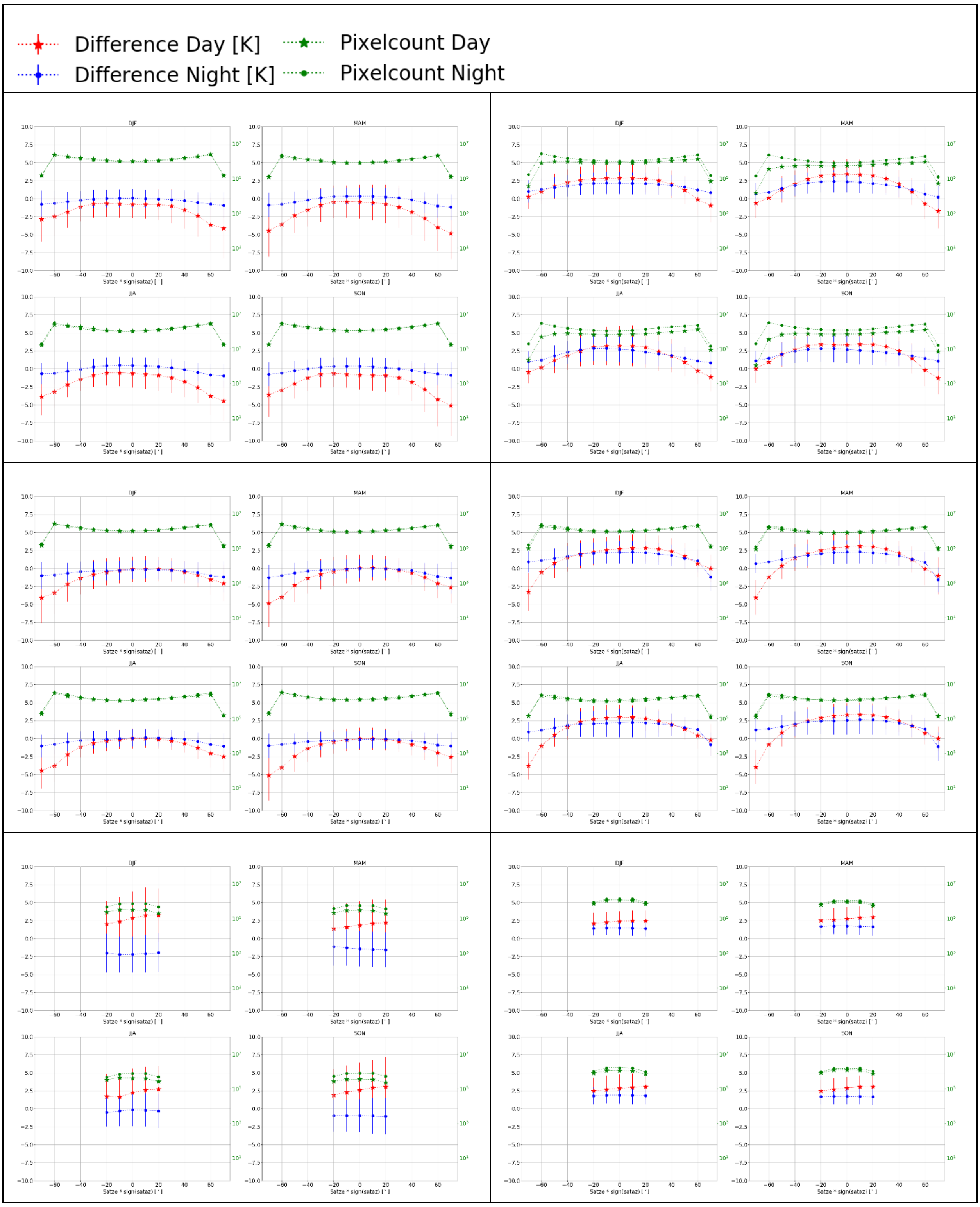

*Figure 58: Seasonal differences versus satze*sign(sataz) of satellite_1; red stars represent the daytime data, blue dots the night-time data, and the green stars and dots on the right axis display the averaged pixel numbers for daytime and night-time data. Upper left plot displays MOD11A-SEVCCI, upper right MODISA-SEVCCI, middle left MOD11T-SEVCCI, middle right MODIST-SEVCCI, lower left ATSOP-SEVCCI, and lower rightATSR_3-SEVCCI.*

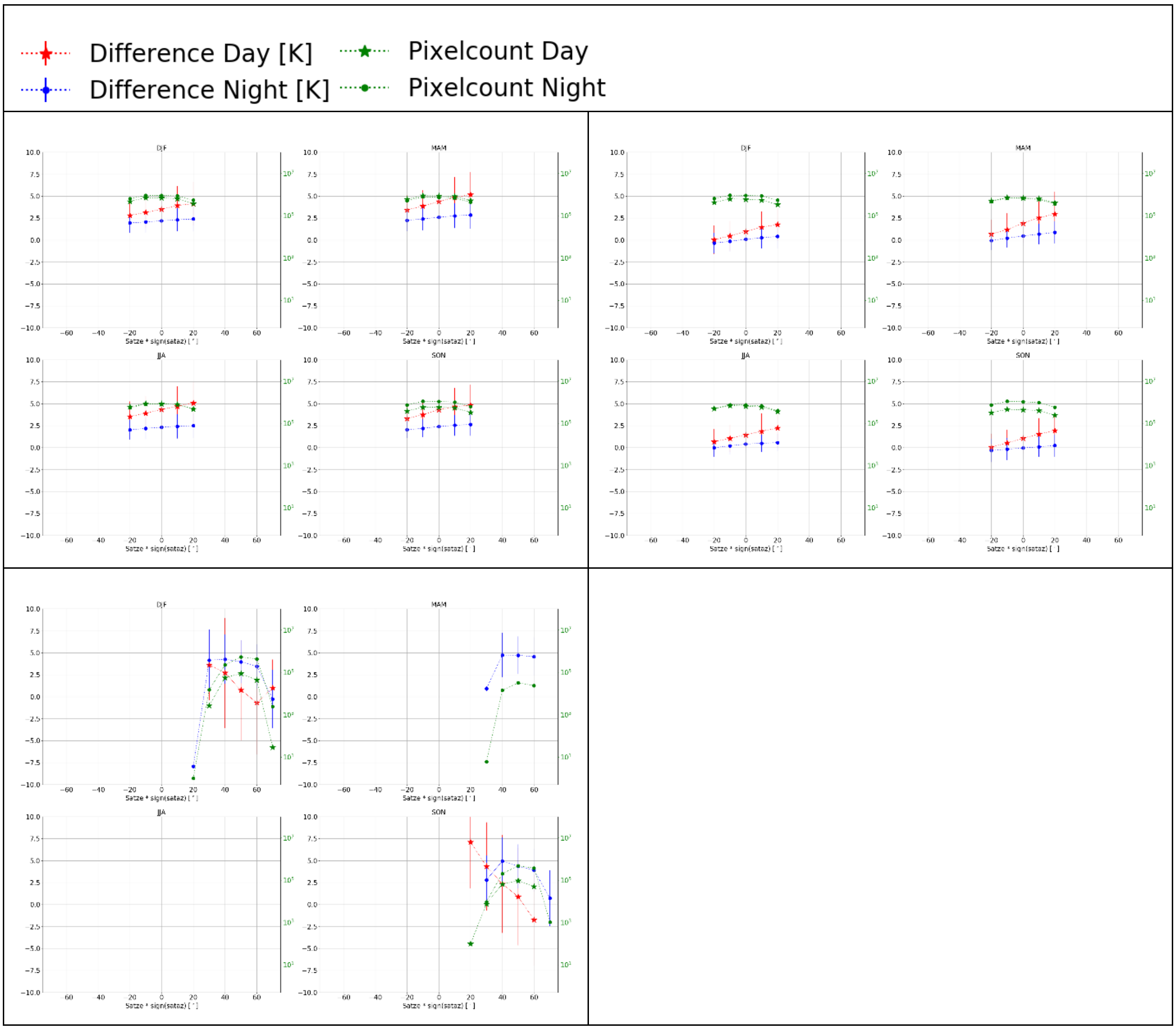

*Figure 59: Seasonal differences versus satze*sign(sataz) of satellite_1; red stars represent the daytime data, blue dots the night-time data, and the green stars and dots on the right axis display the averaged pixel numbers for daytime and night-time data. Upper left plot displays ATSR_3-MOD11T, upper right ATSR_3-MODIST, lower left MODIST-ATSOP.*

7.2. Antarctica

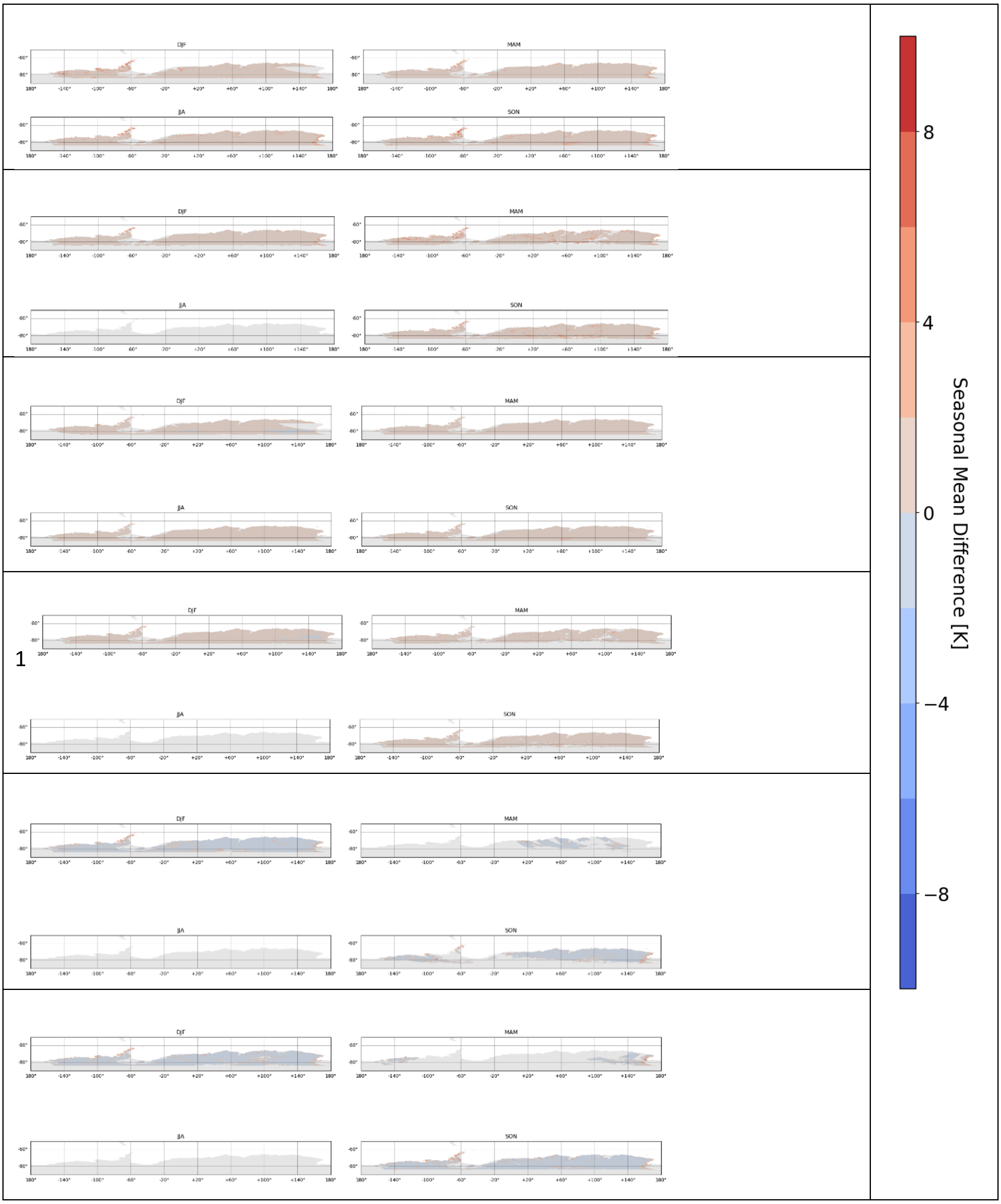

Figure 60: Seasonal mean differences of LST_satellite 1 – LST_satellite 2 in K; two upmost plots are for ATSR_3-MOD11T, two middle plots for ATSR_3-MODIST, and tow lowest plots for MODIST-ATSOPI, each time for night-time and daytime data, respectively.

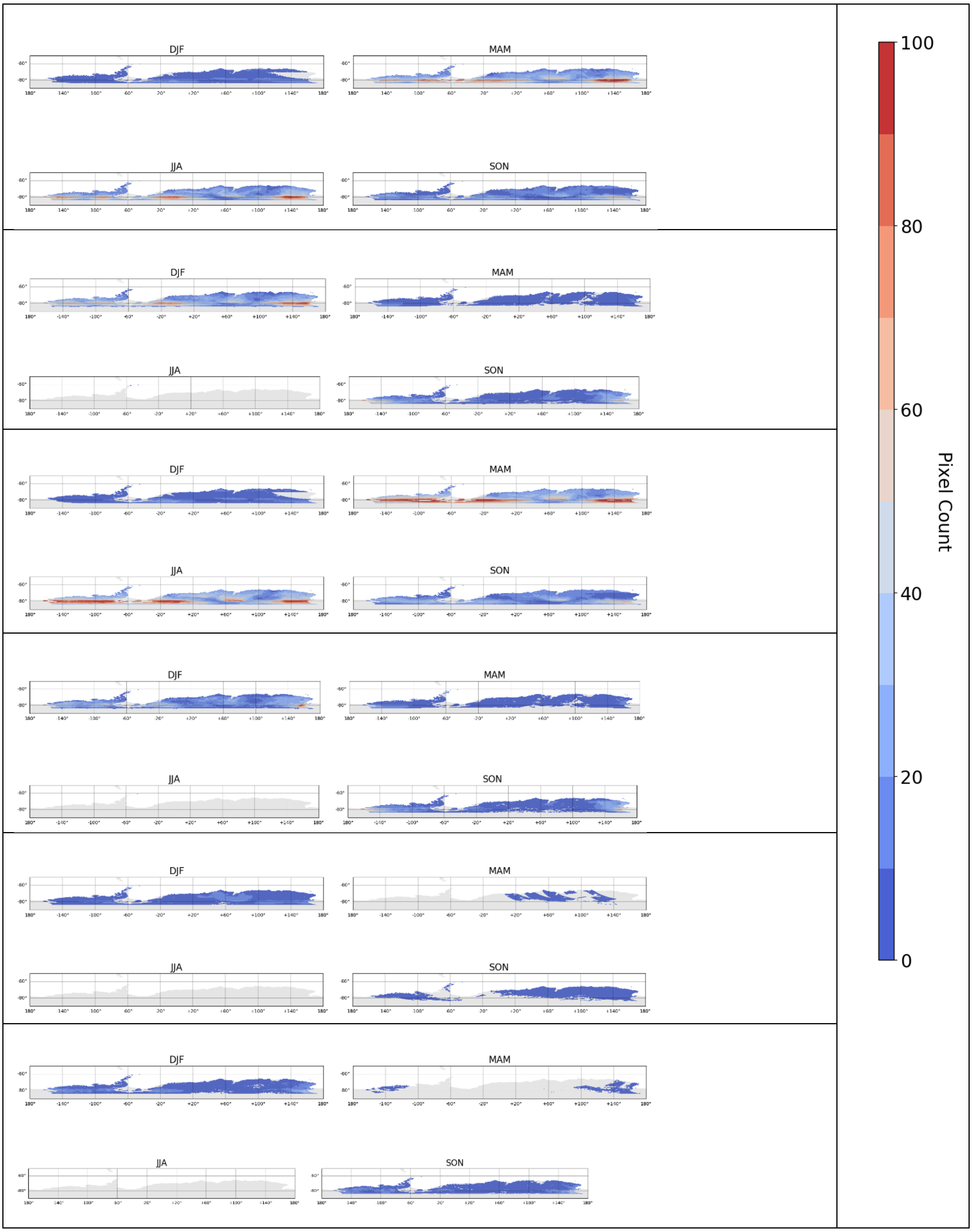

Figure 61: Number of seasonal averaged data points per pixel; two upmost plots are for ATSR_3-MOD11T, two middle plots for ATSR_3-MODIST, and two lowest plots for MODIST-ATSOP. Each time for night-time and daytime data, respectively.

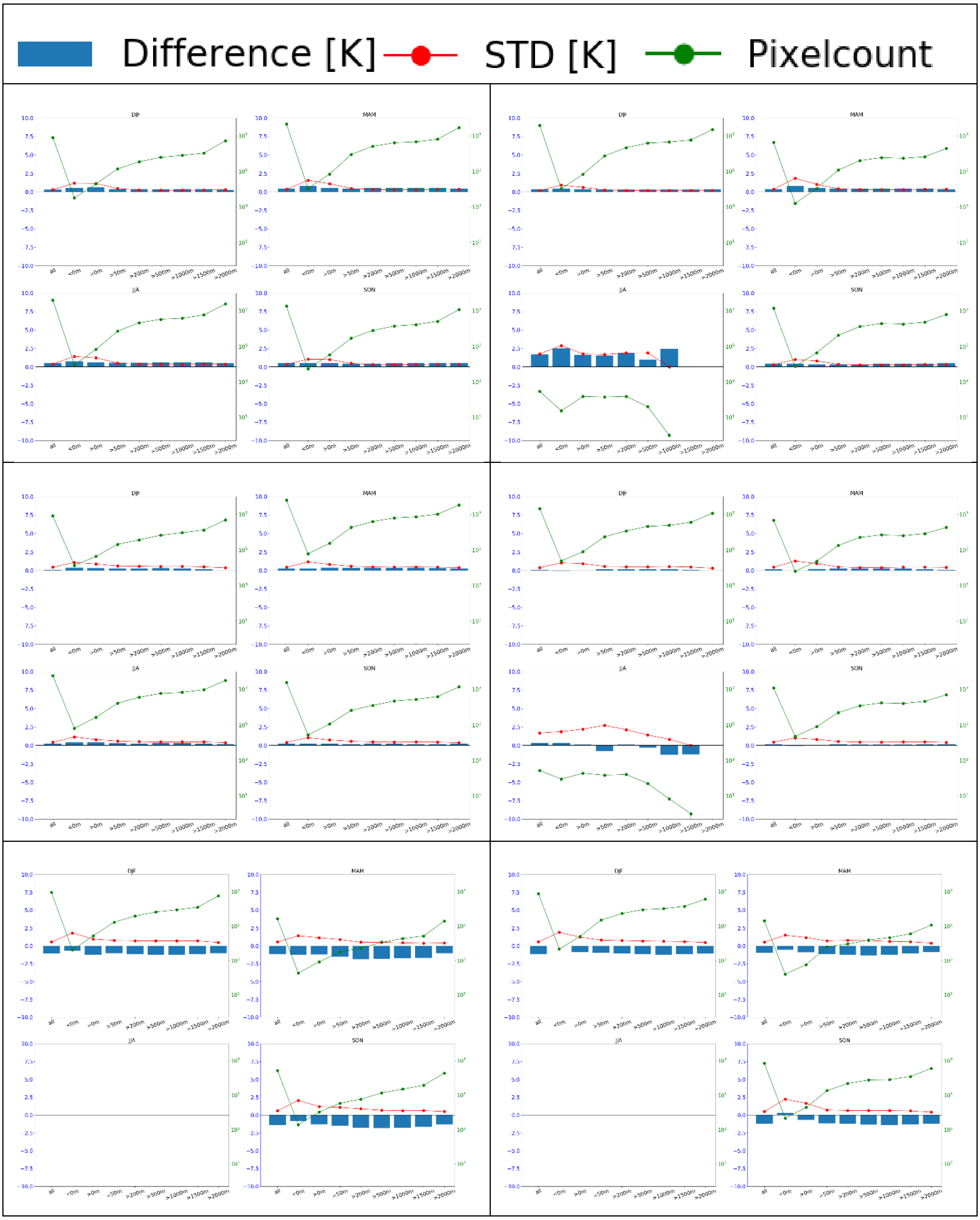

Figure 62: Seasonal differences for different elevation classes; blue bars are the median differences, red points the RSTD and the green points on the right axis show the number of averaged data points Left row displays night-time and right row daytime data. Upper plots are for ATSR_3-MOD11T, middle plots for ATSR_3-MODIST, and lower plots for MODIST-ATSOP.

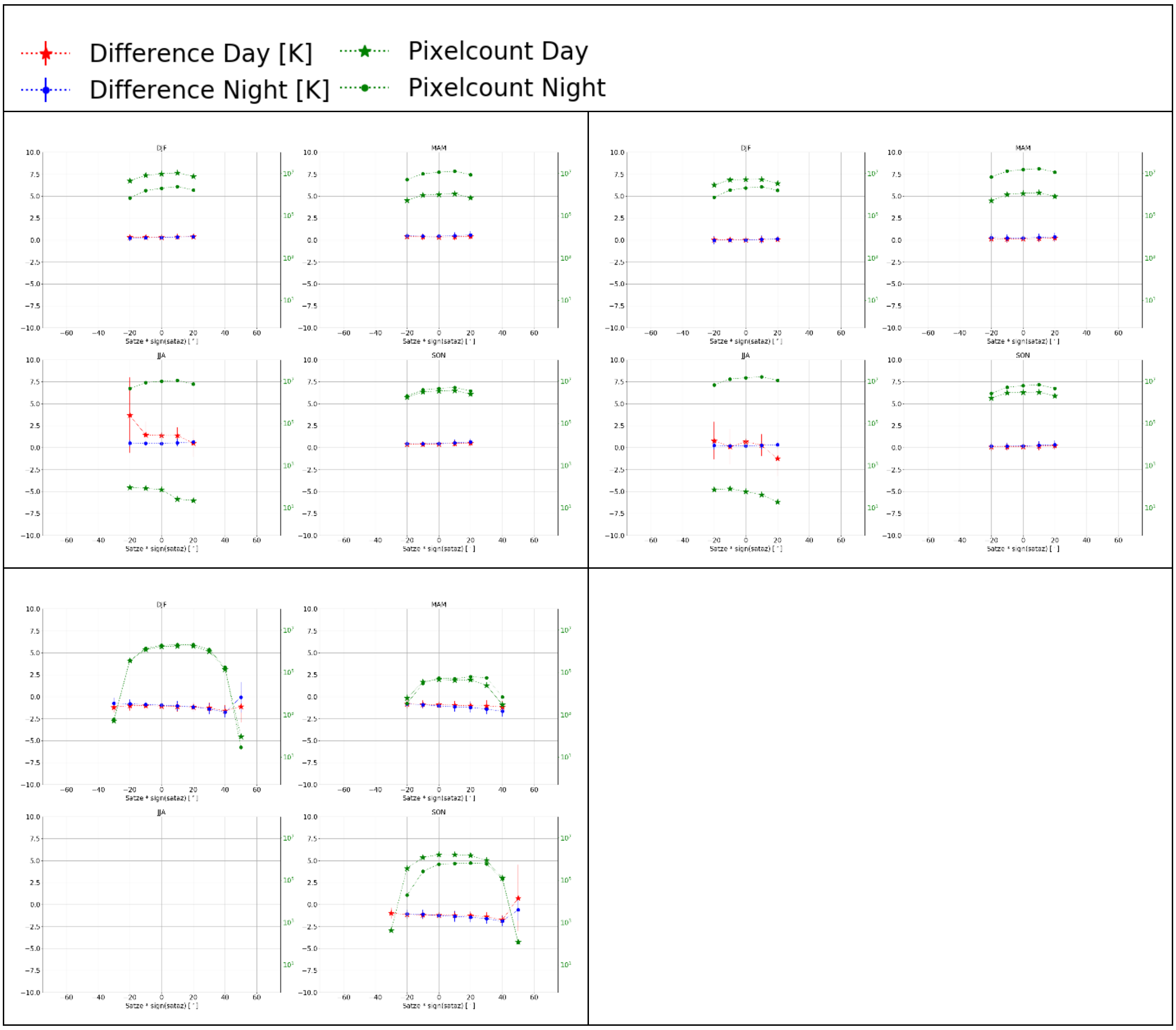

Figure 63: Seasonal differences versus satze*sign(sataz) of satellite_1; red stars represent the daytime data, blue dots the night-time data, and the green stars and dots on the right axis display the averaged pixel numbers for daytime and night-time data. Upper left plot displays ATSR_3-MOD11T, upper right ATSR_3-MODIST, lower left MODIST-ATSOP.

7.3. Asia

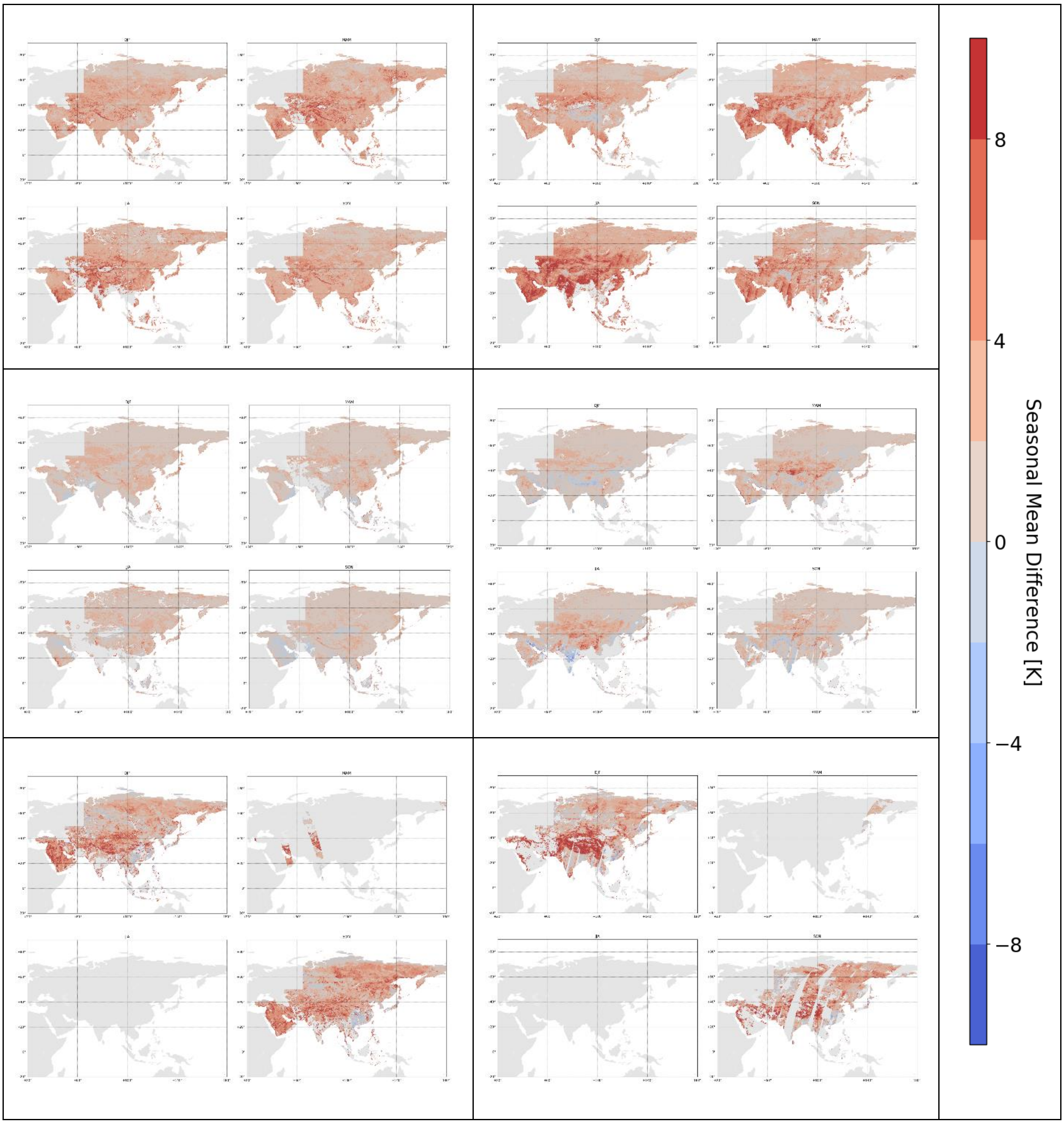

Figure 64: Seasonal mean differences of LST_satellite 1 – LST_satellite 2 in K; left row displays night-time and right row daytime data. Upper plots are for ATSR_3-MOD11T, middle plots for ATSR_3-MODIST, and lower plots for MODIST-ATSOP.

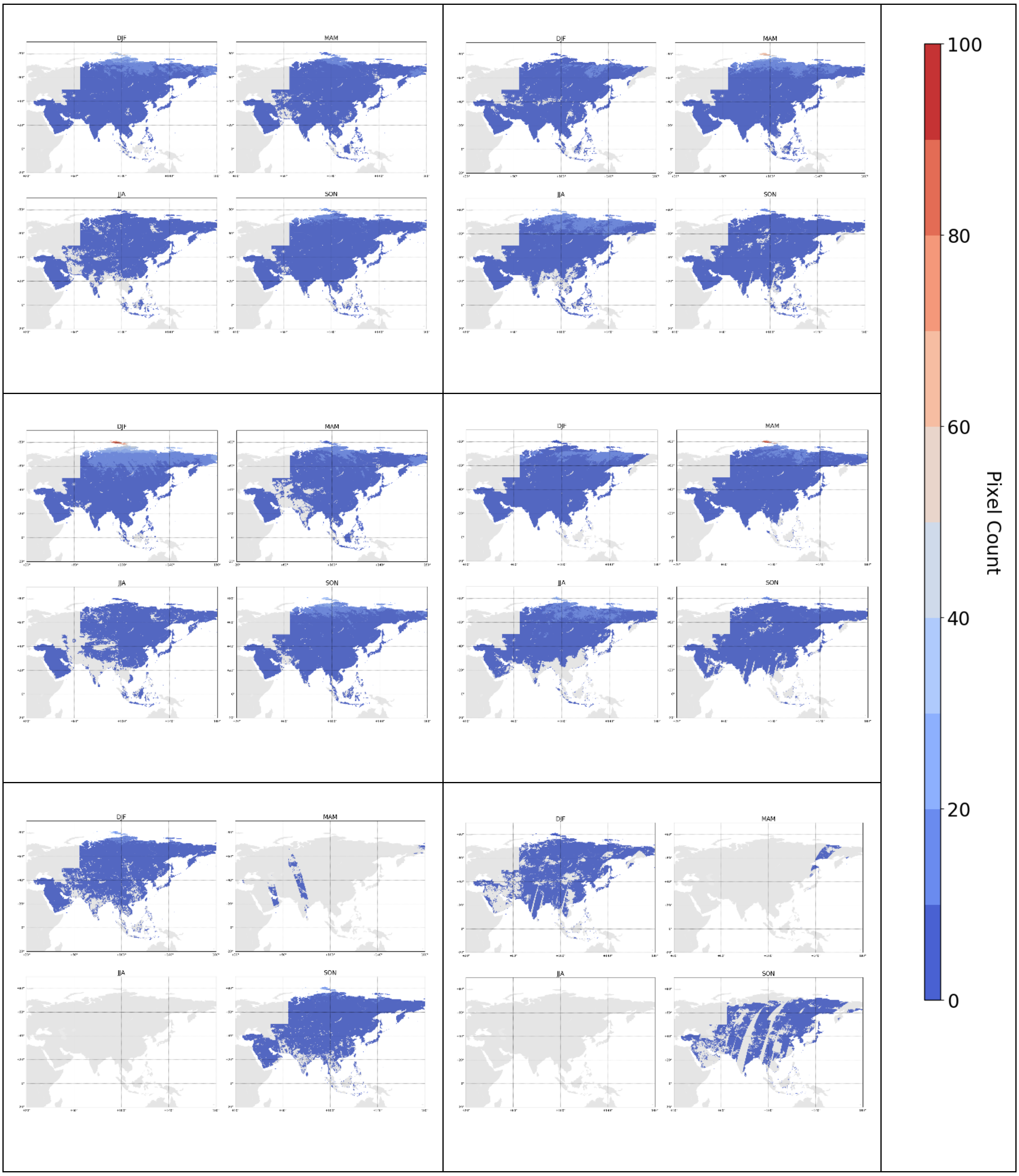

Figure 65: Number of seasonal averaged data points per pixel; left row displays night-time and right row daytime data. Upper plots are for ATSR_3-MOD11T, middle plots for ATSR_3-MODIST, and lower plots for MODIST-ATSOP.

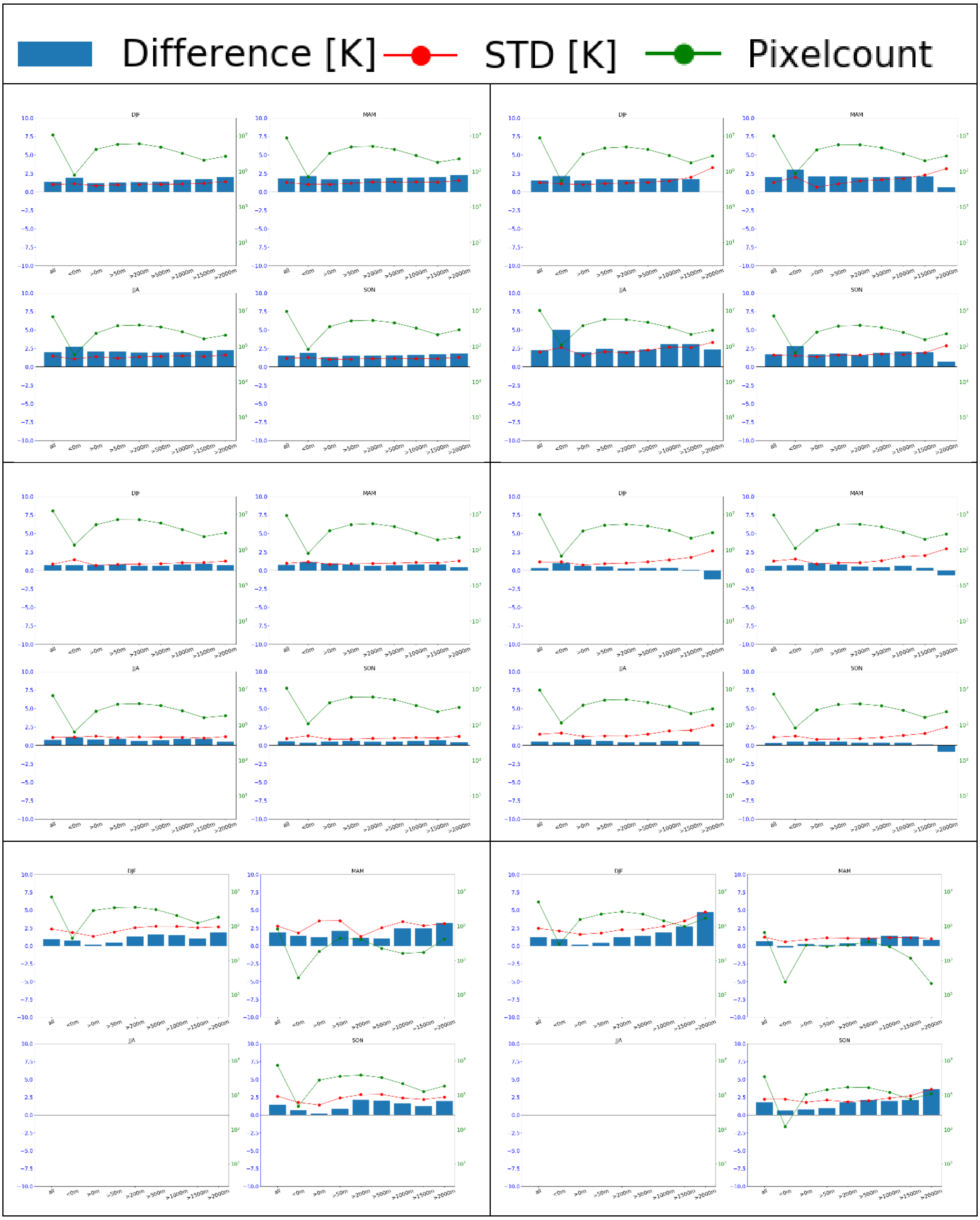

Figure 66: Seasonal differences for different elevation classes; blue bars are the median differences, red points the RSTD and the green points on the right axis show the number of averaged data points Left row displays night-time and right row daytime data. Upper plots are for ATSR_3-MOD11T, middle plots for ATSR_3-MODIST, and lower plots for MODIST-ATSOP.

Figure 67: Seasonal differences for different land cover classes; coloured bars are the differences, red points the RSTD and the green points on the right axis show the number of averaged data points. Left row displays night-time and right row daytime data. Upper plots are for ATSR_3-MOD11T, middle plots for ATSR_3-MODIST, and lower plots for MODIST-ATSOP.

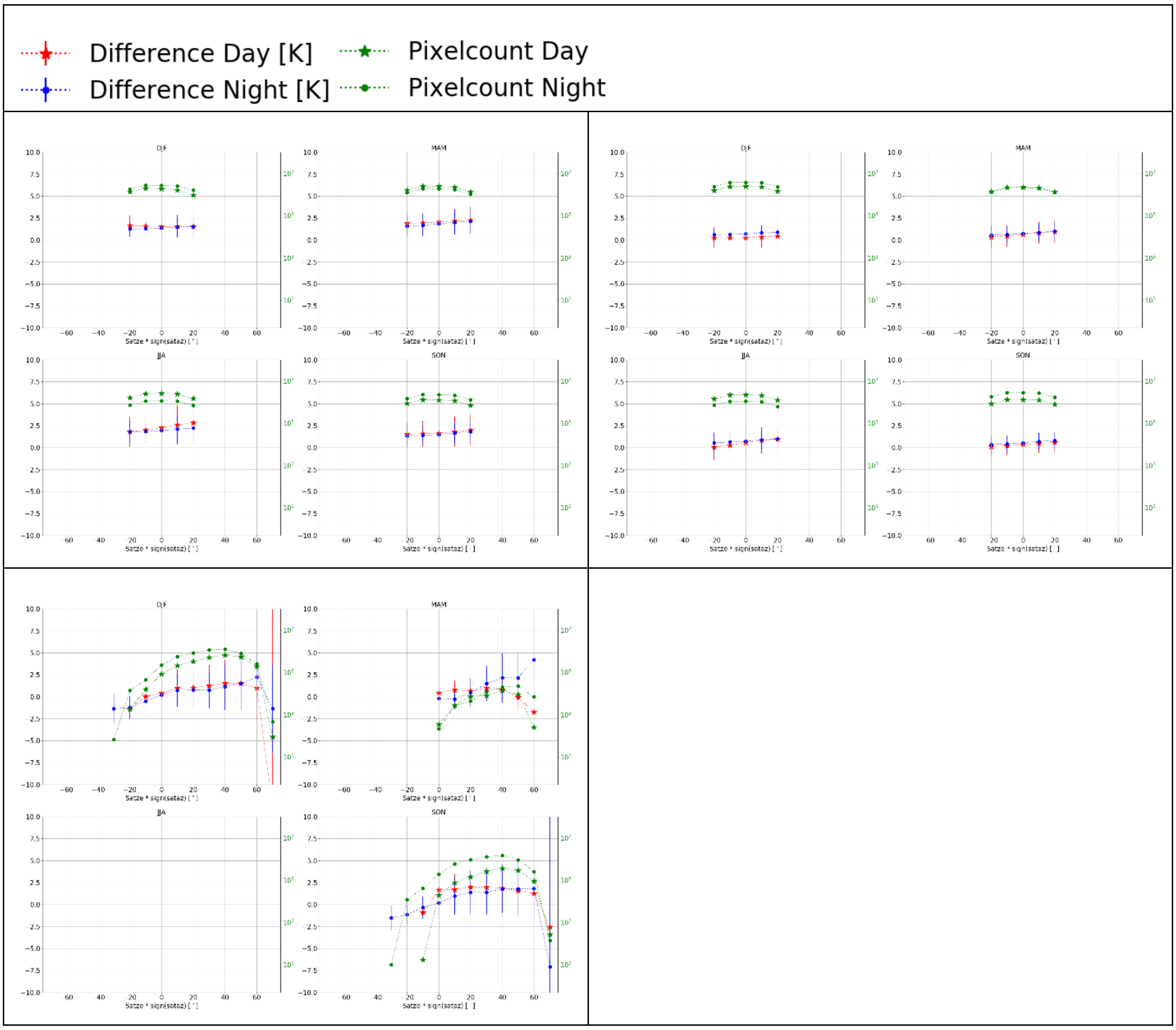

*Figure 68: Seasonal differences versus satze*sign(sataz) of satellite_1; red stars represent the daytime data, blue dots the night-time data, and the green stars and dots on the right axis display the averaged pixel numbers for daytime and night-time data. Upper left plot displays ATSR_3-MOD11T, upper right ATSR_3-MODIST, lower left MODIST-ATSOP.*

7.4. Australia

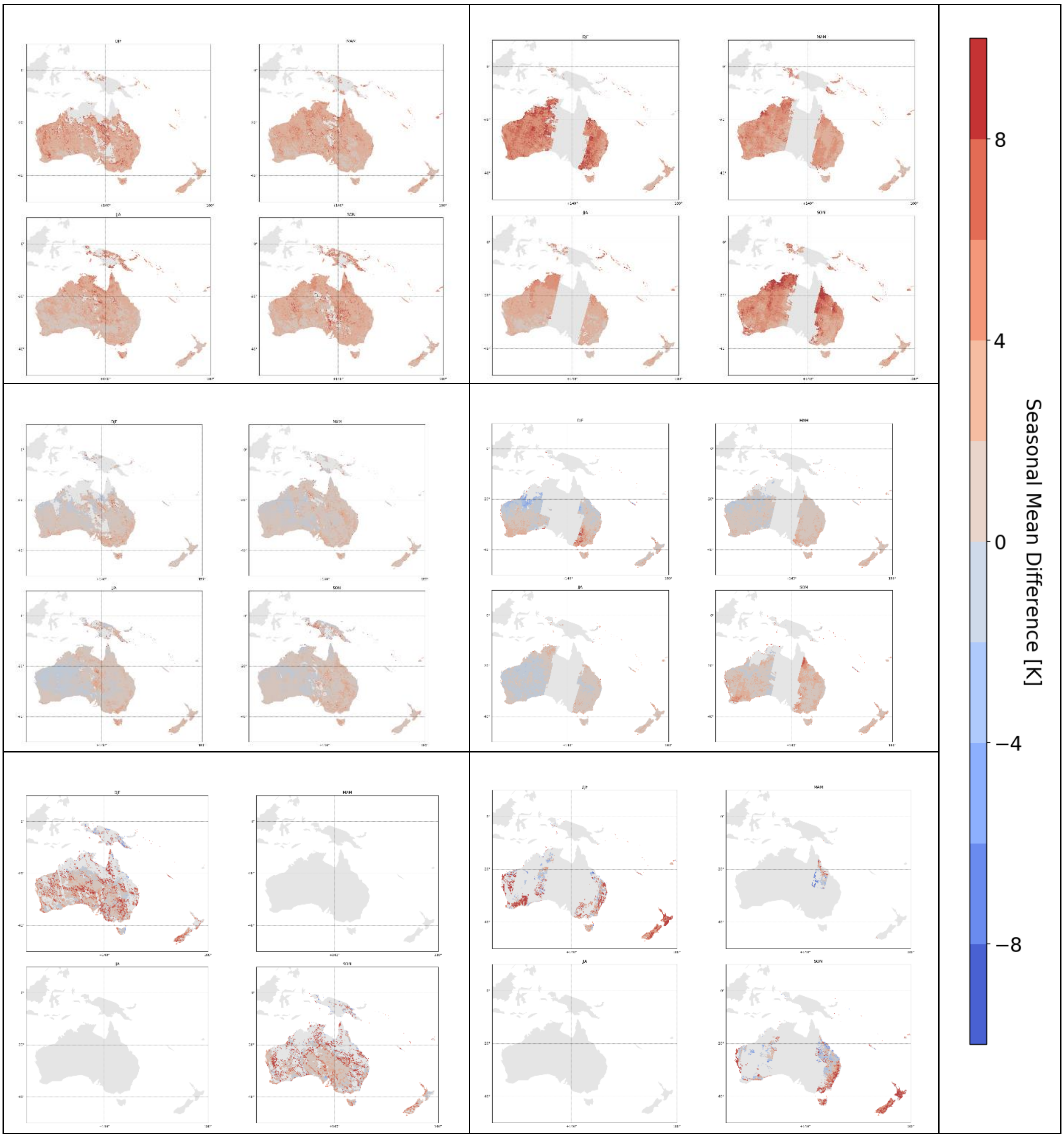

Figure 69: Seasonal mean differences of LST_satellite 1 – LST_satellite 2 in K; left row displays night-time and right row daytime data. Upper plots are for ATSR_3-MOD11T, middle plots for ATSR_3-MODIST, and lower plots for MODIST-ATSOP.

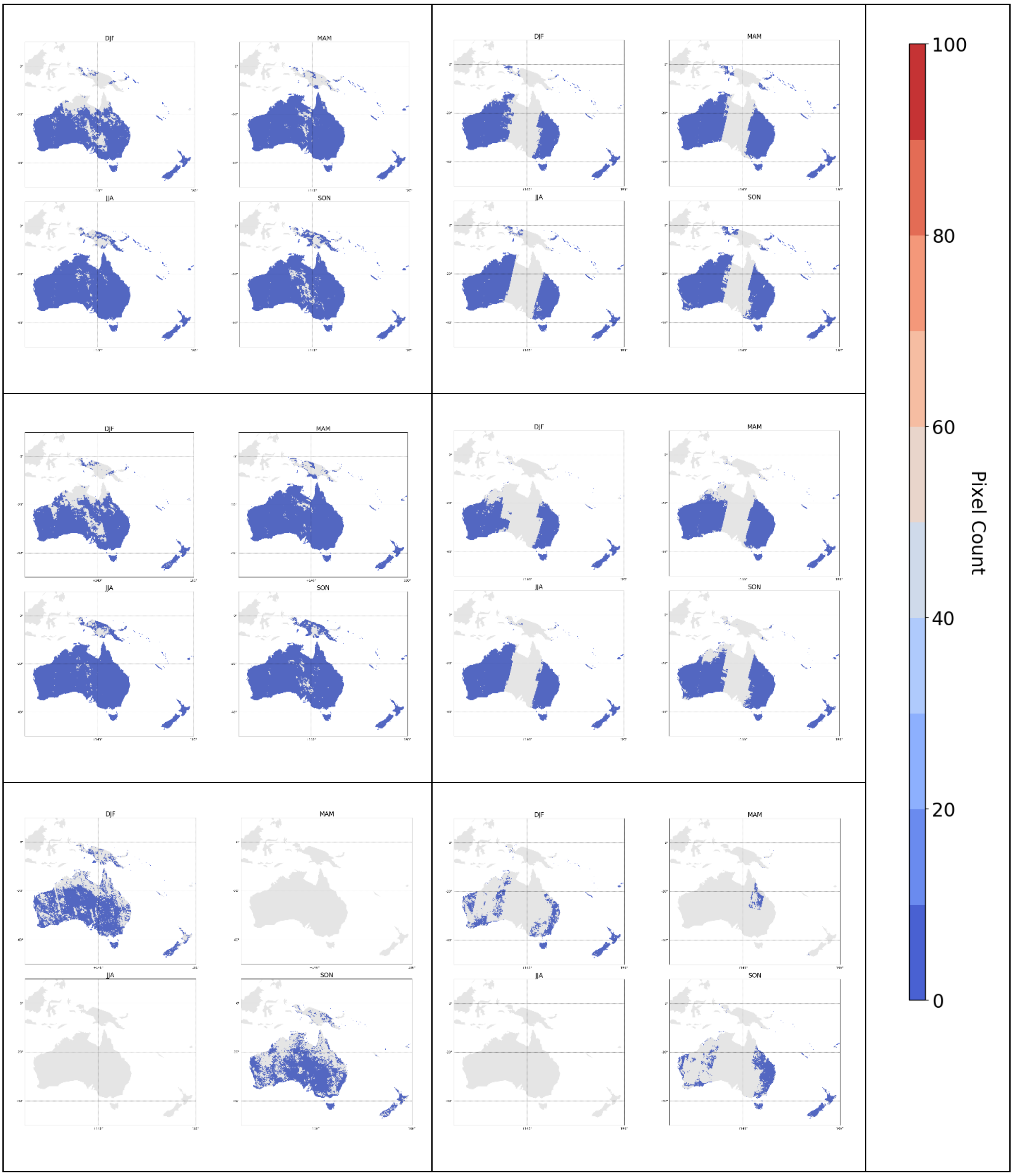

Figure 70: Number of seasonal averaged data points per pixel; left row displays night-time and right row daytime data. Upper plots are for ATSR_3-MOD11T, middle plots for ATSR_3-MODIST, and lower plots for MODIST-ATSOP.

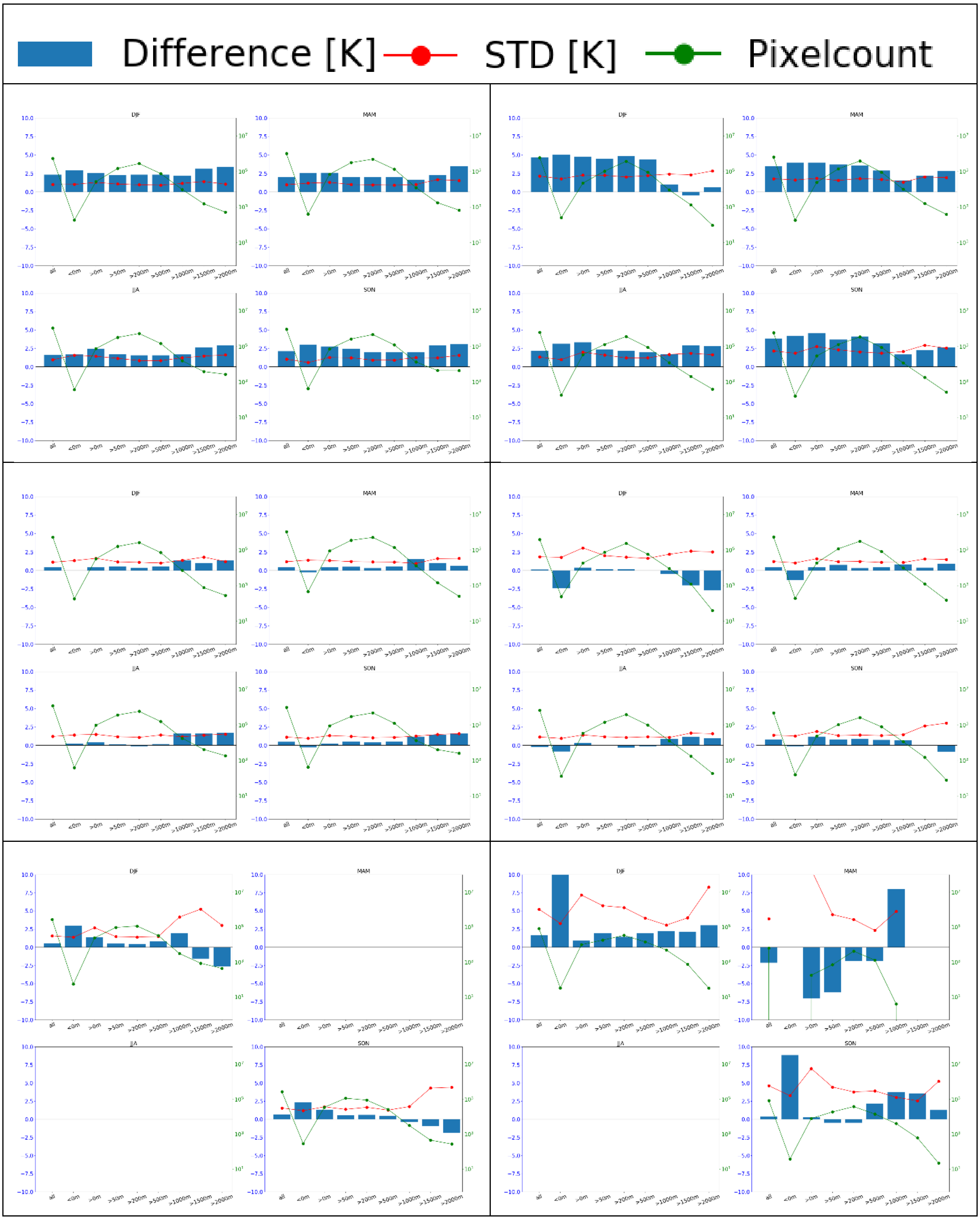

Figure 71: Seasonal differences for different elevation classes; blue bars are the median differences, red points the RSTD and the green points on the right axis show the number of averaged data points Left row displays night-time and right row daytime data. Upper plots are for ATSR_3-MOD11T, middle plots for ATSR_3-MODIST, and lower plots for MODIST-ATSOP.

Figure 72: Seasonal differences for different land cover classes; coloured bars are the differences, red points the RSTD and the green points on the right axis show the number of averaged data points. Left row displays night-time and right row daytime data. Upper plots are for ATSR_3-MOD11T, middle plots for ATSR_3-MODIST, and lower plots for MODIST-ATSOP.

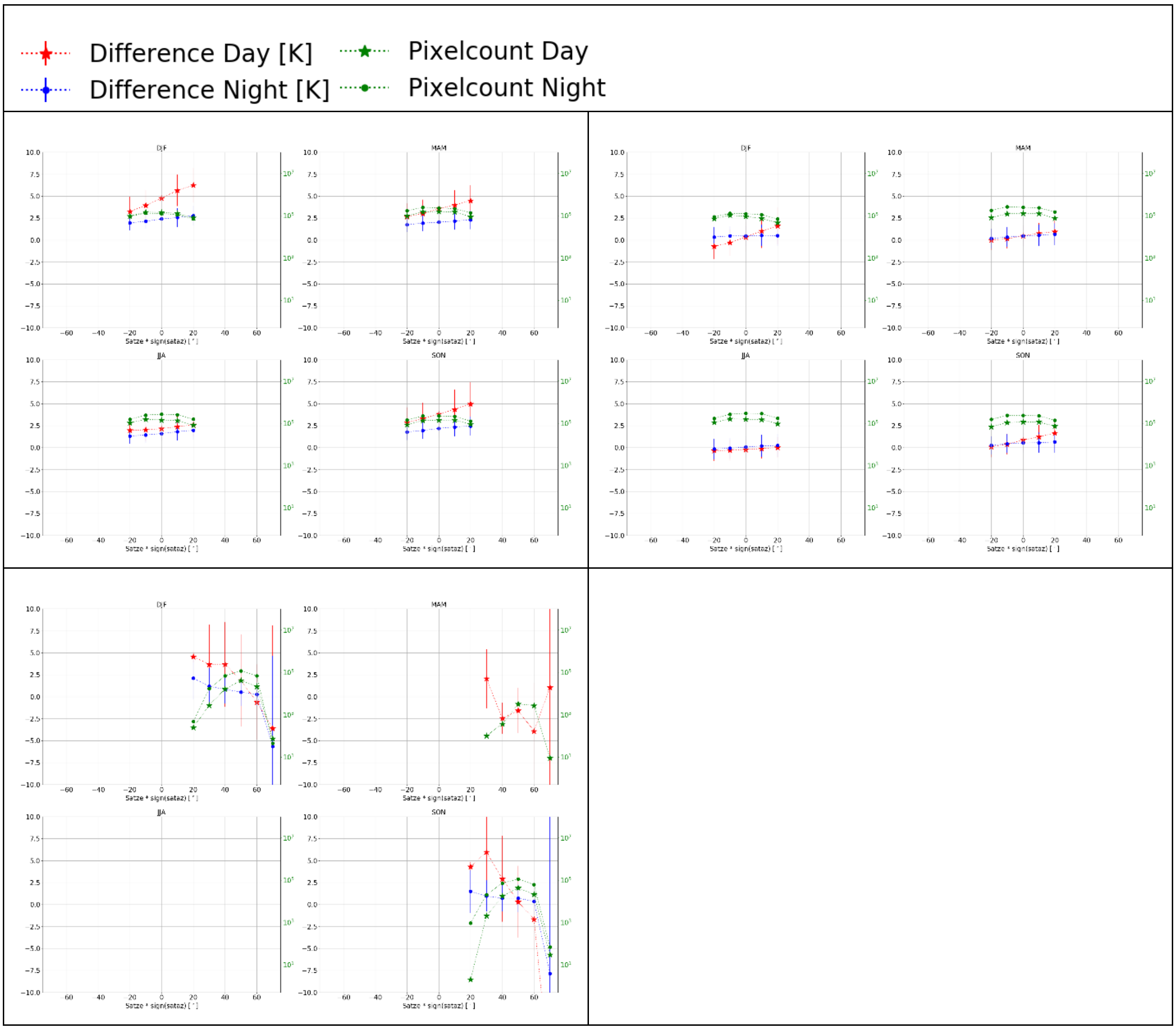

Figure 73: Seasonal differences versus satze*sign(sataz) of satellite_1; red stars represent the daytime data, blue dots the night-time data, and the green stars and dots on the right axis display the averaged pixel numbers for daytime and night-time data. Upper left plot displays ATSR_3-MOD11T, upper right ATSR_3-MODIST, lower left MODIST-ATSOP.

7.5. Europe

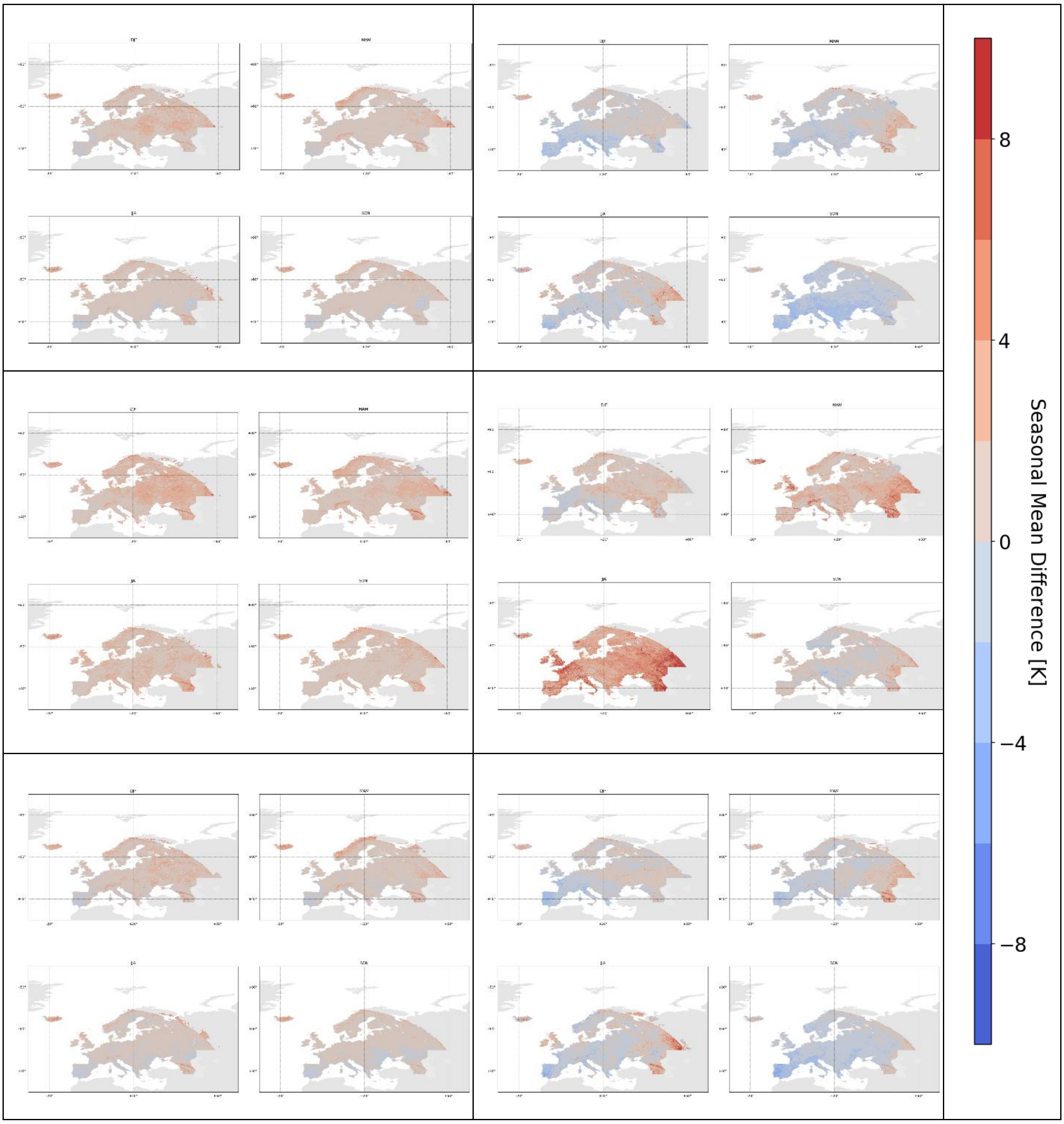

Figure 74: Seasonal mean differences of LST_satellite 1 – LST_satellite 2 in K; left row displays night-time and right row daytime data. Upper plots are for MOD11A-SEVCCI, middle plots for MODISA-SEVCCI, and lower plots for MOD11T-SEVCCI.

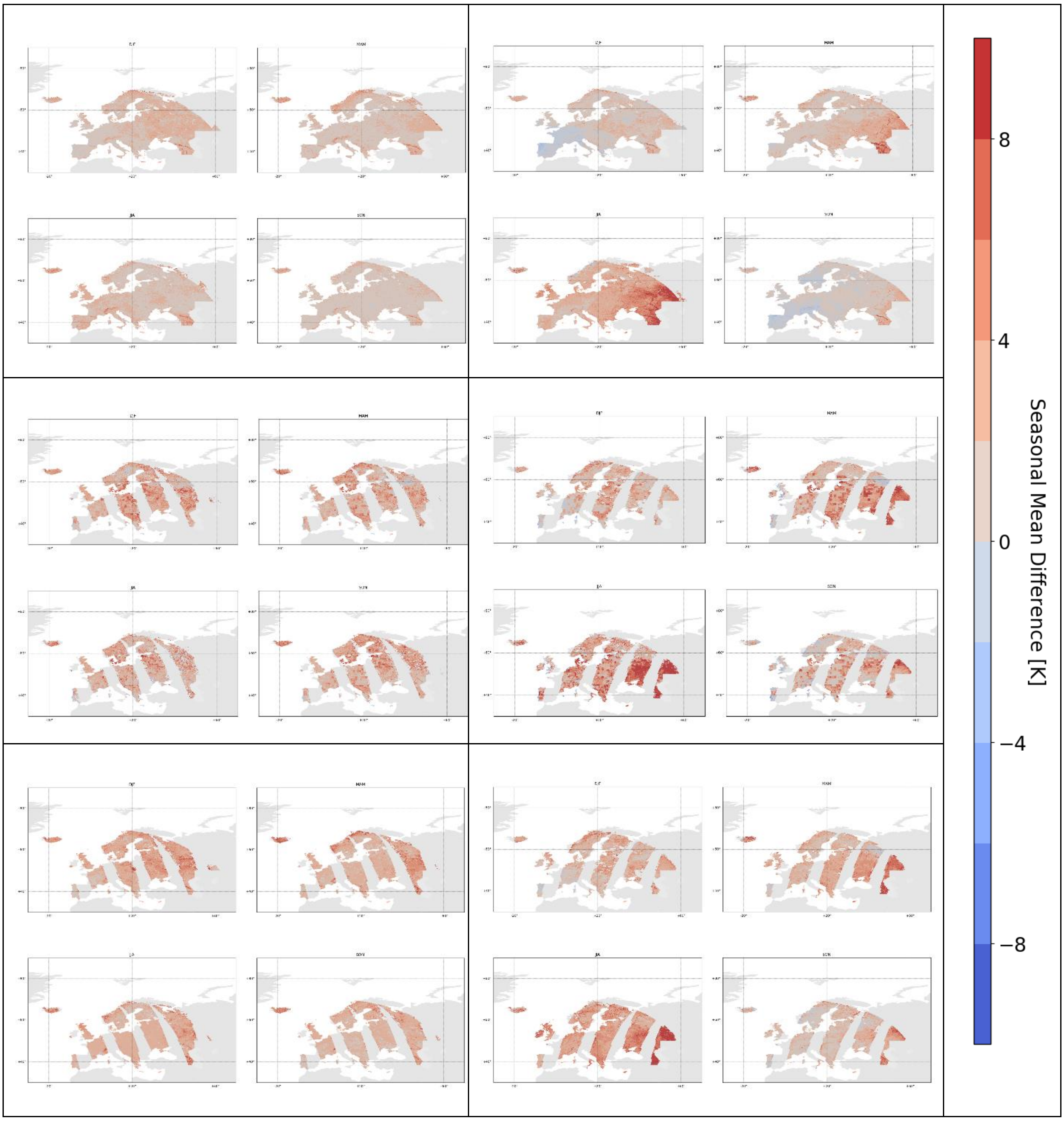

Figure 75: Seasonal mean differences of LST_satellite 1 – LST_satellite 2 in K; left row displays night-time and right row daytime data. Upper plots are for MODIST-SEVCCI, middle plots for ATSOP-SEVCCI, and lower plots for ATSR_3-SEVCCI.

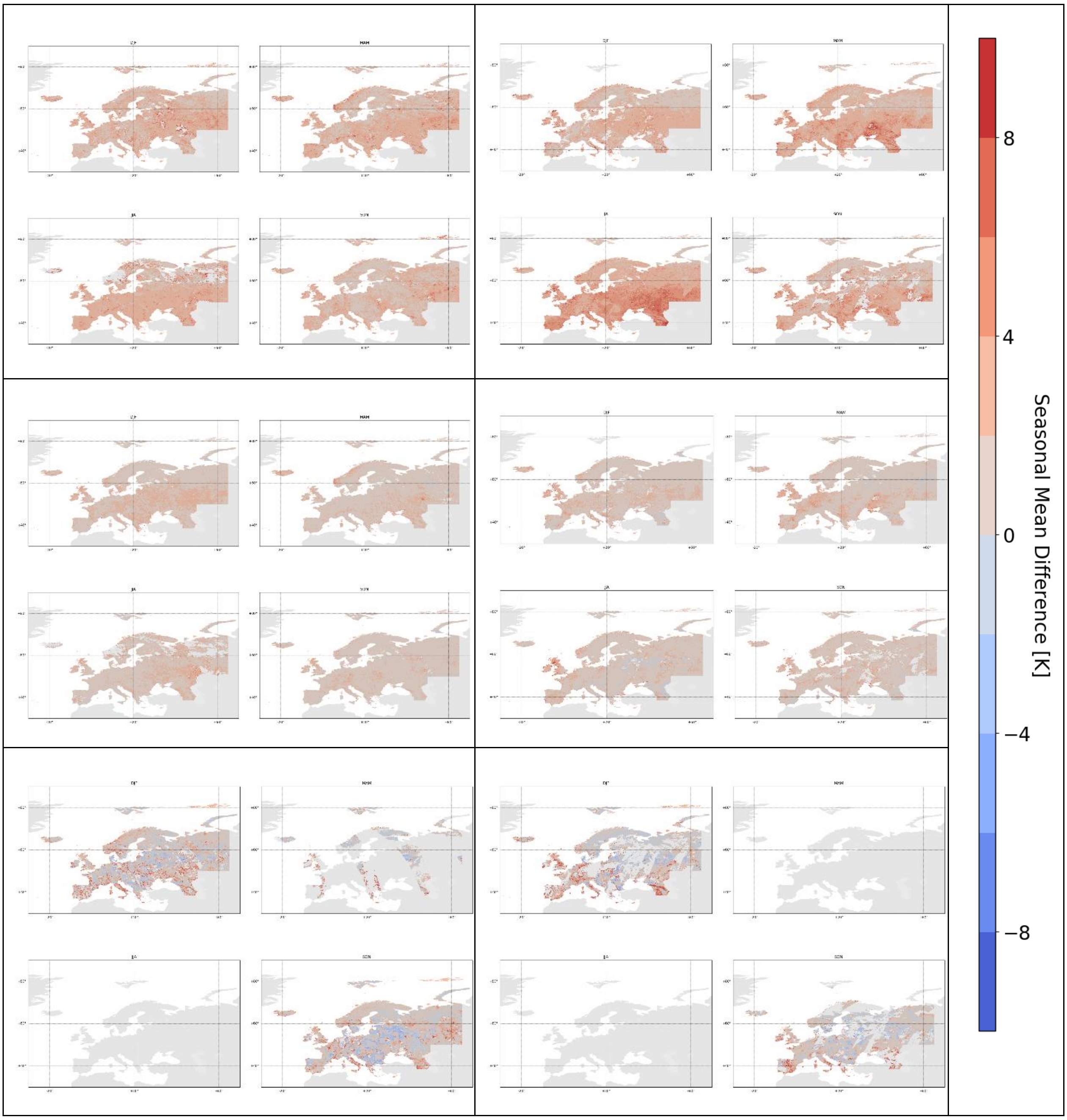

Figure 76: Seasonal mean differences of LST_satellite 1 – LST_satellite 2 in K; left row displays night-time and right row daytime data. Upper plots are for ATSR_3-MOD11T, middle plots for ATSR_3-MODIST, and lower plots for MODIST-ATSOP.

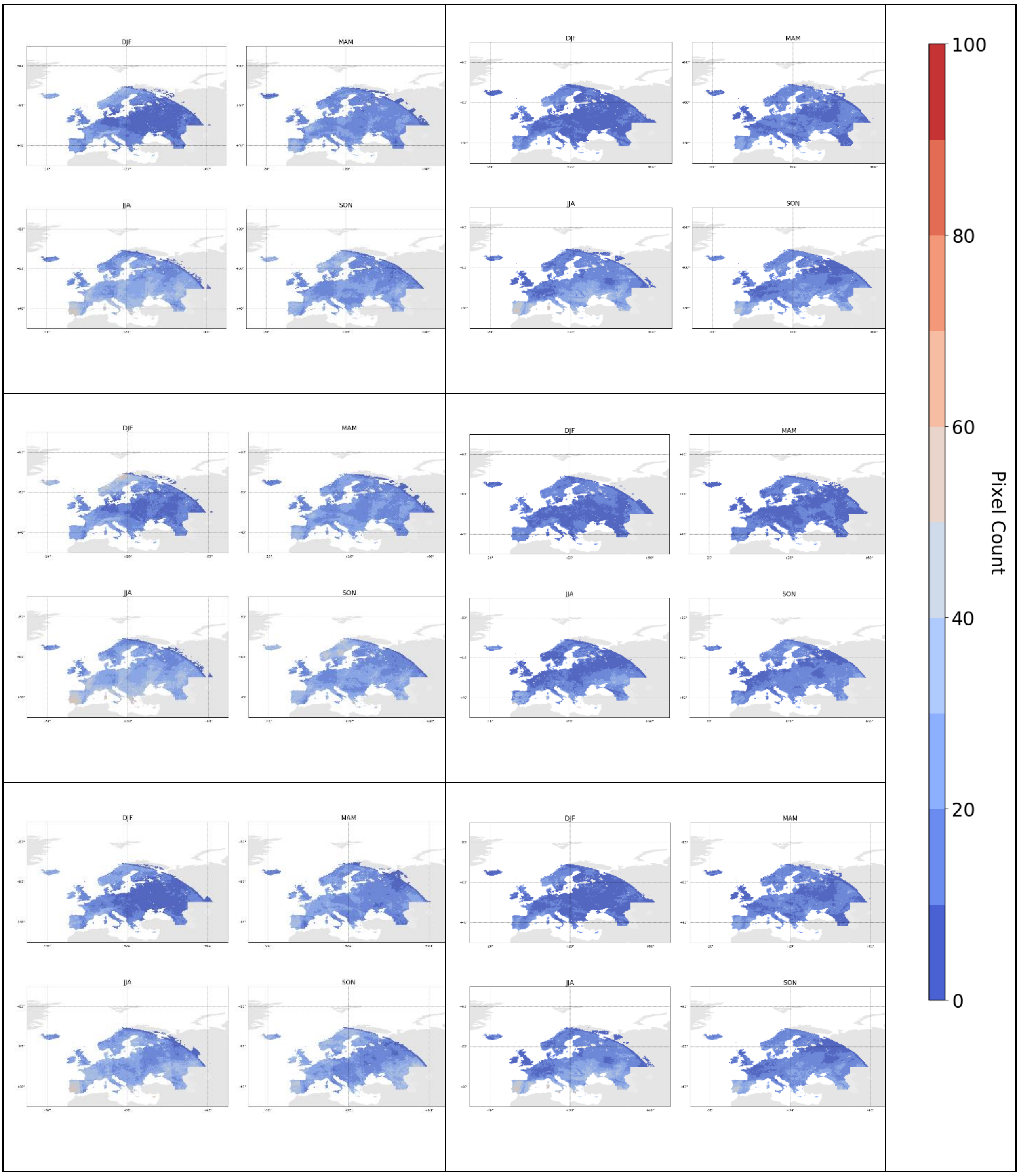

Figure 77: Number of seasonal averaged data points per pixel; left row displays night-time and right row daytime data. Upper plots are for MOD11A-SEVCCI, middle plots for MODISA-SEVCCI, and lower plots for MOD11T-SEVCCI.

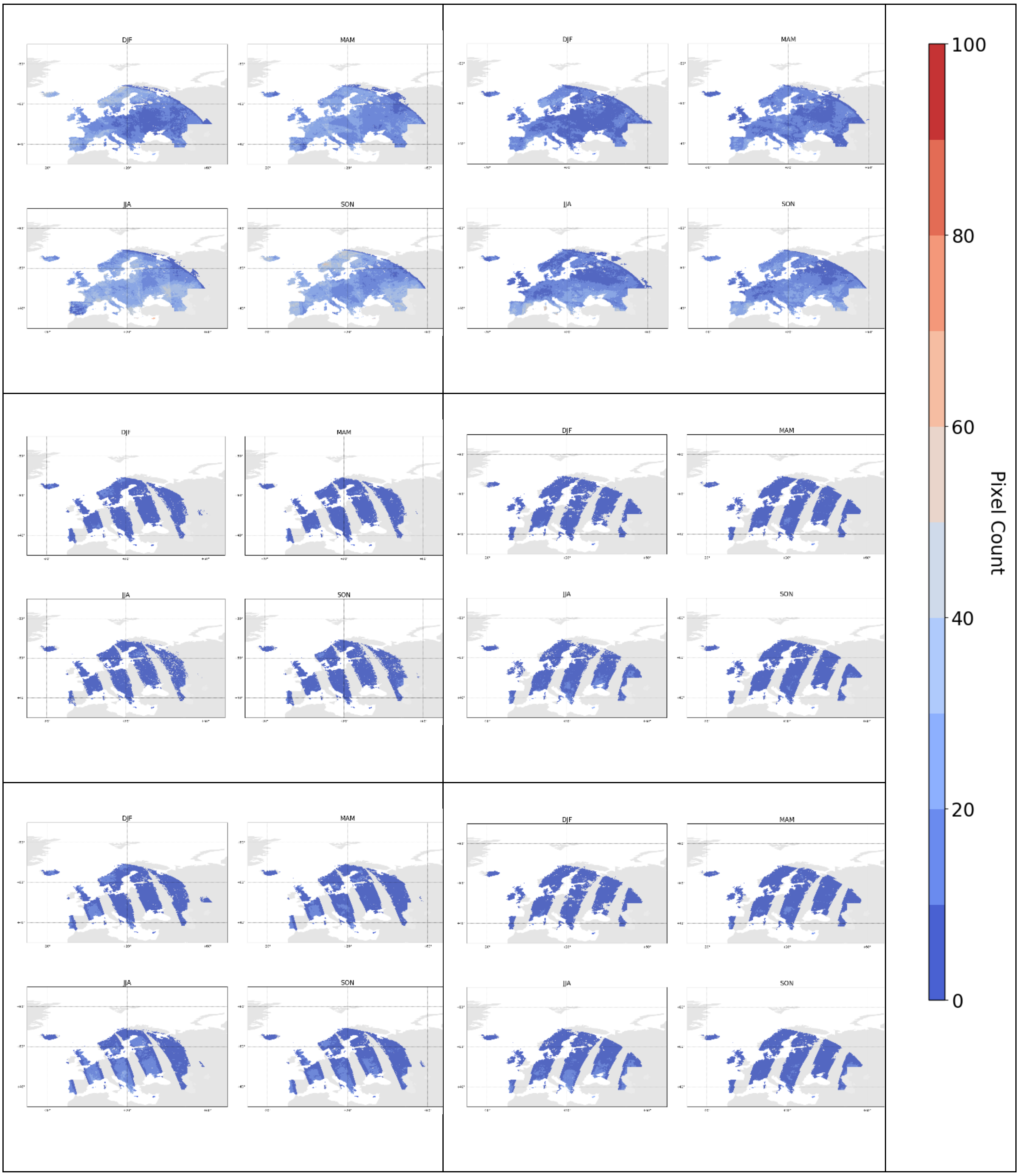

Figure 78: Number of seasonal averaged data points per pixel; left row displays night-time and right row daytime data. Upper plots are for MODIST-SEVCCI, middle plots for ATSOP-SEVCCI, and lower plots for ATSR_3-SEVCCI.

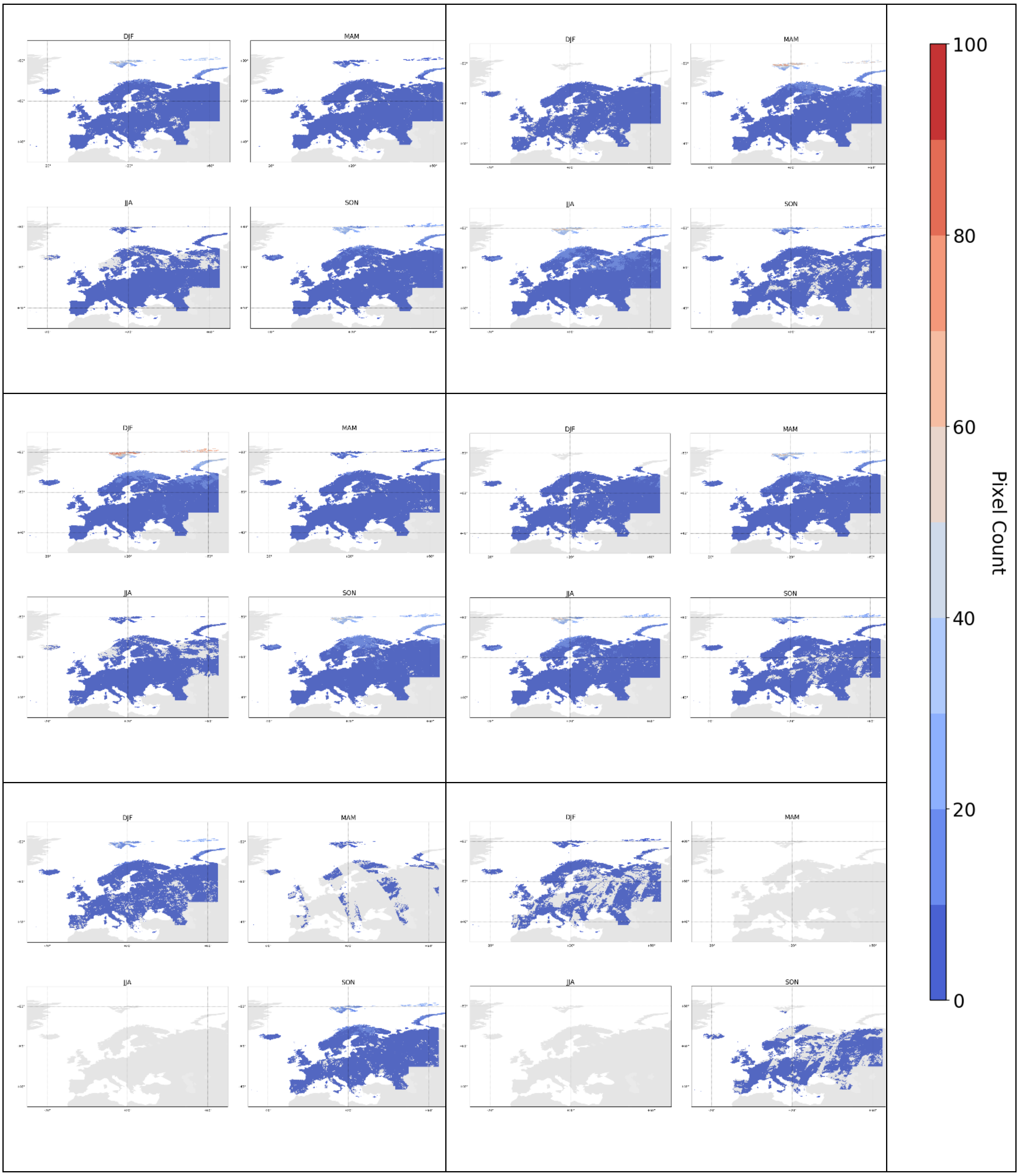

Figure 79: Number of seasonal averaged data points per pixel; left row displays night-time and right row daytime data. Upper plots are for ATSR_3-MOD11T, middle plots for ATSR_3-MODIST, and lower plots for MODIST-ATSOP.

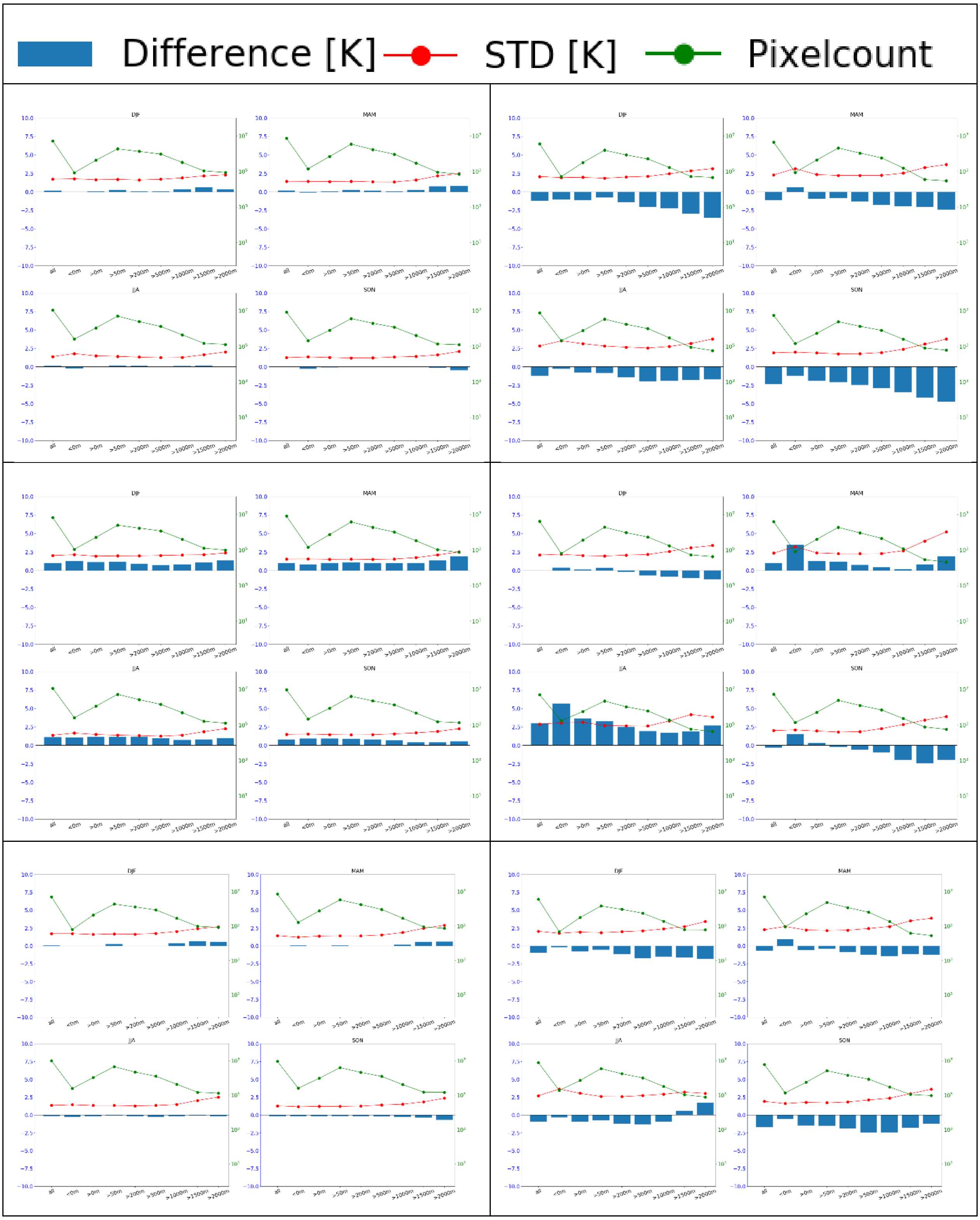

Figure 80: Seasonal differences for different elevation classes; blue bars are the median differences, red points the RSTD and the green points on the right axis show the number of averaged data points Left row displays night-time and right row daytime data. Upper plots are for MOD11A-SEVCCI, middle plots for MODISA-SEVCCI, and lower plots for MOD11T-SEVCCI.

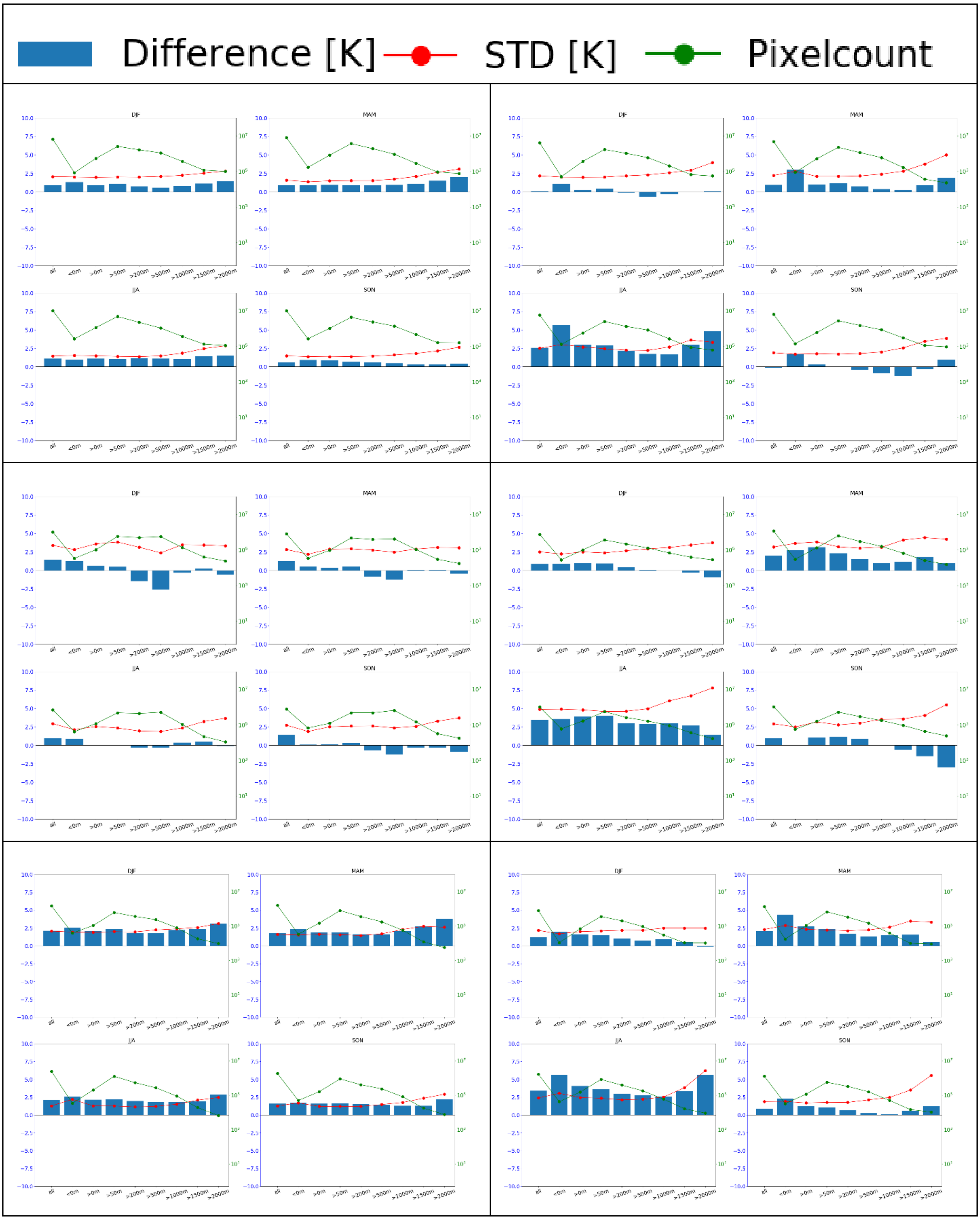

Figure 81: Seasonal differences for different elevation classes; blue bars are the median differences, red points the RSTD and the green points on the right axis show the number of averaged data points Left row displays night-time and right row daytime data. Upper plots are for MODIST-SEVCCI, middle plots for ATSOP-SEVCCI, and lower plots for ATSR_3-SEVCCI.

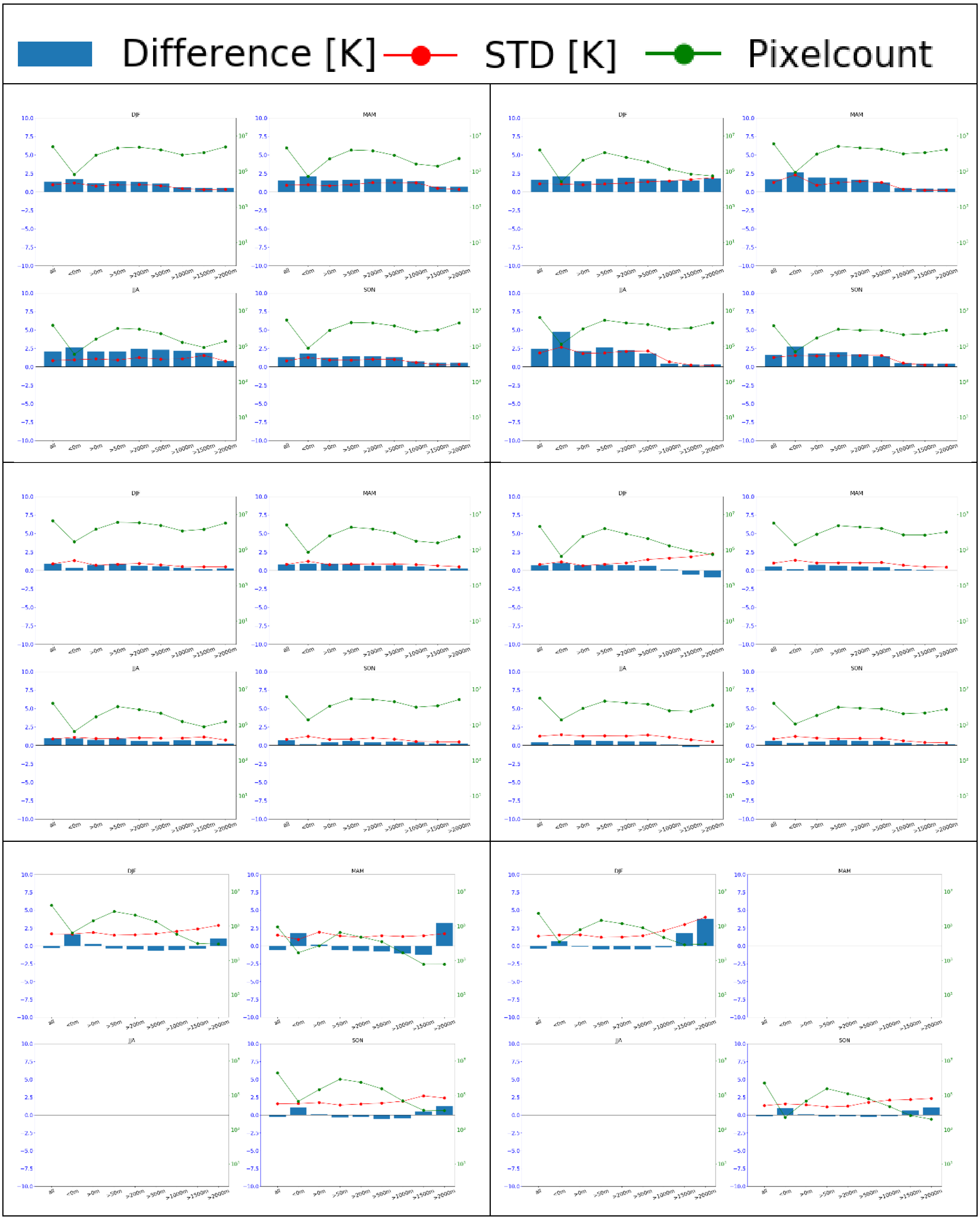

Figure 82: Seasonal differences for different elevation classes; blue bars are the median differences, red points the RSTD and the green points on the right axis show the number of averaged data points Left row displays night-time and right row daytime data. Upper plots are for ATSR_3-MOD11T, middle plots for ATSR_3-MODIST, and lower plots for MODIST-ATSOP.

Figure 83: Seasonal differences for different land cover classes; coloured bars are the differences, red points the RSTD and the green points on the right axis show the number of averaged data points. Left row displays night-time and right row daytime data. Upper plots are for MOD11A-SEVCCI, middle plots for MODISA-SEVCCI, and lower plots for MOD11T-SEVCCI.

Figure 84: Seasonal differences for different land cover classes; coloured bars are the differences, red points the RSTD and the green points on the right axis show the number of averaged data points. Left row displays night-time and right row daytime data. Upper plots are for MODIST-SEVCCI, middle plots for ATSOP-SEVCCI, and lower plots for ATSR_3-SEVCCI.

Figure 85: Seasonal differences for different land cover classes; coloured bars are the differences, red points the RSTD and the green points on the right axis show the number of averaged data points. Left row displays night-time and right row daytime data. Upper plots are for ATSR_3-MOD11T, middle plots for ATSR_3-MODIST, and lower plots for MODIST-ATSOP.

*Figure 86: Seasonal differences versus satze*sign(sataz) of satellite_1; red stars represent the daytime data, blue dots the night-time data, and the green stars and dots on the right axis display the averaged pixel numbers for daytime and night-time data. Upper left plot displays MOD11A-SEVCCI, upper right MODISA-SEVCCI, middle left MOD11T-SEVCCI, middle right MODIST-SEVCCI, lower left ATSOP-SEVCCI, and lower rightATSR_3-SEVCCI.*

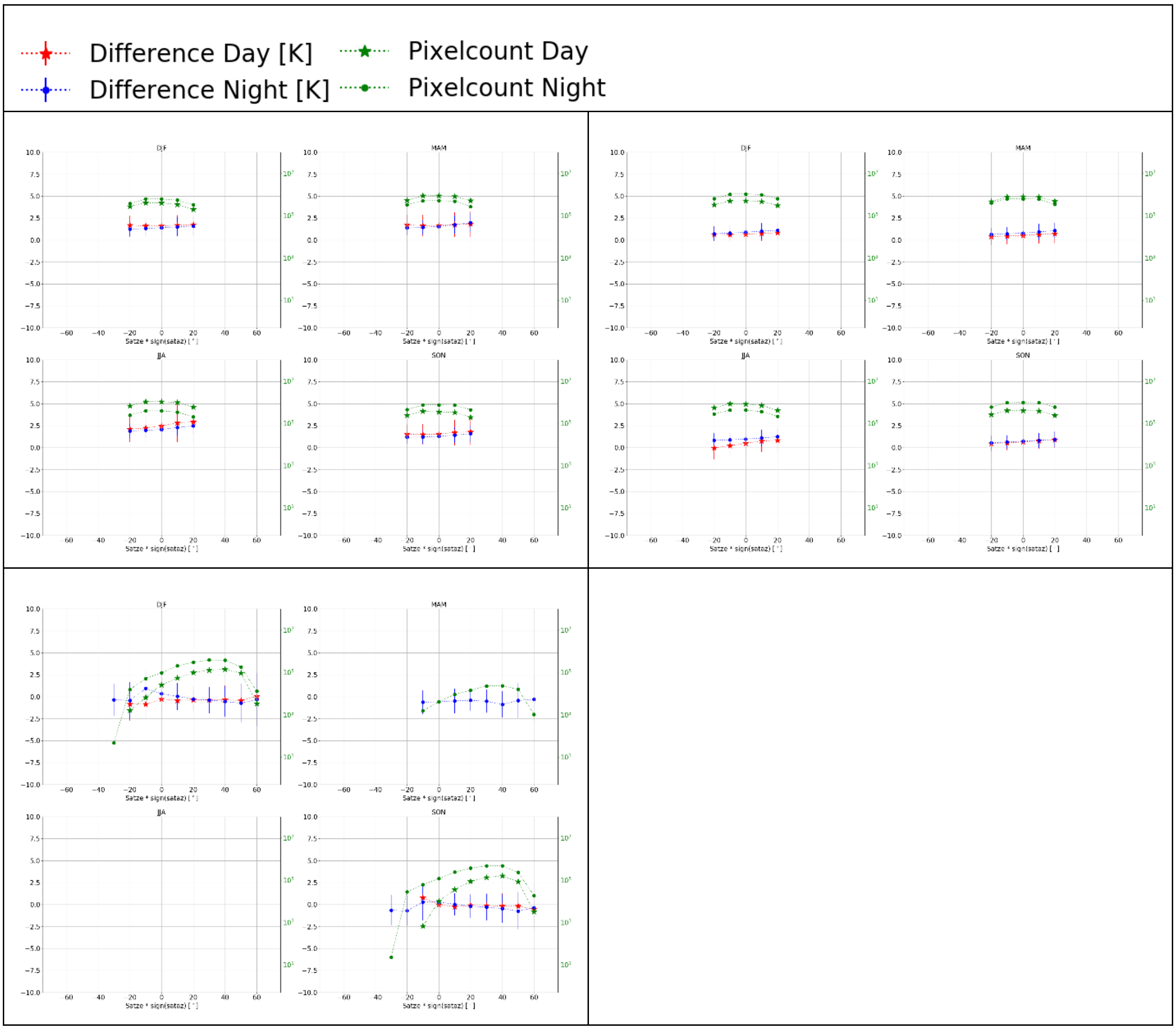

Figure 87: Seasonal differences versus satze*sign(sataz) of satellite_1; red stars represent the daytime data, blue dots the night-time data, and the green stars and dots on the right axis display the averaged pixel numbers for daytime and night-time data. Upper left plot displays ATSR_3-MOD11T, upper right ATSR_3-MODIST, lower left MODIST-ATSOP.

7.6. North America

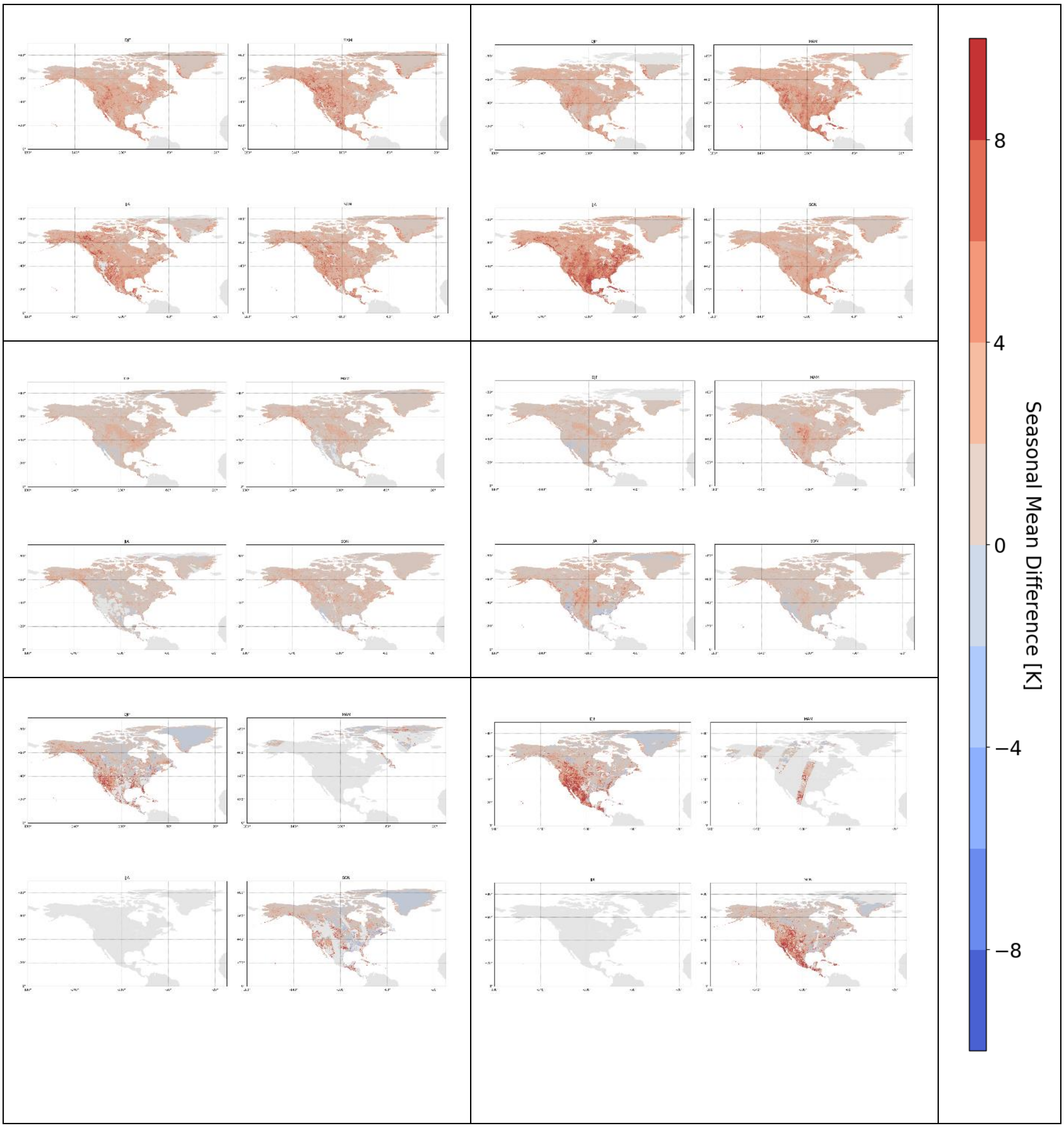

Figure 88: Seasonal mean differences of LST_satellite 1 – LST_satellite 2 in K; left row displays night-time and right row daytime data. Upper plots are for ATSR_3-MOD11T, middle plots for ATSR_3-MODIST, and lower plots for MODIST-ATSOP.

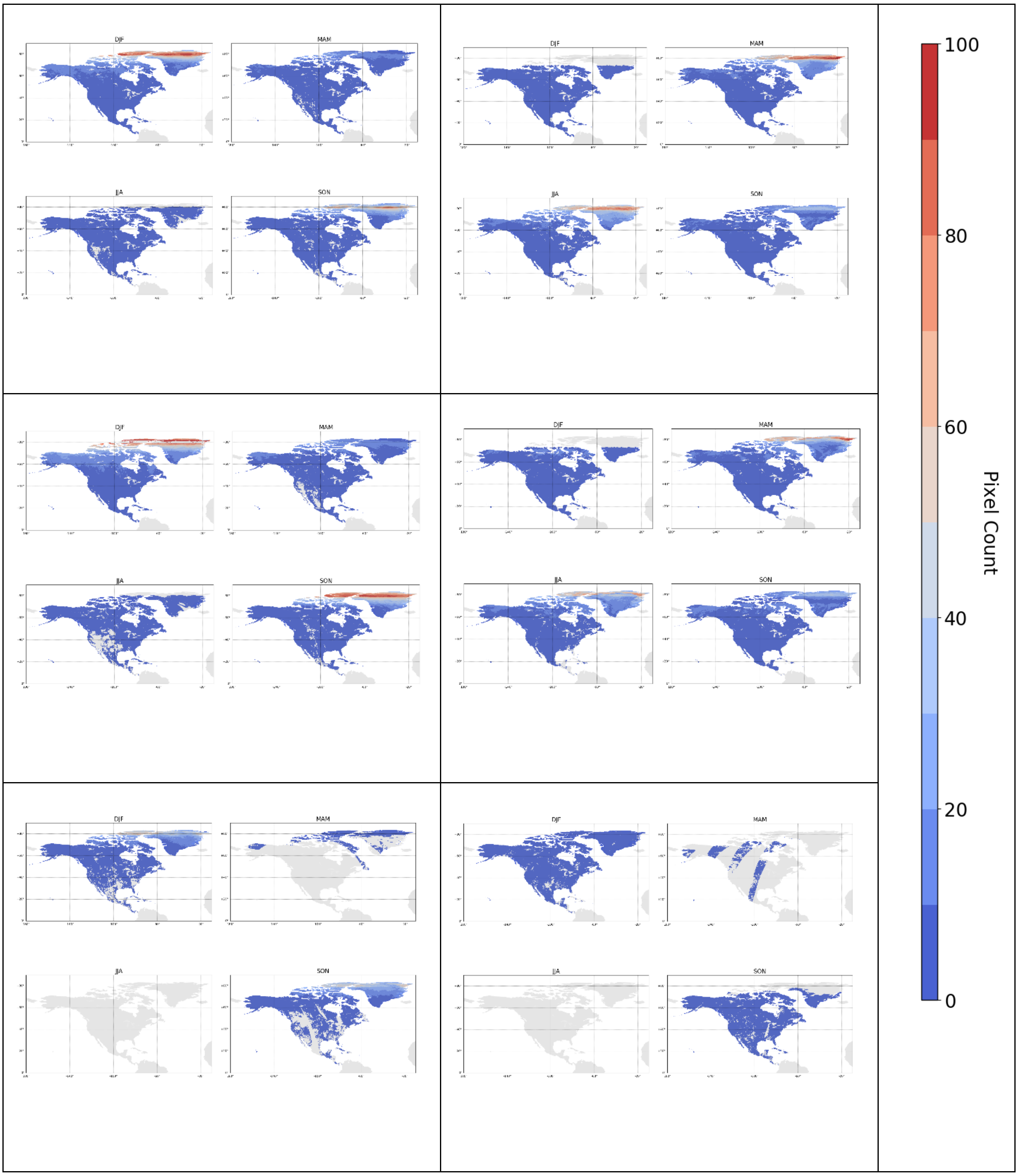

Figure 89: Number of seasonal averaged data points per pixel; left row displays night-time and right row daytime data. Upper plots are for ATSR_3-MOD11T, middle plots for ATSR_3-MODIST, and lower plots for MODIST-ATSOP.

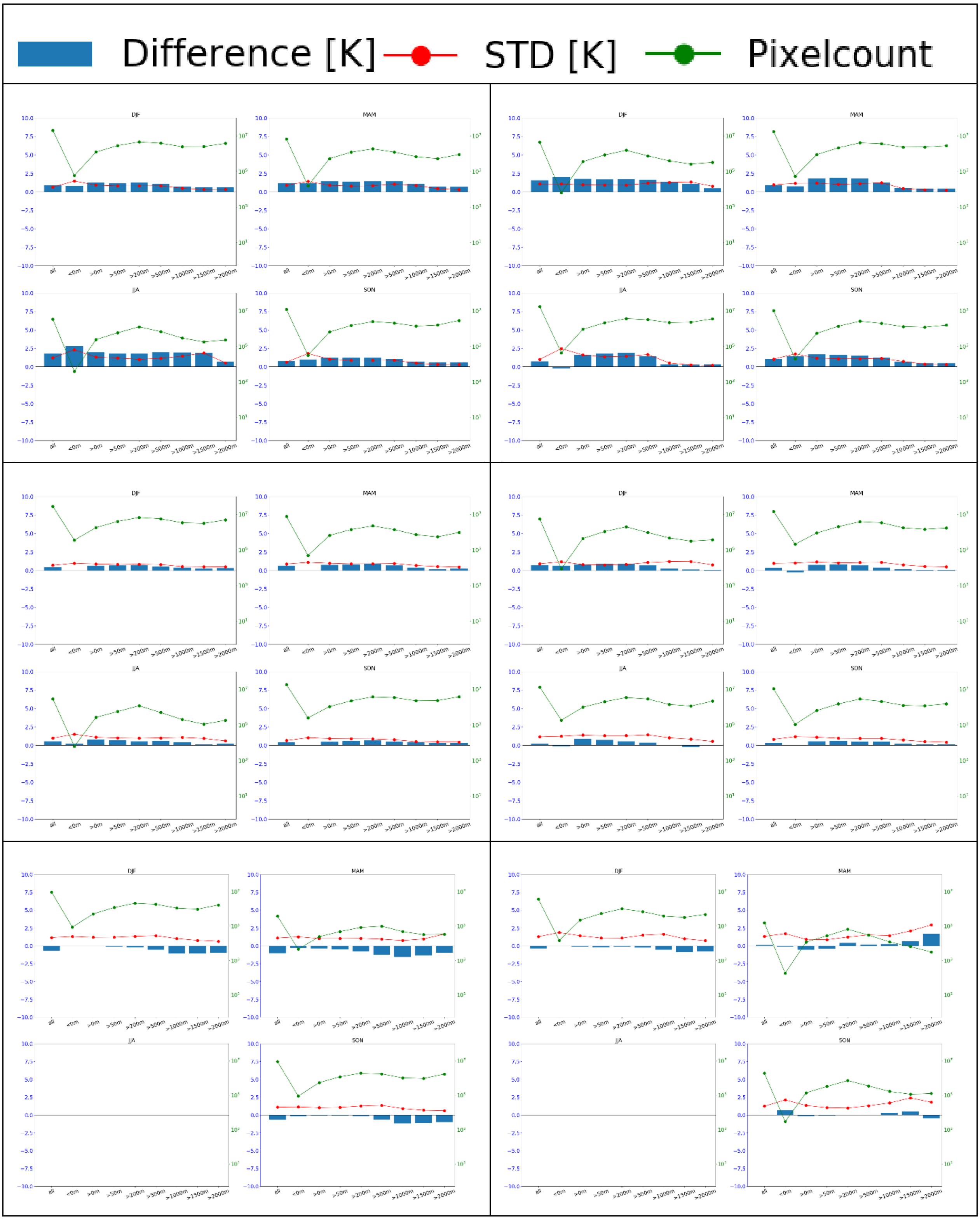

Figure 90: Seasonal differences for different elevation classes; blue bars are the median differences, red points the RSTD and the green points on the right axis show the number of averaged data points Left row displays night-time and right row daytime data. Upper plots are for ATSR_3-MOD11T, middle plots for ATSR_3-MODIST, and lower plots for MODIST-ATSOP.

Figure 91: Seasonal differences for different land cover classes; coloured bars are the differences, red points the RSTD and the green points on the right axis show the number of averaged data points. Left row displays night-time and right row daytime data. Upper plots are for ATSR_3-MOD11T, middle plots for ATSR_3-MODIST, and lower plots for MODIST-ATSOP.

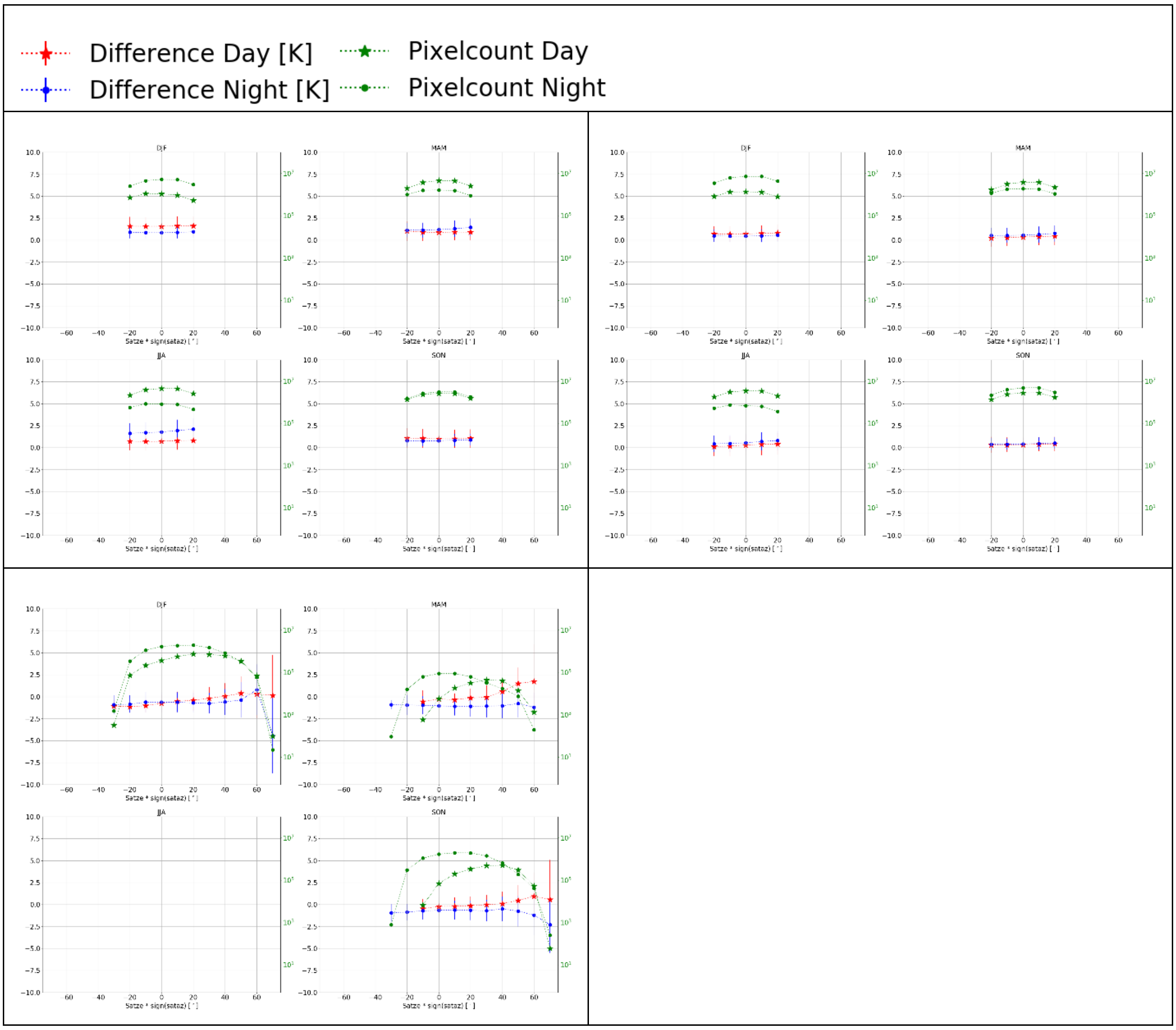

*Figure 92: Seasonal differences versus satze*sign(sataz) of satellite_1; red stars represent the daytime data, blue dots the night-time data, and the green stars and dots on the right axis display the averaged pixel numbers for daytime and night-time data. Upper left plot displays ATSR_3-MOD11T, upper right ATSR_3-MODIST, lower left MODIST-ATSOP.*

7.7. South America

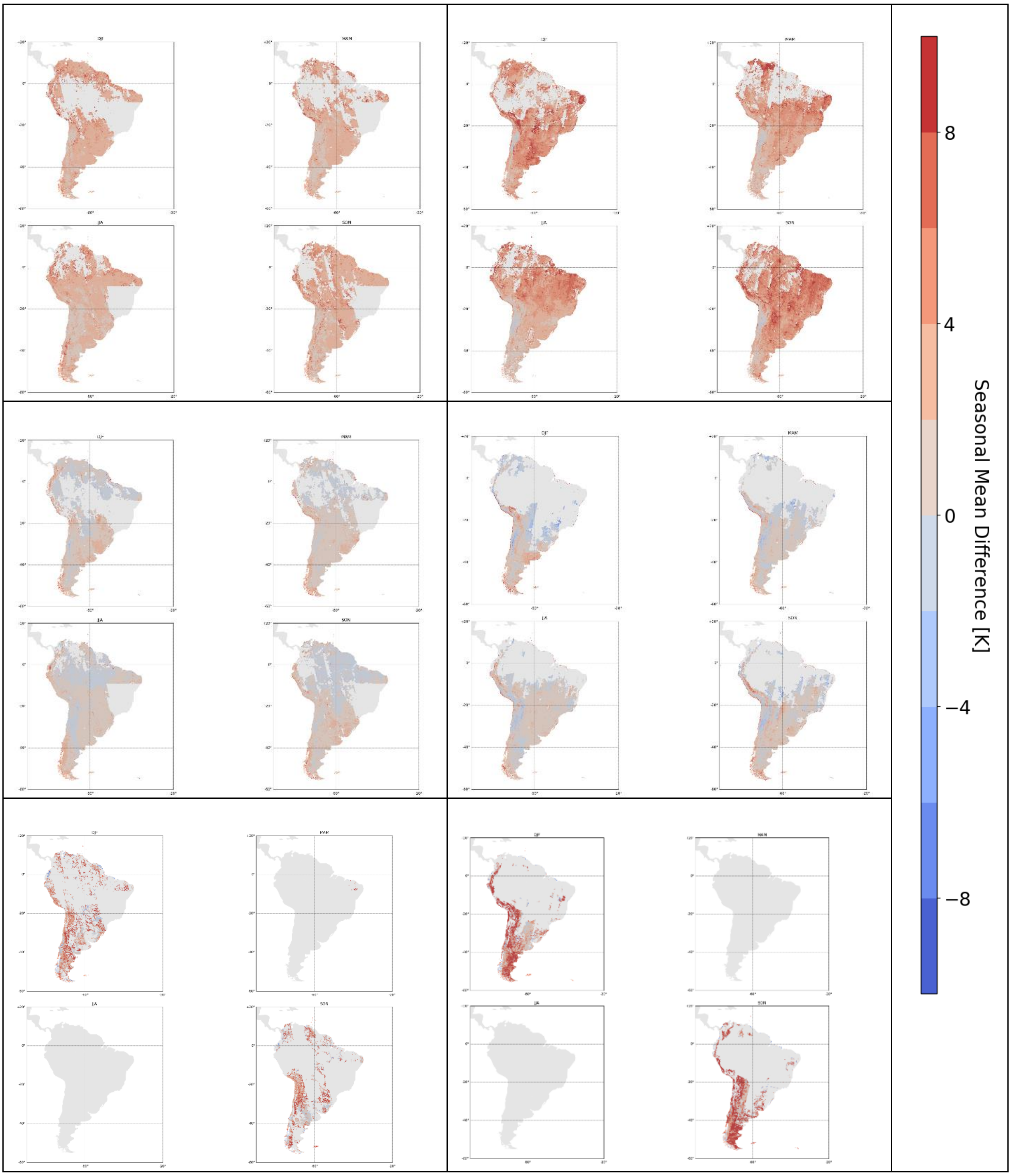

Figure 93: Seasonal mean differences of LST_satellite 1 – LST_satellite 2 in K; left row displays night-time and right row daytime data. Upper plots are for ATSR_3-MOD11T, middle plots for ATSR_3-MODIST, and lower plots for MODIST-ATSOP.

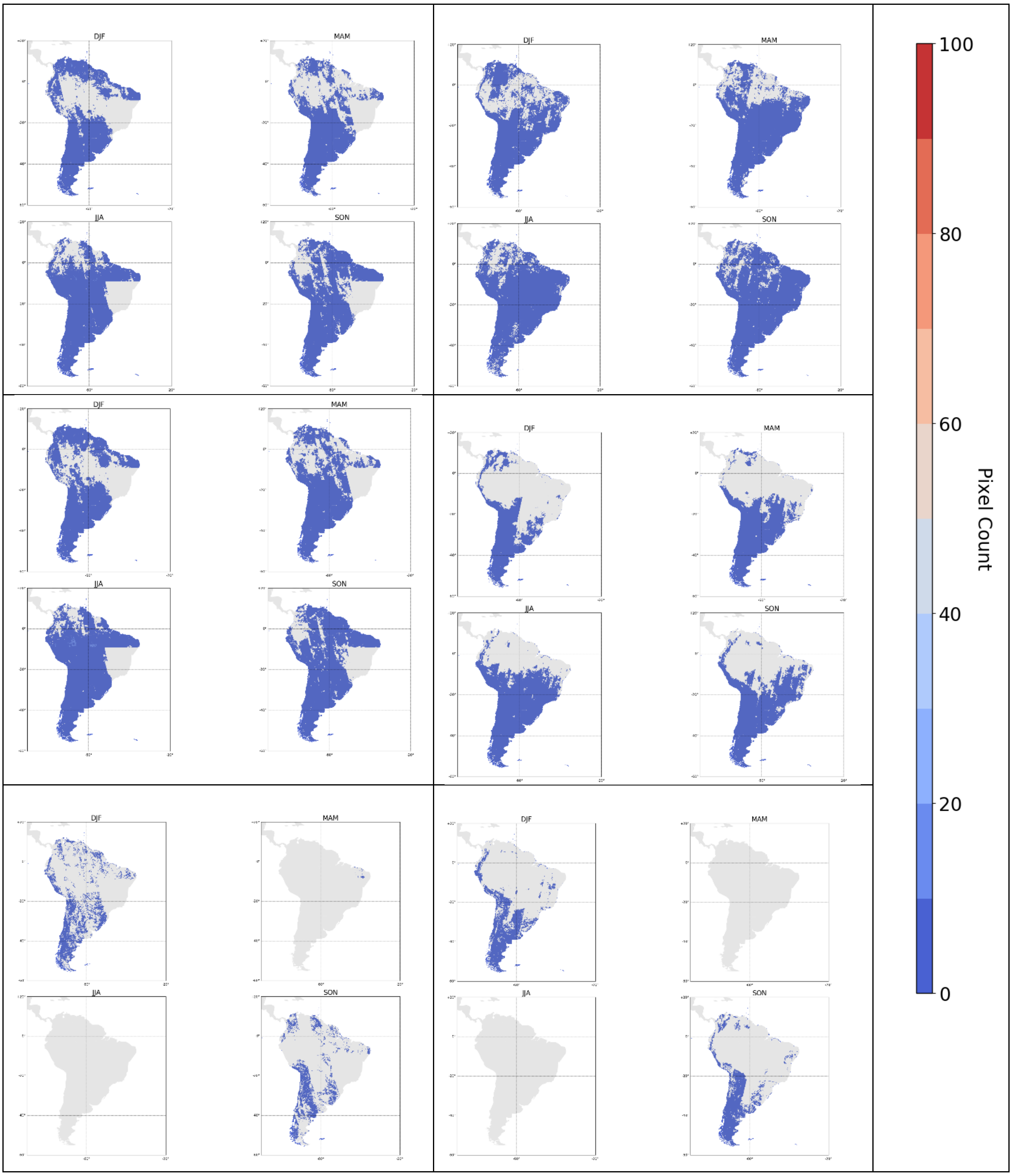

Figure 94: Number of seasonal averaged data points per pixel; left row displays night-time and right row daytime data. Upper plots are for ATSR_3-MOD11T, middle plots for ATSR_3-MODIST, and lower plots for MODIST-ATSOP.

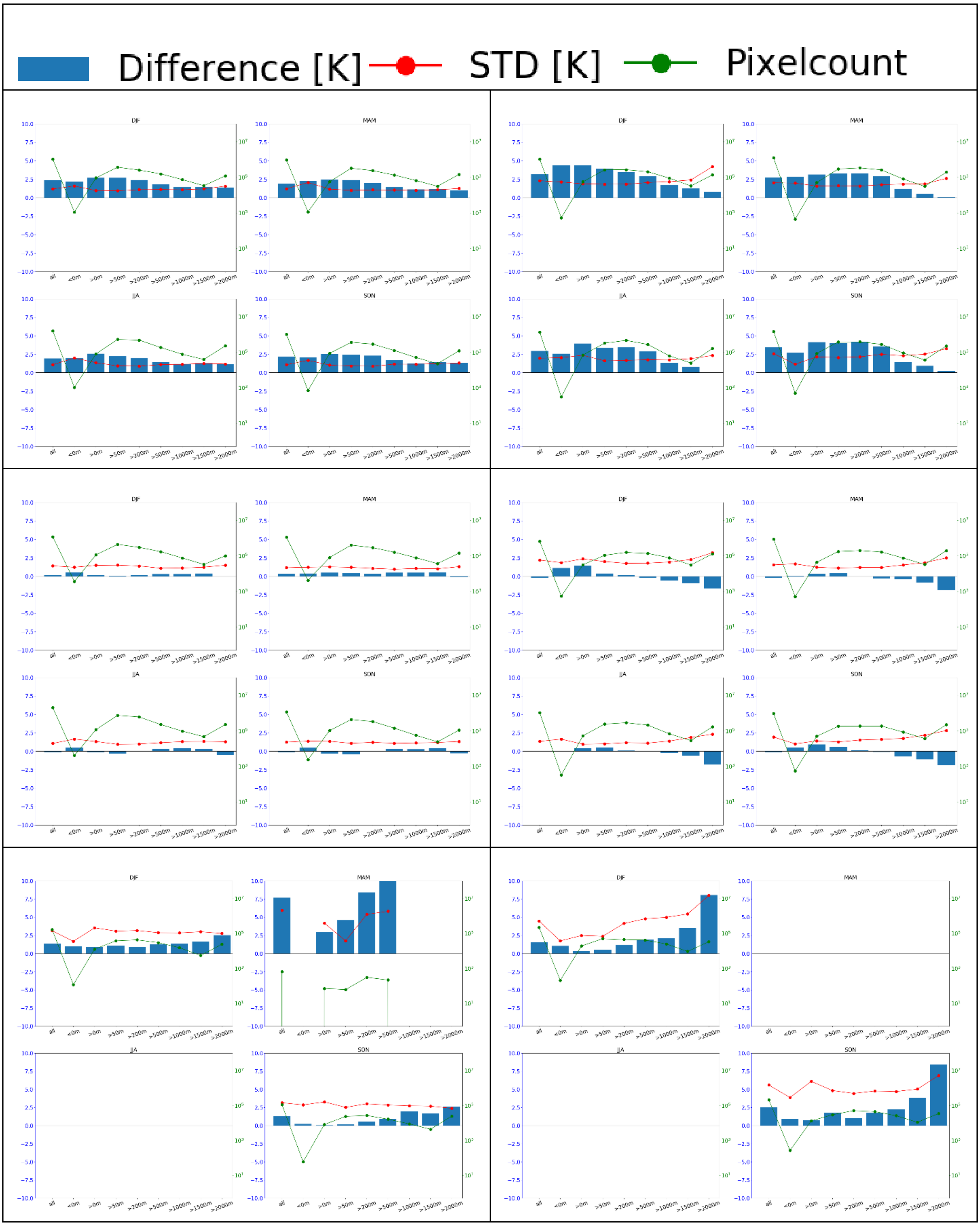

Figure 95: Seasonal differences for different elevation classes; blue bars are the median differences, red points the RSTD and the green points on the right axis show the number of averaged data points Left row displays night-time and right row daytime data. Upper plots are for ATSR_3-MOD11T, middle plots for ATSR_3-MODIST, and lower plots for MODIST-ATSOP.

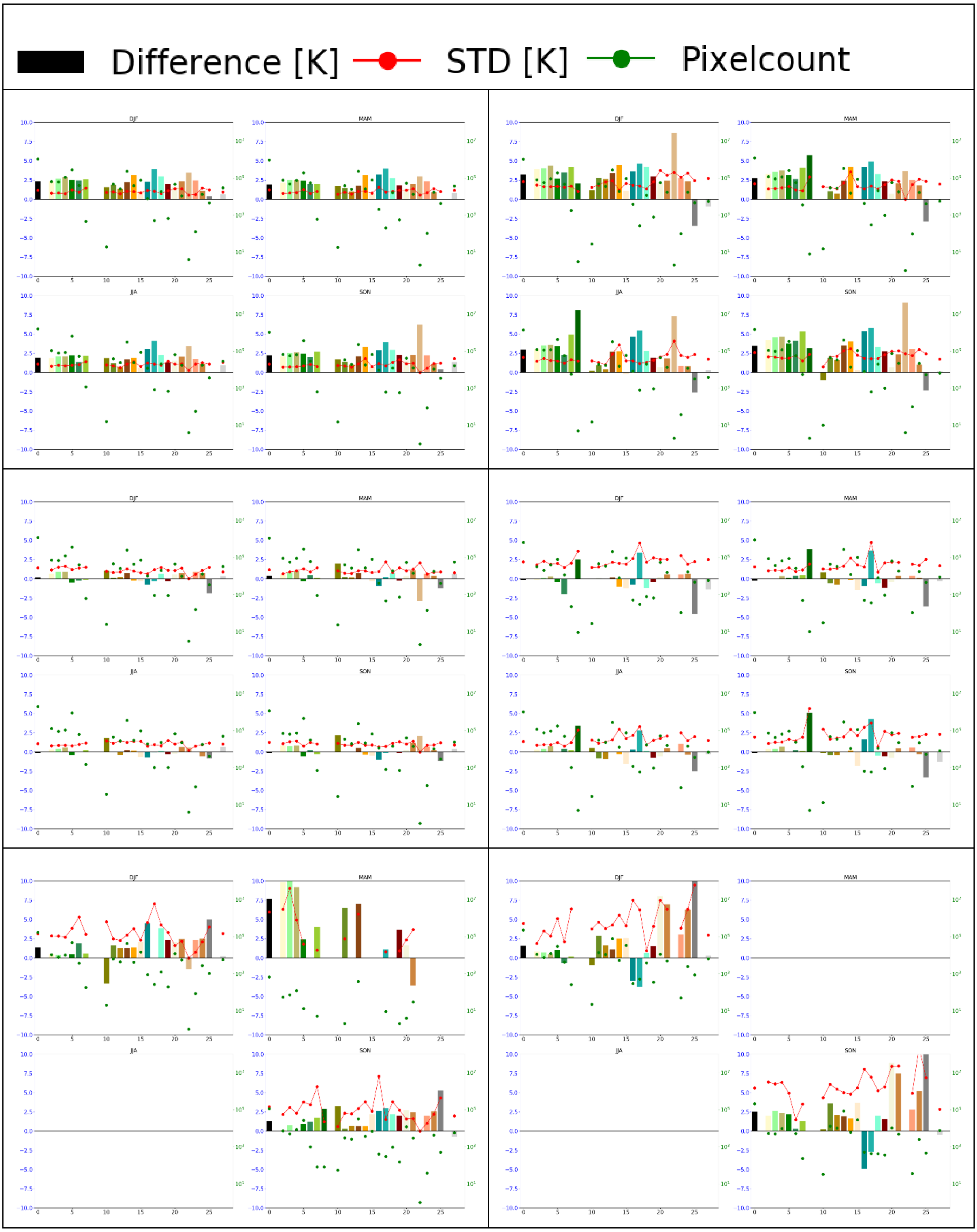

Figure 96: Seasonal differences for different land cover classes; coloured bars are the differences, red points the RSTD and the green points on the right axis show the number of averaged data points. Left row displays night-time and right row daytime data. Upper plots are for ATSR_3-MOD11T, middle plots for ATSR_3-MODIST, and lower plots for MODIST-ATSOP.

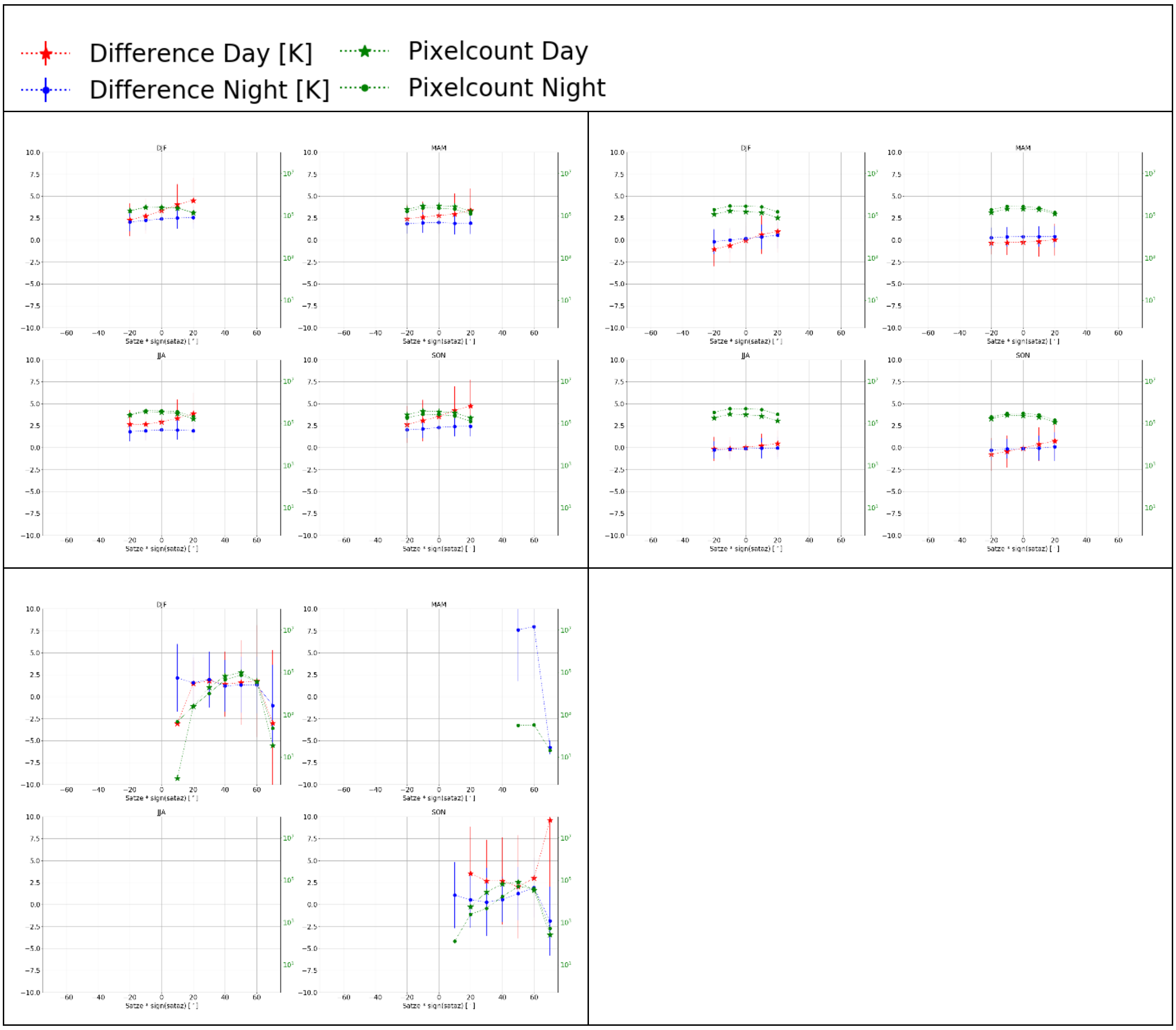

Figure 97: Seasonal differences versus satze*sign(sataz) of satellite_1; red stars represent the daytime data, blue dots the night-time data, and the green stars and dots on the right axis display the averaged pixel numbers for daytime and night-time data. Upper left plot displays ATSR_3-MOD11T, upper right ATSR_3-MODIST, lower left MODIST-ATSOP.